



**Doctoral School in Life and Humanoid Technologies
Course in “Neuroscience and Brain Technologies”**

Cicle XXVII

Title:

**Microchannel scaffolds for axonal biophysics,
electrophysiology and focal microdissection**

Author: Rouhollah Habibey

Supervisor: Dr. Axel Blau



Contents

Abstract	VII
Introduction and background.....	1
1.1 MEA technology for simultaneous recording and stimulation purposes	1
1.2 Neuronal network electrophysiology (Bakkum <i>et al.</i> , 2013b; Obien <i>et al.</i> , 2014; Pirlo, 2009).....	2
1.3 The role of axons in information processing (Debanne, 2004).....	3
1.4 Toward culturing networks with desirable properties on MEA substrates.....	4
1.5 Combined MEAs and microchannel technology for <i>in vitro</i> electrophysiology.....	6
1.5.1 The effect of microtunnel geometry on electrical properties of recording signals	8
1.5.2 Propagation of action potentials (APs) in predefined microchannel confined axons	10
1.5.3 Exploiting microchannels for studying axonal injury, degeneration and regeneration	11
1.6 Combined LMD and microfluidic technologies for axonal regeneration studies.....	12
Materials and methods.....	14
2.1 PDMS microchannel device fabrication:	14
2.1.1 SU-8 photoresist (Chakraborty, 2011).....	14
2.1.2 Chromium mask (Chakraborty, 2011).....	15
2.1.3 Polydimethylsiloxane (PDMS):.....	15
2.1.4 Master molding; SU-8 photolithography.....	17
2.1.5 PDMS device molding; softlithography	19
2.1.6 Fabricated devices properties:	19
2.1.7 Alignment of PDMS devices with MEA electrodes	25
2.1.8 Air bubble removal, coating and wetting the PDMS devices	26
2.1.9 Preparing the primary cortical or hippocampal neurons.....	27
2.1.10 Seeding primary neurons in PDMS microfluidic device	27
2.1.11 MEA electrophysiology.....	29
2.1.12 Laser microdissection	30
2.1.13 Immunofluorescence staining and imaging	33
2.1.14 Statistical analysis.....	33
Results.....	35
3.1 Multicompartment device for multiple axonal compartments	35
3.1.1 Network morphology in multicompartment device	36
3.1.2 Recording activity from microchannel confined axons	38
3.1.3 Activity profile along the time in microchannel confined axons.....	40
3.1.4 Traverse action potential propagation in crossing microchannels	43
3.2 Two compartment devices with open reservoirs.....	44
3.2.1 Recording issue from small networks in open reservoirs	45
3.3 Two compartment devices with closed chambers.....	46
3.3.1 Improved recording in electrodes inside closed chamber	47
3.3.2 Two layer cortical networks provided by sequential seeding	48
3.3.3 Bi-directional propagation in microchannels of two layer cortical cultures	49
3.3.4 Laser microdissection of bi-directional and unidirectional axonal bundles.....	51
3.4 Two compartment devices with working stations (MCh-ws device).....	56
3.4.1 Laser microdissection in microchannels with working stations	58
3.4.2 Morphology and activity in completely dissected axons	58
3.4.3 Morphology and activity in partial-partial dissected axons	61
3.4.4 Morphology and activity in local - partial dissected axons.....	63
3.4.5 Somata response to dissected cortical and hippocampal axons	65
3.4.6 Activity recorded from axons in direct microchannels vs MCh_ws.....	67
3.4.7 Activity recorded from dissected axons vs. intact axons	68
3.4.8 Axonal response to different types of dissection	70
3.4.9 Activity in proximal vs. distal parts of dissected axons in <i>hippocampal cultures</i>	72
3.4.10 Activity in proximal vs. distal parts of dissected axons in cortical cultures	74
Discussion	76

4.5	Multicompartment device for axon guidance and electrophysiology	77
4.1.1	Advantage and disadvantages of multicompartment device	79
4.2	Two compartment devices with straight microchannels	80
4.2.1	Opening the reservoirs from top and recording issue	80
4.2.2	Closed chamber two-compartment device for optimal electrophysiology.....	80
4.2.2.1	Providing bi-directional axonal bundles in microchannels.....	81
4.2.3	Controlled laser microdissection in specific unidirectional or bidirectional axonal tract.....	82
4.2.4	Bi-directional axons morphology and electrophysiology after focal microdissection.....	85
4.2.5	Direct microchannels limitations in studying axonal morphology and electrophysiology	86
4.3	Working stations in microchannels for step wise dissection.....	86
4.3.1	Axonal response to different levels of dissection	87
4.3.2	Network response to the dissection	88
4.4	Conclusion	90
4.5	Limitations	91
4.6	Future works	92
	References	93

Figures:

Figure 1 Master molding and PDMS device fabrication procedure for devices with through-holes ... 20

Figure 2 Master molding and PDMS device fabrication, alignment and cell seeding in devices with closed chambers. 22

Figure 3 PDMS microdevices from backside and downside..... 24

Figure 4 Aligned PDMS microchannels with MEA..... 25

Figure 5 MEA amplifier, chips, electrode layout and PDMS cap 29

Figure 6 Axonal laser microdissection in one layer or two layer networks 32

Figure 7 Optimizing the confinement and coating related issues..... 36

Figure 8 PDMS microchannel tiles on MEAs for neural network compartmentalization..... 37

Figure 9 Sample recording and signal propagation in electrodes inside one microchannel..... 38

Figure 10 Signals with different amplitudes and shapes were propagating in channels. 39

Figure 11 Changes in spike frequency and propagation velocity in axons growing inside crossing microchannels..... 41

Figure 12 Burst propagation along channels and continuous monitoring of axonal morphology..... 42

Figure 13 Traverse axonal growth and AP propagation in crossing microchannels. 43

Figure 14 PDMS mask for cell seeding in the reservoirs of two-compartment PDMS device 44

Figure 15 Very low or lack of recordable activity in the electrodes of open reservoirs..... 45

Figure 16 Cell seeding in two compartment device with closed chambers..... 46

Figure 17 Recording the activity from network growing in the closed chambers..... 47

Figure 18 General concept of crosscorrelation between activity in different electrodes..... 49

Figure 19 Two layer cortical networks and bi-directionally growing axons in microchannels 50

Figure 20 Morphology and activity after dissecting bi-directional axonal bundles connecting two layer cortical networks. 52

Figure 21 Schematic view of dissection in bi-directional growing axons..... 53

Figure 22 Morphology and activity after dissecting uni-directional axonal bundles connecting two layer cortical networks. 54

Figure 23 Sample morphology and recording from cultured neurons in MCh-ws device 57

Figure 24 Axonal morphology and activity after complete dissection..... 60

Figure 25 Axonal morphology and activity after first and second partial dissections 62

Figure 26 Axonal morphology and activity after first and second local – partial dissections..... 64

Figure 27 Somata response to axonal dissection in cortical and hippocampal cultures. 66

Figure 28 Activity recorded from MCh_ws vs MCh_direct 67

Figure 29 Activity recorded from dissected axons vs. intact axons 69

Figure 30 Axonal response to different types of dissection 71

Figure 31 Activity in the proximal and distal parts of dissected hippocampal axons 73

Figure 32 Activity in the proximal and distal parts of dissected cortical axons..... 75

Tables:

Table 1 Physical and chemical properties of PDMS (<i>McDonald and Whitesides, 2002</i>).....	16
Table 2 Master molding detailed procedure for each device.....	21
Table 3 Devices' dimensions and outlines	23
Table 4 Dissection protocol for each type of dissection.....	58

A

bstract

An *in vitro* method for monitoring whole network and axonal electrophysiological activity after induction of the controlled injury to axons would help in investigating network response to injury, as well as understanding axonal function during repair. Laser microdissection could be utilized for highly controlled ablation of microchannel confined axons, while the other parts of the network remain intact. In addition somal and axonal activity and propagation of action potentials could be recorded by custom-made or commercial electrode arrays. Combining these techniques, in the present study, we cultured cortical neurons on top of the commercial microelectrode arrays (MEAs) and forced axons to grow into polydimethylsiloxane (PDMS) microchannels with different configurations. While recording from whole network and axons inside the microtunnels, they were accessible for local laser microdissection (LMD).

The first set of devices including multicompartiment devices with crossing microchannels and two compartment devices with open or closed chambers were used for optimizing the device for network electrophysiology. Finalized PDMS devices included two 100 μm -high rectangular-shaped reservoirs (400 μm X 1600 μm). Reservoirs were connected by eight rows of 30 μm wide and < 5 μm high microtunnels. Axonal LMD was done in axons growing inside two types of microchannels including direct microchannels (MCh_direct) and microchannels with wider areas (MCh-ws). Neurons were seeded from above into one of the freely accessible reservoirs. A PDMS device was aligned with the MEA electrodes to extracellularly record from neurons inside the reservoir and from growing axons inside the microtunnels. Electrical activity recorded before and for weeks after axonal dissection. The pattern of activity and morphology in injured and intact axons, as well as soma was evaluated in different time points.

Combined MEA, microfluidic, and LMD technologies in the present work provided suitable framework for controlled axonal injury and studying network functional and structural response to this injury in compartmentalized manner in soma, intact axons, dissected axons, as well as proximal and distal parts of the dissection point. It is simply possible to add other approaches to the present setup e.g. providing degeneration models, pharmaceutical and molecular studies.

I

ntroduction and background

The complexity of *in vivo* nervous system structure makes it difficult to gain a full understanding of neural cell and network function as well as cell-cell interactions. However, these topics can be almost equally addressed by *in vitro* cell culture assays and methods. To this end, a growing number of investigators pursue the strategy of growing neurons in patterns to evaluate their function and behavior under controlled conditions *e.g.* (Millet *et al.*, 2010). Bruce Wheeler and Gregory Brewer, two of the protagonists in microelectrode array electrophysiology, state that “technology has developed to the point where it is beginning to be appropriate to talk seriously about designing a brain on a chip” (Wheeler and Brewer, 2010). In this spirit, the PhD project will aim at the development of microstructured microchannel confinements to structure and optically dissect selected axons without affecting the other parts of the network. In addition compartmentalizing the network structure gave opportunity to study electrophysiology and function in different compartments separately. These microchannel devices shall be reversibly bondable to substrates for their non-destructive removal and feature cell culture microwells and dedicated microchannels for axonal guidance and electrophysiology. They shall furthermore be compatible with concurrent chemical substrate patterning techniques (*e.g.*, soft lithography) (Blau, 2013).

1.1 MEA technology for simultaneous recording and stimulation purposes

The first prerequisite for studying network electrophysiology is the use of multi- or microelectrode array (MEA) technology which has been developed about three decades ago to study information processing at network level. MEAs have been developed as an on-chip approach to probe and record neuronal communication which fills the gap between cellular

and system neuroscience (Gross, 1979; Nam and Wheeler, 2011; Pine, 1980). These devices consist of multiple microfabricated electrodes, usually with only conductive nodes exposed, often arranged in patterns designed by the user. Wide range of electrodes could be included in MEAs which gives them wide-ranging electrophysiological capabilities, from sub-cellular resolution of single cells to field potentials (Frey *et al.*, 2009). MEAs have been applied for studying primary neurons, stem cell-derived neuronal networks, and brain slices (Baruchi *et al.*, 2008; Illes *et al.*, 2009).

MEA technology makes it possible to simultaneously record from neurons or stimulate them electrically on different channels. However, cultured neurons often migrate over the flat substrate area and thus change position. Furthermore, they tend to cluster if the adhesion chemistry does not sufficiently mimic the extracellular matrix. And, by their nature, neurons make a lot of branched neurites (axon and dendrites) to result in dense networks which make it difficult to ensure one-neuron-per-electrode interfacing (Greenbaum *et al.*, 2009).

1.2 Neuronal network electrophysiology (Bakkum *et al.*, 2013b; Obien *et al.*, 2014; Pirlo, 2009)

Among common activity features of *in vitro* neural networks, the major activities which can be recorded by MEAs are *spikes*, a synonym for action potentials generated by a single cell or a group of cells. A series of spikes is considered as a *spike train*. Many researchers believe that inter-spike intervals in spike trains are important for information procession. *Bursts* are spike flares within a short time window. Bursts are usually recorded simultaneously from different MEA electrodes which, shows that burst activity involves and propagates within large parts of the network (Maeda *et al.*, 1995). Bursting activity of *in vitro* neural networks is different from similar activity in *in vivo* circuits. *In vivo*, bursts occur during development and last only for days or weeks. The bursts persistence in cultured neurons may suggest that culture is arrested in its development. *In vivo*, it usually decreases upon stimulation that resembles sensory input during development (Wagenaar *et al.*, 2005). Different burst features include frequency or rate, duration, inter-burst or inter-spike intervals, spike rates during bursting, peak and mean values of spike and bursting rates, and the change of these values. In addition, the coefficient of variation (CV), the dispersion of the

probability distribution, can also be assessed (Chiappalone *et al.*, 2006; Wagenaar *et al.*, 2005).

In addition to the recording, MEA electrodes have the ability of electrically stimulating the neural cells in culture which can be used as a separate method or in combination with chemical manipulations. Two stimulation types can be distinguished, current pulse and voltage pulse stimulation. From a theoretical point of view, most researchers prefer to apply current pulses instead of voltage pulses for stimulating neural cells through electrodes, because in current pulse mode the electric field and potential near the electrode can be measured directly. In voltage pulse mode, the current depends on the complex impedance of the electrode and is more difficult to control (Madhavan *et al.*, 2006; Maher *et al.*, 1999; Wagenaar *et al.*, 2004). However, there are several drawbacks for current-controlled stimulation for instance good current sources are more complex than voltage sources and current pulses can cause high electrode voltage which may harm the culture or destroy the electrode through chemical reactions. For these reasons most electrical stimulations on MEAs perform on voltage-control mode. Positive and then negative biphasic voltage stimuli is the very effective in induction of APs (Wagenaar *et al.*, 2004).

1.3 The role of axons in information processing (Debanne, 2004)

Axons may have more important roles in neuronal computation than simply propagating the action potentials from soma to post-synaptic neuron. For instance, in cortex and hippocampus, axons not only encode information in digitally but also in an analogue manner through the graded action potential magnitudes which leads to modulated synaptic activity and neurotransmitter release (Alle and Geiger, 2006). On the other hand Sasaki *et al.*, showed that width of axonal APs increased in response to the local application of glutamate to the axon shafts or by uncaging Ca^{2+} from periaxonal astrocytes which activates ionotropic glutamate receptors. Wide APs increase calcium releases in presynaptic buttons and facilitated synaptic transmission to postsynaptic neurons (Sasaki *et al.*, 2011). In addition activity dependent plasticity of AP propagation delay and amplitude has been confirmed in cultured cortical neurons, by increasing the latency time in presence of low frequency patterned stimulus (Bakkum *et al.*, 2008). In the myelinated axons, the thickness of myelin

layer and space of ranvier nodes can affect AP propagation properties of the axon (Fields, 2005). There are some evidence supporting the activity dependent myelination of the axons in white matter during development or in adult (Demerens *et al.*, 1996).

Physical properties of an axon can modify the transmission of action potentials and shape it. These properties include the number and distribution of ion channels, axon diameter, axon length, number of branches and varicosities. They can affect propagation in three ways:

- a) Conduction delay
- b) Propagation failure
- c) Reflected action potentials

1.4 Toward culturing networks with desirable properties on MEA substrates

A desirable network structuring methodology should fulfill the following requirements: (a) a precise and predictable positioning of each neuron, (b) accessibility of each individual neuron for electrical (MEA) and optical (calcium imaging, potential-sensitive dyes, optogenetic probes) recording and electrical (MEA) as well as biomechanical (coated beads) stimulation purposes, (c) arbitrary control of neural polarity, number of neurites and connections between neurons, and (d) long-term network survival to monitor changes in network function and structure for developmental, pharmacological and plasticity studies (Jun *et al.*, 2007). To meet these goals, we can simplify neuronal networks by forcing the geometry of networks into defined patterns, reducing the number of connections between neurons through low-density culture technologies and defining directional growth of neurites (Pirlo *et al.*, 2008). Several preceding studies have already demonstrated the confinement of neurons and neurites by chemical and physical means, *e.g.* (Claverol-Tinture *et al.*, 2007; Wheeler and Brewer, 2010). Physical confinements could be provided by flexible and transparent microfluidic devices which could provide strong as well as reversible bounds with glass slide or MEA substrates (Park *et al.*, 2006).

1.4.1 Microfluidics (Wang *et al.*, 2009)

The terminology ‘microfluidics’ refers to the manipulation of small amounts of fluids (10^{-9} to 10^{-18} liters) in channels with dimensions of tens of micrometers. It is used in different

fields including chemistry, biology and medicine. Because of its ability of precisely controlling, monitoring and manipulating the cell environment, microfluidics is becoming an increasingly useful tool for cell biologists. Several materials have been applied to the fabrication of microfluidic devices. Among them, PDMS-based devices have gained popularity due to several advantages: thermal stability, biocompatibility, low cost and easy fabrication procedures by soft-lithography, optical transparency and gas permeability (Taylor and Jeon, 2010; Wang *et al.*, 2009).

PDMS microfluidic devices can be applied for different biological studies including miniature immunoassays, separation of proteins and DNA, sorting and manipulation of cells, and microscale bioreactors (Andersson and van den Berg, 2004; Sia and Whitesides, 2003). Such structures have been applied to different approaches in the field of neurobiology including cell culture, neural cell manipulation, neuropharmacology, neuroelectrophysiology, neurodegenerative and axon regeneration studies, and neuron biosensors (Berdichevsky *et al.*, 2009; Morin *et al.*, 2006b; Taylor *et al.*, 2003; Taylor *et al.*, 2005; Taylor and Jeon, 2010; Wu *et al.*, 2010).

1- **Neuron cell culture:** PDMS microfluidic devices have been used to provide culture conditions with controlled pH and oxygen concentrations (Mehta *et al.*, 2007), to make high density or very low density cultures within nanoliter-volume devices, or to culture different type of neural cells in close-vicinity chambers (Cullen *et al.*, 2007; Millet *et al.*, 2007).

2- **Separate manipulation of somata or axons:** Because cell body, axon and dendrites have different physiological properties their pathological changes in disease and their responses to treatments are different. Therefore, it would be desirable to have a setup with which we can examine them separately.

Different designs of PDMS microstructures have been developed to trap cells in tiny microwells and scaffolds, and to immobilize them in their specific posts (Luo *et al.*, 2007). This method not only fixes the cells in the predefined position, but also provides an orientation for the network (Recknor *et al.*, 2004).

Axon manipulation is important for neural connectivity studies, axonal plasticity and response to injury in the presence of different molecules as well as for modeling neurodegenerative disease *in vitro*. In total, four protocols have been integrated for axonal

manipulation in microfluidic devices including so far: *a) microstructure guiding* by applying different widths and angles to control the length and shape of an axon (Francisco *et al.*, 2007); *b) external-force assisted microstructure*, by utilizing hydrostatic pressure in microfluidic devices to separate two environments of different chemical composition and help axons to grow in a specific direction or to evaluate the effect of specific agents on the axonal compartment (Taylor *et al.*, 2005); *c) biochemical assisted guiding*, in which a gradient of cell adhesive molecules inside of microtunnels helps axons grow in specific directions (Dertinger *et al.*, 2002); *d) integration of biochemical and topographical cues* (Li and Folch, 2005).

3- Neuropharmacology and neurophysiology: microenvironmental control and delivery of micro- and nano-scale volumes of drugs to the isolated soma or axon is possible by fine structures of PDMS microdevices. In addition, by combining microfluidic devices with commercial or custom-made MEA substrates it is possible to record from cells or axons even during injury or treatment (Morin *et al.*, 2006a; Ravula *et al.*, 2007).

1.5 Combined multi-electrode arrays (MEAs) and microchannel technology for *in vitro* neural networks biology and electrophysiology

The majority of recorded signals from planar MEAs are voltage potentials originating from cell bodies rather than axonal compartments (van Pelt *et al.*, 2004). Because the cell body has a larger surface compared to thin axons currents are larger (Buitengeweg *et al.*, 2002a; Buitengeweg *et al.*, 2002b). To successfully record from neurons or neurites it requires bringing neurons as closely as possible to the electrodes. Microchannel-mediated cell confinement which keeps cells in the vicinity of the recording electrodes has increased the spike rates (Nam *et al.*, 2004). However, the extracellular recording of axonal signals is still a challenge. It would improve biomedical research and drug screening studies, though. In addition, axonal confinement would be helpful in defining the functional connectivity within networks and directionality of pre- and post-synaptic connections (Kondo *et al.*, 2004; Meeks and Mennerick, 2007). To this end, several studies have been conducted in different labs to guide neurites through microchannel or microtunnel structures and record propagating action potentials along axons (Claverol-Tinture *et al.*, 2007) (Claverol-Tinture *et al.*, 2005) (Ling *et*

al., 2012) (Dworak and Wheeler, 2009; Pan *et al.*, 2011). Non-expensive microlithography techniques for the generation of microtunnels have been used recently to structure networks in very variable spatial designs. It allowed microwell-confined populations of neural networks to connect through microchannels (Wheeler and Nam, 2011).

For the first time, Campenot forced axons of sympathetic neurons to grow toward a nerve growth factor (NGF) gradient along 200 μm wide scratches in a glass surface that was coated with collagen (Campenot, 1977). However, the Campenot compartmentalized chamber was not suitable for cortical and hippocampal neurons. Therefore, Taylor *et al.* developed a PDMS microfluidic platform in which microchannels (10 μm wide, 3 μm high) separated axon and soma compartments (1.5 mm wide, 7 mm long, 100 μm high) from each other. Because the microchannels were very small, cell bodies could not enter while axons extended inside the channels and produced pure axonal regions favorable for protein synthesis and axonal regeneration studies (Taylor *et al.*, 2005). Other PDMS microchannel devices were developed in different labs (Berdichevsky *et al.*, 2010; Shi *et al.*, 2010). For instance, Park *et al.* designed a compartmentalized PDMS device for central nervous system axon myelination research with soma and axon/glia compartments separated by axonal microchannels (~ 200 μm length, 30 μm width and 2.5 μm height) (Park *et al.*, 2009a; Park *et al.*, 2009b). Also other materials have been used to design microchannel structures including agarose and parylene (Moriguchi *et al.*, 2002; Tooker *et al.*, 2005).

The other advantage of microchannels is to utilize them for electrophysiological studies of neural networks *in vitro* while cells have been placed in the specific places of substrate including electrodes (Claverol-Tinture *et al.*, 2005; Ravula *et al.*, 2006). Claverol-Tinture *et al.* have described a technique for recording extracellular potentials from different segments of neurites by placing PDMS microstructures including microwells (for somata) and microchannels (for neurites) on the surface of a custom-made MEA. This method fixed cell bodies and neurites on the electrode sites and increased the stability of the cell-electrode interface. They showed that microchannel-confined (20×5 μm^2 cross section) neurites give higher signal to noise (SNR) ratios with large signal amplitudes (~ 300 μV) (Claverol-Tinture *et al.*, 2007). In a complementary study they showed that microchannels (length ≤ 300 μm , cross section ≤ 12 μm^2) can increase the amplitudes of extracellularly recorded signals from

neurites to millivolts. Microchannel devices provide SNR between 18 ± 4 and 428 ± 9 , with a mean value of 101 ± 76 , which is comparable to the maximum SNR obtained from carbon nanotubes CNT coated electrodes (~ 135) or Silicon Nanowire Field Effect Transistors (Si-NWFETs) (~ 210) (Ling, 2011; Ling *et al.*, 2012).

1.5.1 The effect of microtunnel geometry on electrical properties of recording signals

In 2009, Dworak and Wheeler (Dworak and Wheeler, 2009) designed PDMS microtunnel structures to attain high-amplitude signals from axons. Their design included four groups of 11 microtunnels (length (L) = 750 μm , width (W) = 10 μm and height (H) = 3 μm) connecting five 1.5 mm square microwells together (one wells on each side and one in the centre). Line-shaped electrodes of three different widths (25, 50 and 75 μm) were chosen and PDMS microtunnels overlaid on top of them. Thus, the dimensions of the exposed electrode areas were defined by the width of the electrode line and that of the channel. All other conductive paths were insulated by the PDMS device. The resistance R of microtunnels filled with phosphate buffered saline (PBS) solution was modeled to be $R = \rho L / (W \times H)$, where ρ is the resistivity of the solution (75 $\Omega \text{ cm}$). The calculated channel resistance was 15.6 M Ω . However, the actually measured resistivities depended on electrode width and distance from the microtunnel entrance on every side. It ranged from 3.3 M Ω to 13.5 M Ω .

Impedance measurements showed that microtunnels were mostly resistive while the electrode-electrolyte interface was mostly capacitive with a smaller contribution from the spreading resistance. For instance, 50 μm -wide electrodes at the centre of a microchannel had the highest impedance due to their longest distance from the microtunnel entrance while electrode size (between 25 and 75 μm) had less impact on the overall impedance.

The growth of neurites inside the channel increased the resistivity from 75 $\Omega \text{ cm}$ for solution to 300 $\Omega \text{ cm}$ for neural tissue due to effective decrease of channel cross section. The background noise of signals was 10-50 μV p-p and signal amplitudes were 100-200 μV . These are comparably higher than signals recorded from somata (10-100 μV). This led to the conclusion that the higher resistance of microtunnels filled with axons was the reason for such high signal amplitudes. In addition, the action potential amplitude also depended upon the electrodes size and distance from the tunnel entrance. The larger the electrode and its

distance to the channel entrance, the higher were the recorded axonal action potential amplitudes. This design also allowed for determining the action potential propagation speed. However, it is still unknown whether microtunnel geometry has any effect on propagation velocity.

In 2012 Ling *et al.*, tried to characterize the effects of channel geometry on measured signals via numerical simulations and *in vitro* experiments, using the PDMS microchannels with different length and cross section and multielectrode arrays (100 nm thick ITO) with 40 μm width and 60 μm space (Ling, 2011; Ling *et al.*, 2012). Resistance of each channel was measured via a pair of Ag/AgCl electrodes (one as reference in soma compartment and other as recording electrode in the axonal compartment) and patch clamp amplifier in voltage clamp mood. Resistance before cell plating and resistance after 12-14DIV was measured to show how neurites growth inside the channel and sealing the channel entrance can affect the channel resistance. Increased resistivity after cell seeding (12-14 DIVs) for all kinds of cross sections and lengths showed that “spontaneous seal” exist and affects biophysical properties of the channel. Further analysis showed that there is a negative correlation between channel length and clog resistivity (ρ_{clog}) for lengths more than 200 μm . Another important finding was that there is no clear correlation between ρ_{clog} and number of axons (units detected in signal sorting), which suggested a role for glial cells in ρ_{clog} as axons alone cannot account for this resistivity increase. The results of simulation and experimental data showed that for channels with length $< 200 \mu\text{m}$, signal amplitude increases with increasing the length of the channel, however for length 200-3000 μm signal amplitude decreases by increasing the length of the channel. They showed that large amplitude signals can be recorded from electrodes in 200 μm from channel entrance. There was also negative correlation between channel cross section and signal amplitude.

They suggested 2 reasons for decreased signal amplitude in long microchannels:

- 1) Low pass filtering effect: high resistance microchannels combined with stray capacitance acts like a first-order low pass filter and decreases high frequency signal amplitude (*i.e.* positive peaks of AP). As the length of the channel increases, the cut-off frequency decreases and signals getting wide and wider in electrodes which are farther from cell body.

2) Phase-cancelling effect (PCE): even without stray capacitance in simulation, signal amplitude cannot increase beyond 200 μm , which shows that PCE plays an important role in decreasing the signal amplitude. PCE depends on the microchannel length and conduction velocity. For a given channel, fast propagating signals are affected less by PCE effect because the positive phase can spread further. Therefore axons with higher conduction velocity (CV), *e.g.* thick axons or DRG axons, have longer transition length.

Finally they concluded that, to record signals with best SNR the optimal microchannel channel would have 1 μm high, 5 μm wide and 0.3 mm long with electrodes are located in 70-170 μm to the nearest channel entrance from each side.

1.5.2 Propagation of action potentials (APs) in predefined microchannel confined axons

Action potential and burst propagation in the cultured neuronal networks could be useful for extraction of the network functional pattern and plasticity studies. Burst initiation is mainly found in areas with higher neural activity and a lower density of inhibitory neurons (Feinerman *et al.*, 2007). In addition, the initiation point of bursting activity always determines the propagation path through the network (Pan *et al.*, 2009). However, bursts can be propagated in different ways because each may involve different region of culture. By predefining networks through microchannel devices, better control on signal propagation directionality may be achieved. Unidirectional propagation between neural networks had already been proposed by Feinerman *et al.* . However, it was not possible to record from axons in the Feinerman logic gates model (Feinerman *et al.*, 2008).

In 2011, Pan *et al.*, cultured neurons sequentially in two connected wells (10 days delay with respect to the first one), which helped them in creating a structured culture in which most axons from the previously cultured network connected to the other culture through the PDMS microchannels. Their system allowed the recording both from reservoirs and microchannels (150 μV with maximum 1mV) which had been aligned on top of the linear electrodes. In this device, recording of one action potential in 2 subsequent electrodes along the microchannel enabled them to determine the propagation velocity (0.18-1.14 m/s) and direction. Furthermore, they were able to determine the degree to which bursting activity can

be propagated from one population of neurons to other population in another well (Pan *et al.*, 2011).

In a recent study by Bakkum *et al.*, they recorded antidromic or orthodromic AP propagation along cortical axons after stimulation using high density MEAs. They used custom arrays containing 11,011 microelectrodes fabricated by CMOS technology to seed 10,000-40,000 cells over an area of 12 mm². Because of high density nature of array cell body or axon were randomly placed on electrodes, therefore it was possible to activate neural tissue with low artifact (400mV) extracellular stimulation and with high spatial resolution. Selective stimulation of single axon or soma reduces the number of activated neurons which consequently reduces signal overlap. In addition to the somatic action potentials, smaller APs propagating on neurites was also observed in response to stimulation. The velocities measured from axonal spikes were different in different segments of the axon for both antidromic and orthodromic propagation. The velocities were recorded from thinner distal parts of axon was fivefold slower than the thicker parts. More experiments showed that velocity differences existed spatially between neighboring segments, temporally between days and functionally between sites of initiation. The lower threshold in axons is mainly related to higher density of voltage gated sodium channels in it membrane (100-200 channels per μm^2) compared to soma or dendrite (3-10 per μm^2). Therefore activation threshold for axons is 12 mV less than soma for cortical neurons (Bakkum *et al.*, 2013a). However, Uneven and opaque surface of CMOS chip makes it impossible for bright field imaging and very difficult for fluorescent imaging. On the other hand shrinkage during cell fixation process or cell movement before fixation may cause misalignment between recorded activity and cell location. In addition, it was not possible to locally manipulate aforementioned axon by chemicals or optical tools. And most importantly, whole experiment had been done on the stimulation-derived activity while it was not possible to trace the normal propagation along the axons.

1.5.3 Exploiting microchannels for studying axonal injury, degeneration and regeneration

Beyond the physiological role of axon in normal neural circuits, its damage is critical to the etiology of CNS injuries and neurodegenerative disease. Therefore, considerable efforts

have been focused on understanding the mechanisms involved in axonal plasticity and response to injury (Taylor *et al.*, 2005). The complexity of events after injury and lack of tools to monitor them *in vivo*, necessitate the use of *in vitro* models. The first *in vitro* device with separate fluidic environment for growth of axons was developed by Campenot (Campenot, 1977). In this device a Teflon divider is attached to the surface to confine soma in one compartment while letting neurites to grow through the silicone grease into neighboring compartment. However, this device was only useful for PNS neurons because CNS neurons do not respond well to nerve growth factor (NGF) (Park *et al.*, 2009b). PDMS microchannels system developed by Taylor *et al.*, makes it possible to separate CNS neuron soma from axons in two different fluidic environment (Taylor *et al.*, 2005). This device, or similar prototypes, has extensively been applied for studying axonal injury and regeneration, myelination, protein and mRNA synthesis, as well as transport during last decade (Kim *et al.*, 2012; Park *et al.*, 2013; Siddique and Thakor, 2014).

1.6 Combined laser microdissection (LMD) and microfluidic technologies for axonal regeneration studies

Before LMD being utilized for inducing axonal injury, several tools had been used to mimic CAS axonal injury *in vitro*, including the use of sharp metal blades (Quilty *et al.*, 2003), pulled glass electrodes (Mandolesi *et al.*, 2004) and rubber impactors (Fayaz and Tator, 2000). All these methods need sophisticated micro-manipulators, they can cut few axon at time and may affect other parts of the network. LMD is an alternative method which enables precise and rapid dissection of fixed or live axons (Hellman *et al.*, 2010). The ideal LMD setup enables reproducible dissection of individual axon while it is possible to monitor regeneration procedure after injury for long-term.

Kim *et al.*, developed a novel neuro-optical platform to study individual axon injury and regeneration by combining PDMS microchannels and femtosecond laser dissection setup. Single axons of dorsal root ganglion (DRG) neurons were separated individually by seeding them in PDMS microchannel device. Femtosecond laser enabled precise and reproducible axotomy of live DRG or cortical neurons. Regeneration process was evaluated by keeping culture in mini-incubator and differential interference contrast (DIC) imaging system. The

results showed that 0.3 W average power and exposure range of 10-40 ms yields reproducible axotomy. However, these parameters could be different for axons with different thickness. After dissecting the live axon, it snaps like a rubber band from point of injury and detaches from surface. After axotomy distal part is thinned and fragmented while the proximal part starts to regrowth mainly in the original pre-injury track (Kim *et al.*, 2009).

Femtosecond laser radiation is delivered at kHz or MHz rates. Although it seems attractive for *in vivo* microsurgery because of its ability to produce extremely localized damage, the high costs and complex operation is a hinder. In addition, its high intensity can cause production of reactive oxygen species (ROS) or damage biomolecules like DNA. For this reason, Hellman *et al.*, tried to use nano- or picoseconds laser microbeams which are more reliable, less costly and precise in microdissection. Microfluidic device was just used for patterning strips on the surface and cell seeding in specific points. Axons grew in bundles in the patterned areas and dissected by a single 180 ps, 400-800 nJ laser pulse. Time resolved imaging of the events immediately after pulsed laser microbeam irradiation, visualized the cavitations bubble interaction with axon bundle and confirmed the idea that cellular injury is related to direct vaporization by the plasma combined with mechanical shear stress. Dieback and regrowth measured quantitatively after injury and showed that Ca influx into the axon from injury site is the main reason of dieback because Ca induces disassembly of microtubules in the first minutes after dissection. Chelating extracellular Ca by EGTA reduced dieback after dissection. On the other hand Ca also affects regrowth of proximal ends, because chelating Ca with EGTA led to decreased or lack of regrowth compared to the control experiment with normal medium (Hellman *et al.*, 2010).

Combined microfluidic-LMD could be useful for testing the effect candidate drugs on axonal regeneration. In spite of the classic view on inability of CNS axons to regenerate after injury, it has been demonstrated that adult CNS neurons are able to regenerate and extend long processes after injury in presence of favorable environment. The conclusion was that the limiting factor to CNS regeneration is not intrinsic to the neuron, but is the environment in which neurons grow (Kim *et al.*, 2012). Among the factors which inhibit CNS axonal regeneration after injury are inhibitory proteins associated with damaged myelin (Filbin, 2003).

M

aterials and methods

2.1 PDMS microchannel device fabrication:

The whole device has been fabricated in two steps, master molding and PDMS device molding. Master is fabricated in two layer SU-8 resin by photo-patterning through two mask layers. PDMS device fabricated from original SU-8 template or an epoxy master copy.

2.1.1 SU-8 photoresist (Chakraborty, 2011)

Photoresists are composed of three major components; a polymer (base resin), a sensitizer, and a casting solvent. The polymer changes structure when exposed to electromagnetic radiation, the solvent helps for providing uniform photoresist layers on a flat substrate during spin-coating, and the sensitizers control the photochemical reactions in the polymeric phase. Photoresist must meet several rigorous requirements: good adhesion, high sensitivity, high contrast, good etching resistance (wet or dry etching), good resolution, easy processing, high purity, long shelf life, minimal solvent use, low cost, and etc.

SU-8 is an acid-catalyzed *negative photoresist*¹, made by dissolving a SU-8 resin in an organic solvent such as propylene glycol methyl ether acetate (PGMEA) and adding up to 10 wt% of triarylsulfonium hexafluoroantimonate salt as a photoinitiator. Irradiation of the photoresist initiates SU-8 cross-linking. Irradiation generates a low concentration of a strong acid, hexafluoroantimonic acid, which opens the epoxide rings and acts as a catalyst of the chemically amplified cross-linking process that gets further activated by the application of heat, post bake.

¹ In *negative photoresist*, the photochemical reaction strengthens the polymer by cross-linkage of main chains or side chains, thus becoming less soluble. In *positive* photoresist, the photochemical reaction during exposure weakens the polymer by rupture or scission of the main and side chains, and the exposed resist becomes more soluble in developing solutions. In other words, in *negative photoresists* light cross-links, whereas in *positive photoresists* light scissions.

2.1.2 Chromium mask (Chakraborty, 2011)

The stencil used to repeatedly generate a desired pattern on resist-coated substrates is called a mask. Photomasks are optically flat glass (transparent to near UV) or quartz plate (transparent to deep UV) with an absorber pattern metal layer (e.g., an 800-Å-thick chromium layer). Like resists, masks can be positive or negative. A positive or a dark-field mask has clear patterns with dark background. A negative or a clear-field mask has dark patterns in a clear background. In present work we used positive masks for fabrication of all SU-8, negative photoresist, templates.

2.1.3 Polydimethylsiloxane (PDMS):

Among the multiple approaches for fabricating microfluidic devices, PDMS soft lithography has become standard for cell culture applications. By soft lithography micrometer resolution structures were molded from hard master into PDMS (Fig.). PDMS possesses many desirable qualities for use in microfluidic devices, including high flexibility, low chemical reactivity and the ability to reversibly bind to the other substrates. PDMS is a biocompatible (Belanger and Marois, 2001), transparent polymer (240nm-1100nm) with low auto-fluorescence (Piruska et al., 2005), permeable enough to gas to allow O₂ supplying for on chip mammalian cells culture (Leclerc et al., 2003). PDMS can be molded and cured in a template (original template made of SU-8 structures on a silicon wafer, or epoxy copy from original template made of epoxy 655) (Blau et al., 2011). Fabricated PDMS could be used for production of master copies without damaging the original template (Fig.). In addition to highly controlled cellular microenvironment, PDMS based microfluidics provides excellent live cell imaging because PDMS is transparent material with stable optical features (Mehling and Tay, 2014). The non-polar nature gives it a hydrophobic surface and makes it mostly impermeable to water. It consists of repeating -OSi(CH₃)₂- units; the CH₃ groups make its surface hydrophobic (Mata et al., 2005). This hydrophobicity results in poor wettability with aqueous solvents, which makes it susceptible for trapping of air bubbles.

Cured PDMS becomes impervious to chemical attack from anything other than organic solvents. Exposure to organic solvents results in temporary swelling of the PDMS substrate as the solvent diffuses into the material. The swelling subsides as the solvent evaporates and diffuses back out of the PDMS. PDMS can seal to itself and other at surfaces reversibly by

conformal contact (via van der Waals forces), or irreversibly if both surfaces are Si-based materials and have been oxidized by an air plasma before contact (a process that forms a covalent O-Si-O bond). Seals are watertight and can be formed under ambient conditions. The surface can be made hydrophilic by exposure to air plasma; the plasma oxidizes the surface to silanol (Si-OH). The plasma-oxidized surface remains hydrophilic if it stays in contact with water. In air, rearrangements occur within 30 min, which bring hydrophobic groups to the surface to lower the surface free energy. The surface of oxidized PDMS can be modified further by treatment with functionalized silanes (Mata et al., 2005).

Table 1 Physical and chemical properties of PDMS (McDonald and Whitesides, 2002)

Property	Characteristics	Consequence
Optical	Transparent; UV cutoff, 240 nm	Optical detection from 240 to 1100 nm
Electrical	Insulating; breakdown voltage, 2×10^7 V/m	Allows embedded circuits; intentional breakdown to open connections
Mechanical	Elastomeric; tunable Young's modulus, typical value of ~ 750 kPa	Conforms to surfaces; allows actuation by reversible deformation; facilitates release from molds
Thermal	Insulating; thermal conductivity, 0.2 W/(m - K); coefficient of thermal expansion, 310 $\mu\text{m}/(\text{m} - ^\circ\text{C})$; stable up to $\sim 300^\circ\text{C}$	Can be used to insulate heated solutions; does not allow dissipation of resistive heating from electrophoretic separation
Interfacial	Low surface free energy ~ 20 erg/cm ²	Replicas release easily from molds; can be reversibly sealed to materials; not wetted by water unless oxidized to SiOH presenting surface
Permeability	Low permeability to liquid water; permeable to gases and nonpolar organic solvents	Contains aqueous solutions in channels; allows gas transport through the bulk material; incompatible with many organic solvents
Reactivity	Inert; can be oxidized by exposure to a plasma	Unreactive toward most reagents; surface can be etched; can be modified to be hydrophilic and also reactive toward silanes
Toxicity	Nontoxic	Can be implanted in vivo; Supports mammalian cell growth

Adapted from J. C. McDonald and G. M. Whitesides, "Poly(dimethylsiloxane) as a material for fabricating microfluidic devices," *Acc. Chem. Res.*, 35, (2002), 491–499.)

2.1.4 Master molding; SU-8 photolithography

In photolithography light is applied through a photomask (Cr- mask) to pattern a substrate (SU-8). The most common form of the lithography is UV photolithography which mainly is used in IC industry. Other resist-patterning techniques include x-ray, electron, and ion-lithography as well as soft lithography, and etc.

Following steps are generally applied for SU-8 photolithography:

1. Photoresist deposition (spin coating)
2. Soft bake
3. Exposure (UV 365 through the Cr-mask)
4. Post-exposure treatment (including post bake)
5. Development (SU-8 developer)

Detailed information about SU-8 original master fabrication for each PDMS device has been presented in Table 2.

The general structure of the device including the reservoirs and microchannels has been designed in two layers, one including reservoirs and microchannels and the other without microchannels using a layout editor (Silvaco Expert, version 4.8.8). Figure 2 shows the first and second layers for direct microchannels used in laser dissection experiment. Each layer copied in an individual quartz glass as positive mask in which microchannels and reservoir areas were free and the rest of the glass had been coated by chromium layer to absorb the light (Figure 1 and Figure 2). Mask layer 1 was used for photo patterning of the first SU-8 layer and mask layer 2 for patterning the SU-8 layer 2 (Figure 1).

SU-8-25 and SU-8-50 (MicroChem) were used for fabrication of two layer template Figure 1. SU-8 25 was spin coated onto silicon substrates to provide the first layer with heights between 3.5 μm to 7 μm depending on the device (Table 2 and Figure 1). The second layer fabricated by SU-8 50 with 100 μm thickness on top of the first layer (Table 2 and Figure 1). At each step, the SU-8 layer was photo-patterned in a mask aligner (MJB4, SUSS Microtec) with chrome masks to form SU-8 stripes, and reservoirs. SU-8 layers thickness was controlled by the spinning speed (Ws-650Sz Spin Coater; Table 2). Thicknesses and widths of the final structures were determined by a stylus profiler (Wyko NT1100, Veeco)

and quantitative microscopy measurements (Leica, Leica Microsystems CMS GmbH) and Zeiss Axiovision 4.8 software.

To not destroy the SU-8 master, polymer copies were made from it. To provide copies from original master a reverse copy of original SU-8 master template was molded on a thick (> 5 mm thickness) PDMS. Mixed and degassed PDMS was poured into a cylindrical plastic frame placed on the surface of the SU-8 master to generate an approximately 7 mm high inverse copy of the master features. After 2 days of curing at room temperature, the thick PDMS slab was peeled from the master and used for the production of several epoxy master copies (Blau et al., 2011). After trying different epoxy materials with different physical properties an optimized epoxy material (Epoxy A cast 655; formerly Metalset® A-30; SMOOTH-ON) was selected for fabrication of copies from thick PDMS because it was dimensionally stable especially for fabrication of very thin structures with higher aspect ratio. Epoxy A cast 655 is a versatile aluminum filled castable epoxy that is very hard and strong. Different hardener speed options are available depending on requirements. To fabricate master copies in present study a two-component epoxide "resin" with polyamine "hardener" was mixed and rubbed into the microstructured PDMS cavities from different directions. A thick glass slide was pressed onto the thin epoxy layer as a flat carrier. After curing at room temperature for two days, the PDMS layer was detached carefully. The resulted copy was used for fabrication of thin PDMS microchannel devices which were used in all experiments. Before using the copies for fabrication of PDMS microchannel devices, epoxy master copies were placed in a desiccator for being exposed to trichloro (1H,1H,2H,2H-perfluorooctyl) silane (Sigma 448931) for 1 h under constant vacuum to deposit a thin anti-stick film on the molding master. Silane-substrate binding was stabilized in an oven at 120 °C for 1 h thereafter. Silane coating only for one time was enough in most cases to facilitate peeling of cured PDMS devices from template for several times.

2.1.5 PDMS device molding; softlithography

Soft lithography is based on self-assembly and replica molding using elastomeric stamps with the patterns of interest in bas-relief. It represents a non-photolithographic, easy and low cost strategy for fabrication of micro- and nanostructure. Patterns and structures fabricated by softlithography could have feature sizes ranging from 30 nm to 100 μm . Five soft lithography techniques have been demonstrated: replica molding (REM), microcontact printing (μCP), microtransfer molding (μTM), micromolding in capillaries (MIMIC), and solvent-assisted micromolding (SAMIM) (Whitesides et al., 2001). In present work we applied replica molding method for fabrication of PDMS microchannel devices from original master or from epoxy master copies.

PDMS (Dow Corning, Sylgard 184) pre-polymer and curing agent was mixed (10:1), degassed and poured on an epoxy copy of the SU-8 master. In case of the devices with open reservoirs, it was leveled to the highest topographies by squeezing the PDMS out with the help of a laser copier transparency, a foam cushion and a screw clamp. To fabricate devices with closed chambers as reservoir, laser copier transparency left on top of the PDMS to push extra PDMS with a light and homogenous pressure while a very thin layer of PDMS left on top of the highest structures, reservoirs, to close them from the top. PDMS was cured at room temperature for 48 hours before peeling it from the epoxy copy. In most cases, PDMS sticks tightly to the epoxy surface and it is difficult to peel it off without rapturing the thin PDMS layer. Ethanol (75%) helped in separating PDMS from its epoxy master. Silanizing the epoxy surface dramatically improves PDMS detachment. In case of PDMS devices with closed chamber, after peeling the thin PDMS device from SU-8 wafer, big seeding reservoirs were punched on the two far edges of each small reservoir (Figure 1 and Figure 2).

2.1.6 Fabricated devices properties:

In general we designed three different categories of devices:

- I. Multicompartment microfluidic device for producing multiple axonal compartments and recording from mixture of direct and indirect growing axons in crossing microchannels.
- II. Two compartment microchannel devices with direct microchannels, microchannels with working stations (MCh_ws), as well as long microchannels for recording action

potential propagation, laser microdissection and long-term monitoring axonal electrophysiology.

III. Multi modular devices for providing small world quasi-3D neuronal networks on top of the electrodes. These devices were used for studying the electrophysiology of patterned quasi-3D networks and compare them with random large-scale networks.

Regardless of the designs variability, fabrication procedure for all devices was similar with small differences. Below are the design schemes and details for each class of devices:

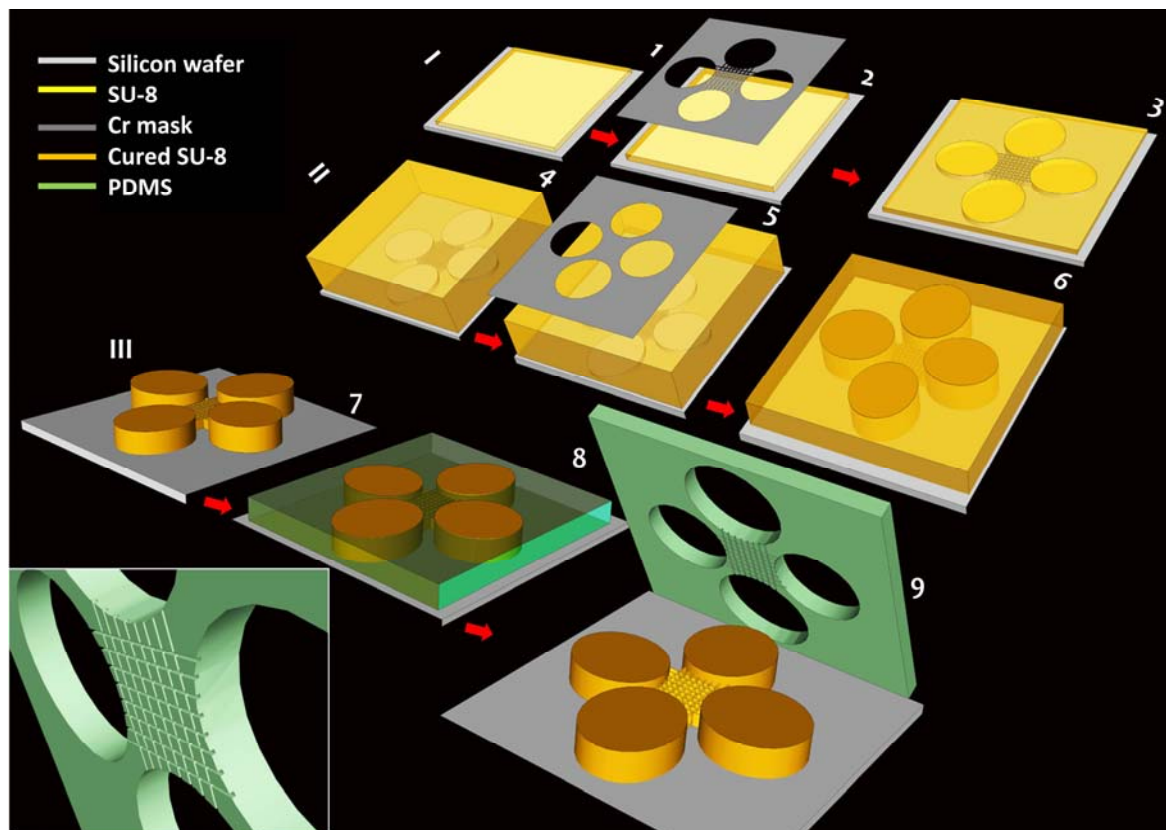


Figure 1 Master molding and PDMS device fabrication procedure for devices with through-holes

Master molding: I (layer 1, a: SU-8 25 spin coated on silicon wafer in $< 70 \mu\text{m}$ thickness, b: SU-8 exposed to UV through first layer mask, c: SU-8 cured areas including first layer of master), II (layer 2, d: SU-8 50 spin coated on top of first layer in $100 \mu\text{m}$ thickness, e: SU-8 50 exposed to UV through the second layer mask, f: Cured SU-8 in places of through holes). PDMS molding: III (g: developed 2 layer master, h: PDMS was cured on the surface of master or its epoxy copy, i: peeling of cured PDMS from the template).

Table 2 Master molding detailed procedure for each device

	Multi-compartment		Two-compartment	
	MCh_crossing	MCh_direct	MCh-direct	MCh-ws
Photoresin	SU-8 5	SU-8 5	SU-8 5	SU-8 5
Viscosity (cst)				
Spin	5 s (100 rpm/s) 500 rpm 10 s (300 rpm/s) 3000 rpm 30 s in 3000 rpm	5 s (100 rpm/s) 500 rpm 10 s (300 rpm/s) 3000 rpm 30 s in 3000 rpm	5 s (100 rpm/s) 500 rpm 10 s (400 rpm/s) 4000 rpm 60 s in 4000 rpm	
Pre-bake				
65 °C	1 min	1 min	1 min	
95 °C	3 min	3 min	3 min	
Expose				
Time	17 s	40 s	35 s	
Gap	30 µm	30 µm	15 µm	
Post-bake				
65 °C	1 min	1 min	1 min	
95 °C	1 min	1 min	1 min	
Photoresin	SU-8 50	SU-8 50	SU-8 50	SU-8 50
Viscosity (cst)				
Spin	5 s (100 rpm/s) 500 rpm Kept in 500 rpm for 5 s 5 s (300 rpm/s) 1500 rpm kept at 1500 rpm for 30 s	5 s (100 rpm/s) 500 rpm Kept in 500 rpm for 10 s 4 s (300 rpm/s) 1500 rpm kept at 1500 rpm for 30 s	5 s (100 rpm/s) 500 rpm Kept in 500 rpm for 10 s 6 s (150 rpm/s) 1500 rpm kept at 1500 rpm for 40 s	
Pre-bake				
65 °C	10 min	10 min	10 min	
95 °C	30 min	30 min	30 min	
Expose				
Time	17 s	70 s	60 s	
Gap	40 µm	30 µm	30 µm	
Post-bake				
65 °C	1 min	1 min	1 min	
95 °C	10 min	10 min	7 min	
Development				
Developer	10 min	10 min	8 min	
IPA	2 min	2 min	2 min	
Features				
MCh-strips	5 µm – 10 µm	5 µm – 7 µm	3.5 µm – 5 µm	
Reservoir	100 µm	100 µm	70-100 µm	

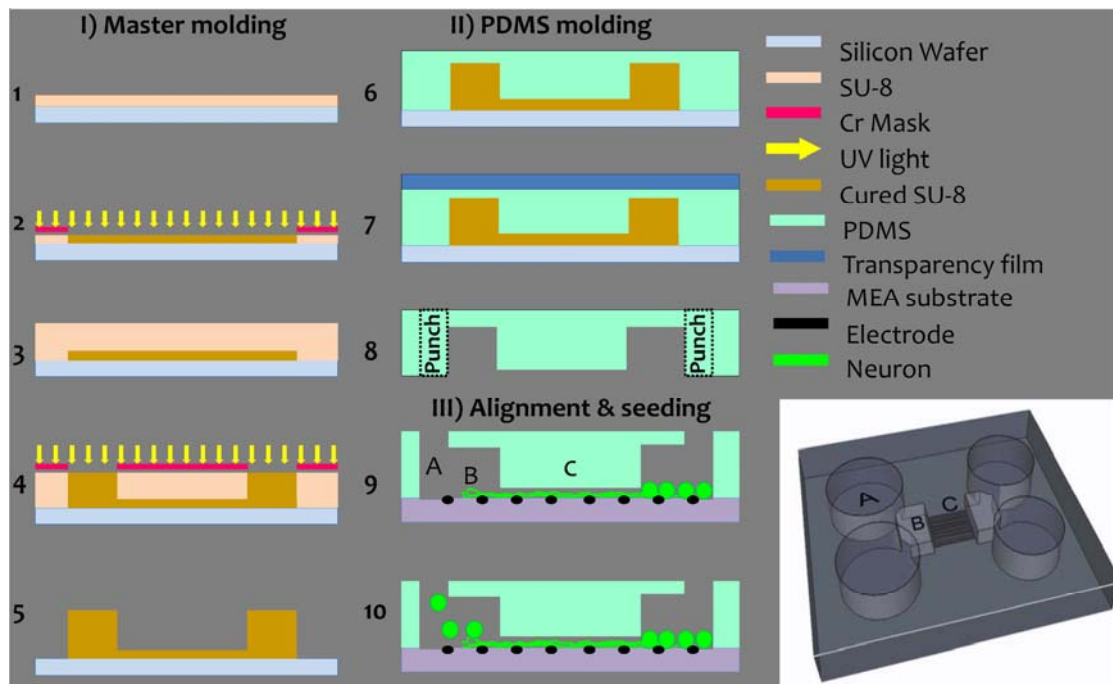
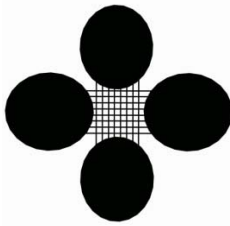
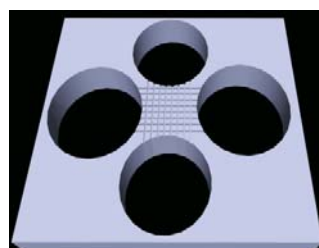
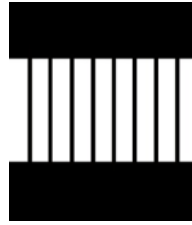
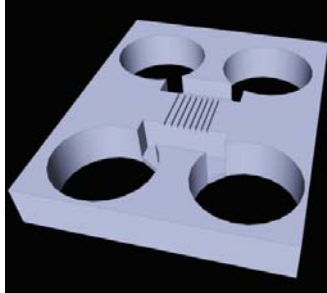
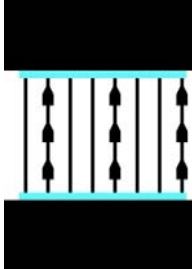
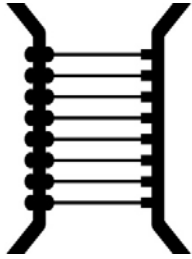
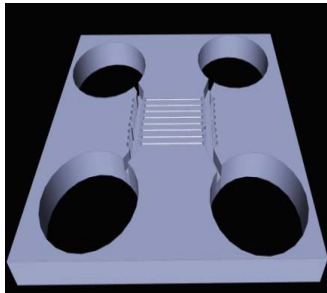


Figure 2 Master molding and PDMS device fabrication, alignment and cell seeding in devices with closed chambers.

- I) Master molding in 5 steps (1: spin coating the SU-8 25 on silicon wafer in $< 5 \mu\text{m}$ thickness, 2: exposing to UV and curing the first layer, 3: spin coating SU-8 50 on top of the first layer in $< 100 \mu\text{m}$ thickness, 4: exposing and curing the second layer, 5: developing the 2 layer SU-8 structures). Master molding steps was same for devices with through-holes or closed chambers.
- II) PDMS molding in 3 steps (6: purring PDMS on the surface of original template or epoxy copy, 7: leveling the PDMS with transparency foil and leaving very thin layer of PDMS on top of the highest structures and curing it, 8: pealing the PDMS from template and punching the round opening from two far edges of each closed chamber).
- III) Alignment and cell seeding (9: closed chamber aligned on top of 2 electrode rows and 4 electrodes left for each microchannel, cells were added from the openings into the closed chamber in one side, 10: after 14 DIVs and axonal release into the counterpart reservoir, freshly prepared neurons were added into the closed chamber). A: shows the punched big opening, pools, B: shows the closed chamber, and C: shows microchannels.

Table 3 Devices' dimensions and outlines

Class	Features	Dimensions (h×w×l) μm	2D outline	3D view
I	Res Oval n = 4	170×1600×1800		
	MCh Crossing 8 × 8	7 × 40×1400 7×40×2000		
II	Res Rectangular n = 2	100×400×1600		
	MCh Direct n = 8	5×30×800		
	Pool Round n = 4	r = 1 mm h = 200 μm		
II	Res Rectangular n = 2	100×400×1600 fi (5×100×1500)		
	MCh ws n = 8	ch (5×30×800) ws (5×50×100)		
	Pool Round n = 4	r = 1 mm h = 200 μm		
II	Res Wavy n = 2	100×150×2000 di (r = 70) di (100×40×70)		
	MCh Direct n = 8	30×1100		
	Pool Round n = 4	r = 1 mm h = 200 μm		

Res: reservoir, MCh: microchannel, ws: working station, fi: filtering cavity, di: diode. Filtering cavity has been mentioned by blue highlighted area. Diodes are round or square areas.

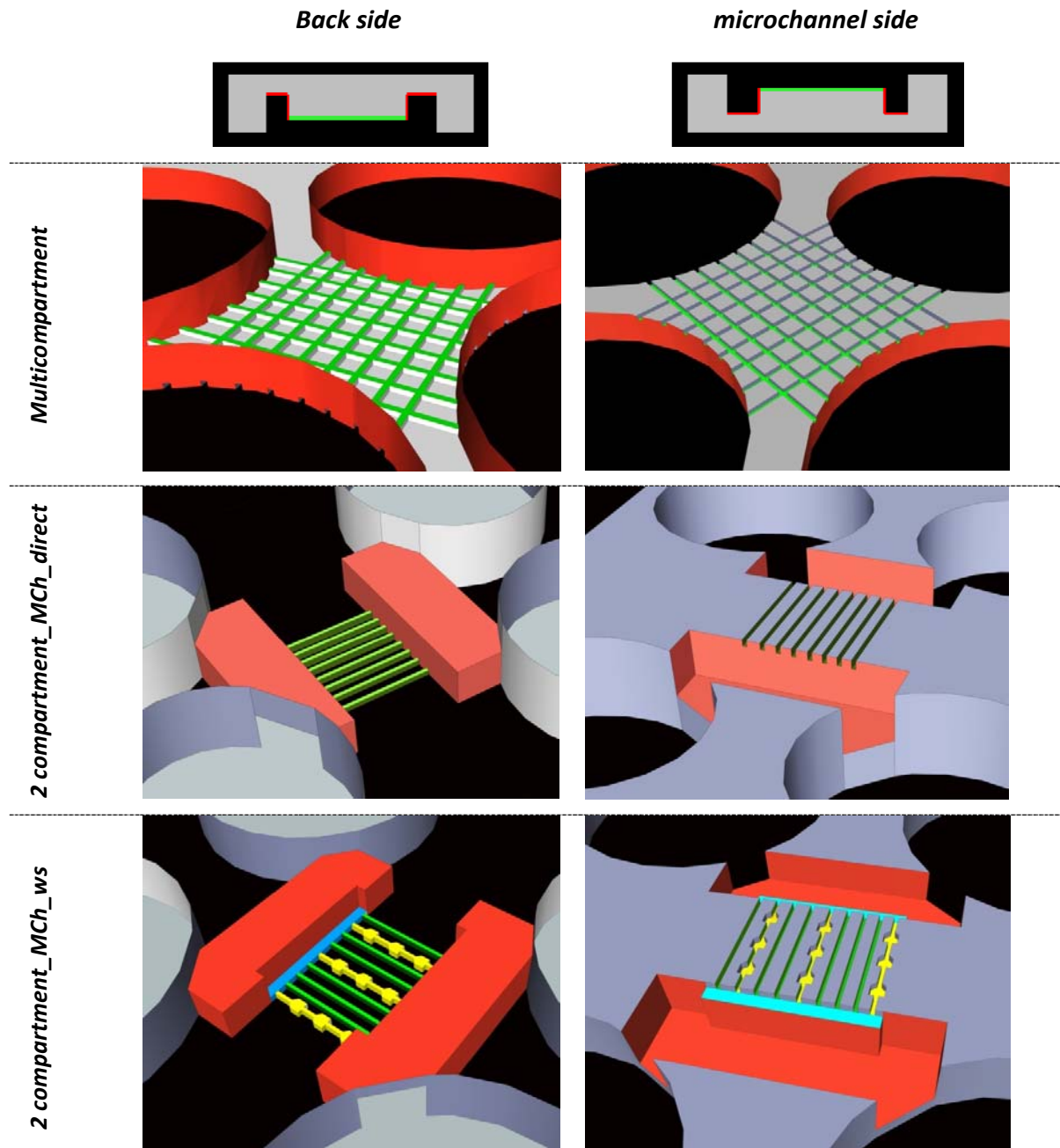
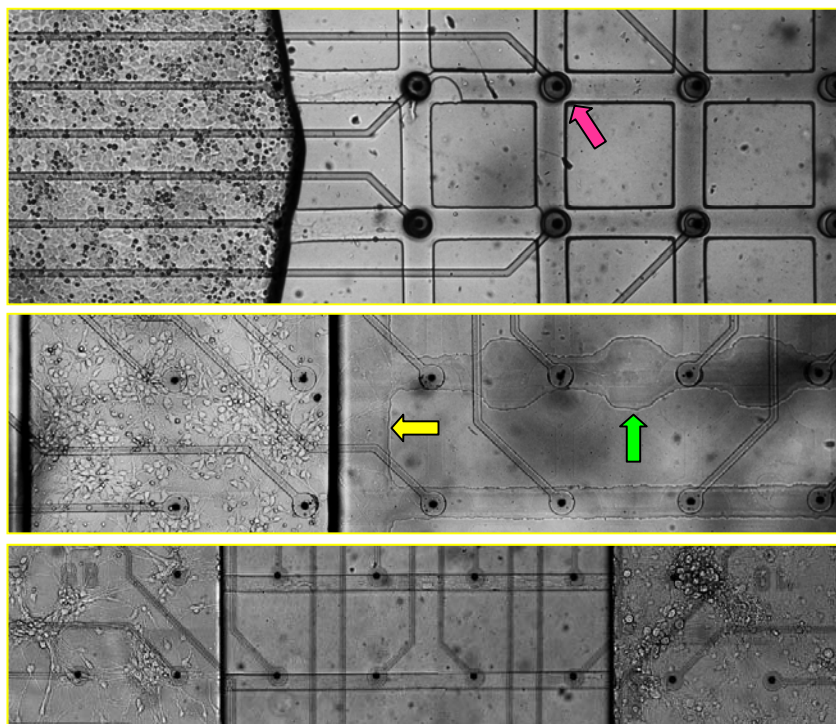


Figure 3 PDMS microdevices from backside and downside.

Left and right pictures in each row show the backside and downside of each device, respectively. Red color represents the reservoir area, where cells were seeded. Green shows microchannels. Yellow shows microchannels with working stations (ws). Blue shows neurite filtering cavity. In multicompartment device through-holes have been fabricated during the PDMS molding by pressing the transparency film. In two-compartment device closed chambers (reservoirs) were fabricated during PDMS molding and through holes, pools, punched later. MCh: microchannel, ws: working station. Dimensions are not real.

2.1.7 Alignment of PDMS devices with MEA electrodes

PDMS microchannel tiles were first post-baked at 100 °C for 24 hours to crosslink any uncured oligomers, then autoclaved at 120 °C for 20 minutes before being moved to a sterile hood. Each device was aligned on a MEA (60 electrodes, 30/200 ir or 10/200 ir; Figure 2 and Figure 4). In multicompartment device (device I) each microchannels aligned on to fit 8 electrodes of each row, while there was no electrode recording from reservoir section (Figure 4). Electrodes were aligned corresponding to the crossing points in each microchannel (Figure 4). To align two-compartment devices with MEA electrodes we fit four electrodes in each microchannel and 14 electrodes in each closed chamber (Figure 2 and Figure 4). In the case of microchannels with working stations (MCh-ws) we tried to align the working stations (wider areas) between the electrodes where it was possible to cut axons without damaging the electrodes or connecting tracks (Fig. 6). Because PDMS sticks to the dry MEA surface, we used an ultrapure water (MilliQ, MQ) or ethanol (96%) droplet to facilitate the manual alignment procedure under the light microscope (5 X magnifications).



Multicompartment PDMS device aligned on MEA electrodes. Electrodes are in the crossing points of the microchannels. Dense neuronal networks inside the reservoir. Red: an electrode in the crossing point.

Aligned two-compartment device (MCh_ws and MCh-direct). In MCh_ws wider areas aligned between each pair of the electrodes. Yellow: neurite filtering cavity. Green: working station (ws)

Aligned two-compartment device (MCh-direct). With seeded cells in both reservoirs.

Figure 4 Aligned PDMS microchannels with MEA.

2.1.8 Air bubble removal, coating and wetting the PDMS devices

Because the microchannels are hydrophobic and trap air bubbles it is necessary to remove air bubbles before seeding the cells into the device. In present study we applied two different protocols for removing the air bubbles from microchannels.

In the multicompartiment device reservoirs were open from top therefore the assembly of MEA and aligned device was hydrophilized by oxygen plasma (2 - 3 min, 60 W, 2.45 GHz, 0.4 mbar O₂) [femto, Diener]. Cell adhesive material, mixture of 0.1 mg/ml poly-D-lysine (PDL) and 0.05 mg/ml laminin in MQ water, was added through one open pool and rapidly covered the MEA surface in reservoirs and microchannels and reached the counterpart reservoirs through the microchannels by capillary action. This method allowed the coating material to cover only the areas of the interest, which included reservoirs and microchannels. The coating was dried in a vacuum chamber for one minute before immersing the whole device in MQ water three times for 10 min each. To remove entrapped air bubbles, the merged device was vacuumed for a few seconds to remove air bubbles and then MQ water replaced by cell culture medium before adding the cells into the reservoir.

In the two-compartment devices with closed chambers, reservoirs, and < 5 µm height microchannels it was almost impossible to remove air bubbles just by hydrophilizing the surface. Therefore, after applying the plasma (2 - 3 min, 60 W, 2.45 GHz, 0.4 mbar O₂) [femto, Diener] we coated the surface by adding mixture of 0.1 mg/ml poly-D-lysine (PDL) and 0.05 mg/ml laminin in MQ water through one opening pool, washed for three times with MQ water and then vacuumed. Later we added sterile MQ water or PBS 1% and vacuumed the whole device for less than 30 seconds in plasma chamber [femto, Diener], which replaced all trapped air bubbles inside the microchannels or neurite filtering cavities with rinsed solution. Because this procedure was done after coating and outside the hood there was possibility of device contamination. The whole device assembly left under the hood and UV exposure for 1 to 2 hours to remove any contamination. Then MQ or PBS 1% drained from the MEA ring and device and replaced by already prepared cell culture medium (Neurobasal, B27 2%, Glutamax 1%, penicillin/streptomycin 1%) and incubated for 12 to 24 hours in incubator (5% CO₂, 37 °C, 95% RH). Long-term incubation before cell seeding increased device wettability and cell seeding procedure.

2.1.9 Preparing the primary cortical or hippocampal neurons

Rats were anesthetized and killed and then embryos (E 18) were removed and decapitated. Brain was removed from the skulls and rinsed in cold HBSS. Then hemispheres were divided, meninges were removed and hippocampus and/or cortex dissected out. Four cortex were placed in 5 ml of trypsin 0,125% + DNase and incubate in water bath at 37° for 30 minutes. Seven to ten hippocampi were placed in 5 ml of trypsin-EDTA and incubate in water bath at 37° for 30 minutes. After incubation 1 to 5 ml of complete Neurobasal + 10% FBS were added to trypsin solution and centrifuged for 5 min at 1200 rpm. Supernatant was discarded and fresh Neurobasal + 10% FBS was added to the rest of the solution. Then hippocampi or cortex dissociated gently by pipetting for not < 10 times with P1000 pipette. The resulted solution was filtered with a cell strainer (from BD, 40um pore size) and centrifuged 7 min at 700 rpm. Supernatant was discarded and cells were resuspended in complete Neurobasal or complete Neurobasal + 10% FBS and counted. The desired cell concentration acquired either by adding Neurobasal to decrease the concentration or centrifugation the cell suspension and discarding the part of solution for increasing the cell concentration.

2.1.10 Seeding primary neurons in PDMS microfluidic device

If not stated differently, all cell culture chemicals were purchased from Invitrogen. For multicompartiment device on commercial MEAs, a small drop (~ 5 µl; 10,600 cortical neurons/µl, ~ 50,000 cells per device) was placed into just one out of four reservoirs and Cells were allowed to settle for 30 min in a cell culture incubator before adding 1 ml of serum-free medium (Neurobasal medium, B27 2%, Glutamax 1%, penicillin/streptomycin 1%). Cultures were protected by a PDMS cap against evaporation and contamination (Blau et al., 2009) and stored in the incubator. Every week, 450 µL of media was exchanged with fresh warm media. Cultures were imaged once a week on an inverted microscope (Leica Microsystems, Germany, 20X) with a 5 Mpixel camera (Leica, DFC420C, Germany).

In two-compartment devices it was not possible to add cells directly into the reservoirs and we had to add cells through the opening pools which had already been punched in two far edges of the reservoir. The device wettability was necessary for adding the cells otherwise

cell suspension will not enter into the closed chamber from very tiny entrance. Incubation for 12 to 24 hours facilitates the cell seeding procedure. Just before adding the cells, the old cell culture medium was drained from the MEA glass ring, but not from the microchannels. Rat cortical or hippocampal neurons (6000 cells/ μ l to 12000 cells/ μ l) were added through one of the big pools which automatically let them enter into the 5 small cell culture chambers and settle there. The small reservoirs produced almost closed chambers for small network formation on top of the electrodes. Cells were distributed homogenously in the small reservoirs with a maximum number of 2240 cells per module (reservoir; Figure 4). After incubation for five minutes, 1.5 ml pre-warmed cell culture medium (Neurobasal, B27 2%, Glutamax 1%, penicillin/streptomycin 1%) was added into each MEA and all cultures were returned to the incubator (5% CO₂, 37 °C, 95% RH). Cells were kept inside the incubator over the entire study period except for recording, microscopy and dissection. To establish a secondary network for bi-directional axon growth inside the microchannels, we added freshly prepared neurons (5000 cells/ μ l) into the second cell culture compartment two weeks later in the same way as before after draining the medium in the counterpart reservoir (Figure 2).

In two compartment PDMS devices with direct microchannels we cultured cortical neurons in two layers and in two compartment devices with working stations (ws) neurons were seeded cortical or hippocampal neurons in one compartment and left another compartment as pure axonal compartment. This was done to simplify the analysis of the signals inside the microchannels because in the case of two-layer networks axons growing in both directions which make the signal analysis inside the microchannels difficult.

2.1.11 MEA electrophysiology

The classical MEA-System consists of a data acquisition computer, MEA amplifiers, MEAs, and a temperature controller. The core element is the MEA amplifier with 60 channels (Figure 5). It is possible to build a setup with one, two or four amplifiers, resulting in a system with 60, 120 or 240 channels respectively. Data acquisition computer and analysis program MC_Rack is used for visualization and recording the electrical activity. MEA chips are provided in different configurations with variations in electrodes numbers, orientation and spacing, presence or absence of an internal ground electrode, presence or absence of a glass ring, and the size of the glass ring. The electrodes are embedded in a carrier material, usually glass. Standard tracks made of titanium (Ti) or indium tin oxide (ITO) are electrically isolated with silicon nitride (SiN). Standard contact pads are made of titanium nitride (TiN) or indium tin oxide (ITO). ITO contact pads and tracks are transparent, for a perfect view of the specimen under the microscope. In present study we mainly used the standard micro-electrode array containing 60 electrodes in an 8 by 8 grid arrangement with 10 μm or 30 μm diameter titanium nitride electrodes (TiN) and 200 μm distances between electrode centers (60MEA200/30iR-ITO). One of the electrodes is larger and functions as the ground or internal reference electrode (Figure 5).

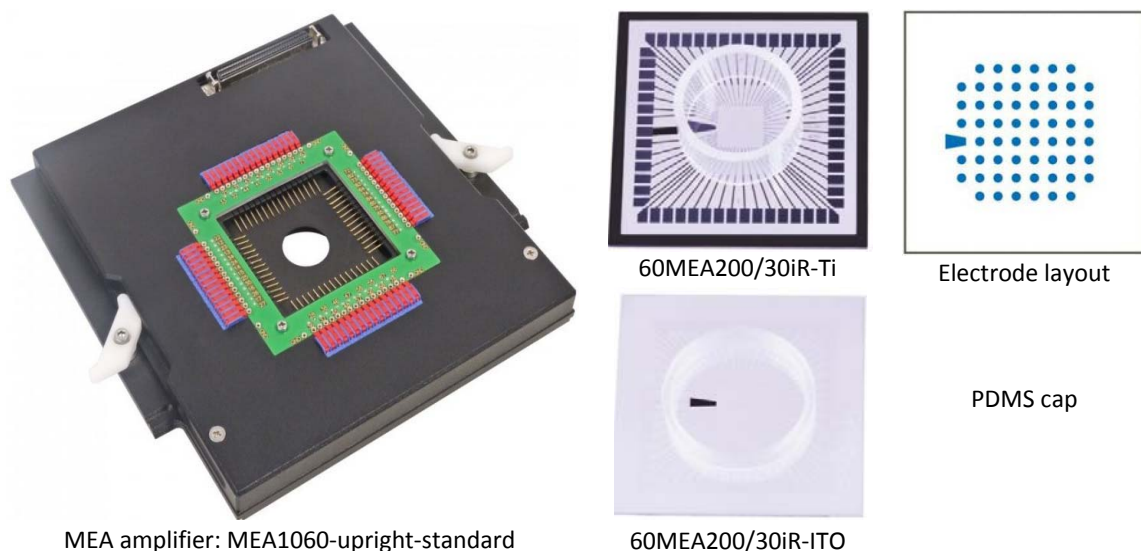


Figure 5 MEA amplifier, chips, electrode layout and PDMS cap

Network activity was recorded using a commercially available 60-channels MEA filter-amplifier system (0.1 Hz - 25 kHz, 1200 x amplification, MEA1060-upright-standard,) with an A/D conversion card (64-channels, 25 kHz sampling frequency/channel, PCI-bus) and software interface (MC_Rack) (all from Multi Channel Systems).

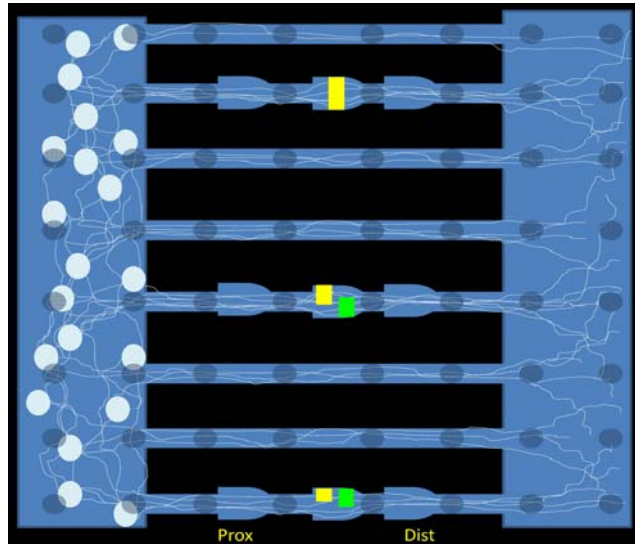
In the cultures seeded in multicompartiment device recording was done randomly in different DIVs (DIV 10 to DIV 70) lasting 10 to 15 min each. In the two-compartment devices recording was done daily (10 DIV to 45 DIV). On dissection days, activity was recorded three times from each culture starting with the baseline activity, followed by the activity just after the dissection and the activity three to five hours after dissection. During recordings, the temperature was kept at 37 °C using a built-in thermal sensor and heating element controlled by an external temperature controller (HC-1, MCS). Raw signals were digitally filtered by a second-order Bessel high-pass filter (cut-off at 200 Hz) and analyzed offline. Spikes were detected in the filtered data stream by passing a negative threshold set to -4.5 StDev of the peak-to-peak noise. Spike trains were transformed to time stamps (NeuroExplorer, Nex Technologies) before extracting the mean spike frequency on each electrode.

2.1.12 Laser microdissection

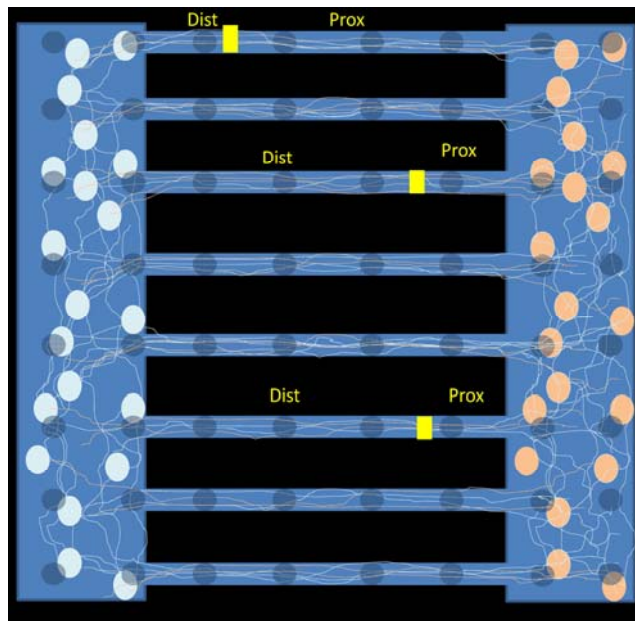
Laser microdissection was applied in the cultures in two-compartment PDMS devices. A pico-second pulsed laser (Teem Photonics, PNV-M0150, 355 nm; ~ 2V), installed on an inverted Nikon Eclipse Ti microscope, was applied for dissection using a motorized stage and simultaneous bright field time-lapse imaging (iXON 897, Andor Technology). All dissection and imaging experiments were performed at RT within 10 min using a 20x objective (CFI Plan Apo VC 20x Air 0.75NA, Nikon). In the unidirectional cultures inside the devices with MCh_ws, dissection was performed only in the central working stations (ws) of microchannels with working stations (MCh-ws) (Figure 6). Three different dissection levels in three different microchannels of each culture were applied at 17 DIV. In the first microchannel, all axons were completely dissected by passing twice across the working station (Figure 6). In the second microchannel, only half of the axons were dissected by partially passing with the laser up to the center of the working station and leaving the rest of the axons intact (Figure 6). In the third microchannel, a very local point injury was induced

in one corner of the working station (Figure 6). One week later at 24 DIV, the dissection was completed for the previously partially dissected axons in the second microchannel by completely passing across the working station (Figure 6). On the same day, a partial dissection was performed in the third working station with the local dissection. Microchannels were selected randomly in each culture to provide complete, partial-partial or spot-partial dissections. Network morphology and activity were monitored and recorded at different instances before and after laser microdissection (Figure 27). Control cultures were kept for 10 minutes on the same microscopy stage on the same DIVs and times to record their activity and image their morphology.

In an extra group including cortical neurons in the two-compartment PDMS microdevice with direct microchannels (MCh_direct), dissection was done in DIV 25. These cultures composed of two-layer cortical neuronal networks with direct microchannels composed of bi-directional or uni-directional growing axons originated from one of the reservoirs. Complete dissection in these cultures was done in one side of the microchannel in vicinity of dominant or counterpart reservoir (Figure 6 and Figure 21). In these cultures we applied different numbers of dissection in different cultures. In general axonal bundles in one to three microchannels experienced complete dissection in each culture (Figure 6 and Figure 20).



Two compartment device with one-layer cortical or hippocampal neurons and growing axons in direct microchannels (MCh-direct) or microchannels with working stations (MCh_ws). Dissection performed only in MCh_ws in the middle ws in each microchannel. Yellow shows the first dissection in DIV 17 which was complete, half or very local. Green shows the second dissection in DIV 24 which completed dissection or provide half dissection. Gray circles show the layout of corresponding electrodes recording from somata in reservoir, ctrl axons in direct microchannel, as well as proximal and distal parts of dissected axons.



Two compartment device with two-layer cortical neurons and growing axons in direct microchannels (MCh-direct). White circles show the first layer and orange circles show the second layer seeded two weeks after first layer. This picture shows a two-layer network with dominant second layer because in accordance to cross-correlograms most propagated signals was from layer 2 to layer 1. Most microchannels showed bi-directional axonal growth originated from one of the reservoirs.

Yellow shows the complete dissection in each microchannel. Dissection performed in one to three microchannels in vicinity of dominant reservoir or counterpart reservoir. In all cases electrodes close to the dominant reservoir consider as proximal electrodes and electrodes after the dissection point considered as distal electrode.

Figure 6 Axonal laser microdissection in one layer or two layer networks

2.1.13 Immunofluorescence staining and imaging

Selected cultures were fixed with 4% paraformaldehyde and 4% sucrose solution after draining the cell culture medium and washing with warmed 1% PBS. Cell membranes were permeabilized with 0.2% Triton X-100 in PBS for 10 min and incubated with blocking buffer (2% goat serum and 3% bovine serum albumin (BSA) in PBS) for 30-45 minutes. Cultures were incubated with primary antibodies 3 hours at room temperature, then with secondary antibodies for 1 h at room temperature. The primary antibodies were anti-rabbit β -tubulin III IgG (a neuronal marker; Sigma-Aldrich), anti-mouse glial fibrillary acidic protein (GFAP) IgG (a glial marker; Sigma-Aldrich). The secondary antibodies were Alexa Fluor 488 (goat anti-mouse) and 633 (goat anti-rabbit) (both from Molecular Probes). Finally mounting solution including DAPI, to stain nuclei, added to each culture on MEA and cover by coverslip. Fluorescence was observed using either an upright fluorescence microscope (Olympus BX51, Tokyo, Japan) or an inverted confocal microscope (Leica TCS SP5).

2.1.14 Statistical analysis

To analyze the data obtained from multicompartiment devices spike trains from were transformed to timestamps (NeuroExplorer, Nex Technologies) for mean frequency and burst analysis. Individual units on each electrode were detected by k-means clustering (Offline Sorter, Plexon). Thereafter, sorted units were checked manually to merge the same units or exclude unsorted rare signals from analysis. Numerical results were further analyzed by a one-way repeated measures analysis of variance (ANOVA) or a two-way ANOVA, followed by a Bonferroni post-test for all groups (GraphPad Prism). A probability of $p < 0.05$ was considered significant. Data are expressed as mean \pm SEM or as quartiles (Whisker-bars) with maximum and minimum values.

In the case of two compartment device and dissection experiments extracted spike frequencies and time stamps were transferred into Microsoft Excel spreadsheets. The information for each electrode in each culture was categorized according to its position with respect to the aligned microchannel device and dissection point. The analysis was performed on different levels to distinguish the activity recorded from the somata in the reservoirs, from control axons in intact microchannels, from completely, partially or locally dissected axons, as well as from proximal and distal parts of dissected axons. The mean spike frequency

(spikes/s) was calculated separately for each section by combining the data gathered from all electrodes in that section from all cultures of the same group. Usually, the activity recorded from different electrodes varies in same culture, between cultures of the same group as well as for different DIVs in same culture. To account for these activity fluctuations, we normalized the activity on each electrode in each culture to the maximum activity in that culture for each DIV. Both raw and normalized data were then subjected to the same statistical analysis. Because the variables were evaluated for different groups over time, we performed a mixed analysis of variance (mixed ANOVA) to allow for ‘between group’ or ‘in group’ comparisons over the entire experiment. The resulting data was compared to baseline values by repeated measure ANOVA based on estimated marginal means and multiple comparison adjustments by Bonferroni (). The mixed ANOVA was followed by a post hoc Tukey range test to identify ‘between groups’ differences at specific time points. Data are expressed as mean \pm standard error of the mean (SEM). $p < .05$ was considered to be significant.

R

esults

3.1 Multicompartment device for multiple axonal compartments

To understand the least-required micro-well and channel geometries for plating and growing neurons inside the PDMS microstructures, we designed channels with different dimensions (10-40 μm widths and 70 – 7 μm height). In very high microchannels the overall channel cross section was large and some cells migrated into and within the channels and produced very low-density networks with growing axons or dendrites. Therefore in the fabrication procedure for the Su-8 template we tried to decrease the thickness of the first layer from 70 μm to 7 μm and prevent from cell body penetration into the microchannels.

Another challenge in the first set of the experiments was the neuronal networks growth beneath the device outside the microchannels (Figure 7 A). This happened for two reasons: first because coating was done before device alignment, and it covered whole central parts of the MEA, which let axons or cells found their way through very tiny clefts between device and MEA substrate to grow outside of the physical confinements. Second, and related to alignment of the device after coating, it was not possible to provide stronger bond between PDMS microdevice and MEA substrate, because plasma after coating would remove the adhesive materials. To prevent from network formation underneath the device and provide strong bond between device and MEA substrate, device was aligned on MEA substrate before coating. This method also gave opportunity to utilize physical confinements for chemical patterning of the surface. After alignment MEA and device assembly was vacuumed and then plasmalized which hydrophilized the MEA surface only in the place of reservoirs and microchannels. Thereafter, adding the coating materials let it to cover reservoirs and microchannels and left areas outside of the microchannel and reservoir uncoated (Figure 7). This method was successful in providing the networks inside the PDMS microdevice barriers on top of MEA electrodes (Figure 8).

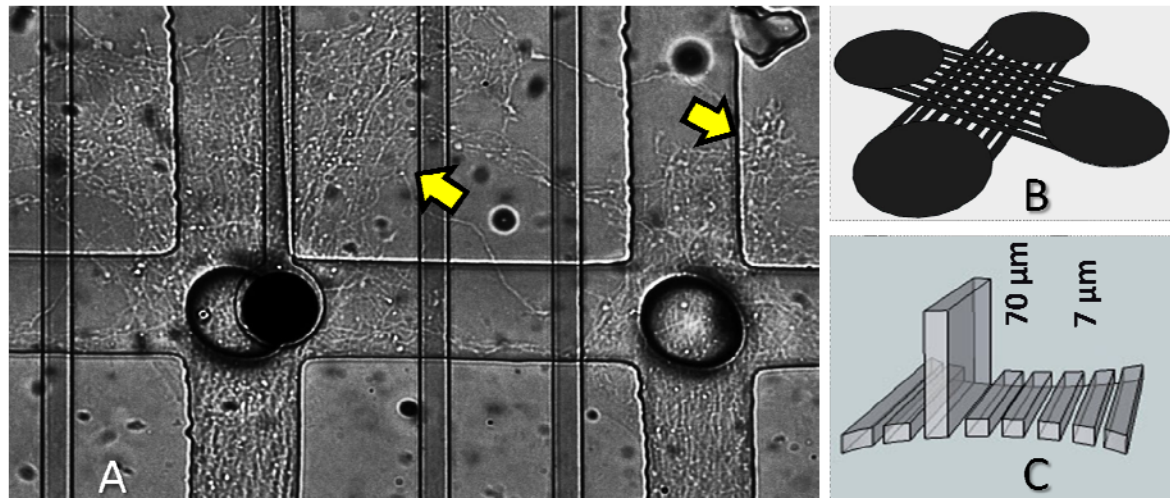


Figure 7 Optimizing the confinement and coating related issues.

A) Growing networks in and outside of microchannel tiles. B) A schematic view of coated surface when PDL was added after PDMS device alignment on MEA substrate. C) Microchannel height decreased from 70 μm to 7 μm to prevent from cell body penetration into the microchannels.

3.1.1 Network morphology in multicompartment device

A small drop of cortical cell suspension ($\sim 5 \mu\text{l}$; 10,600 cortical neurons/ μl , $\sim 50,000$ cells per device) was placed into just one out of four reservoirs. The device was enough transparent to see and prepare microscopy images from growing neurites inside the microchannels (Figure 8). Cells started to grow their neurites into the microchannels after 3 DIV. After 9 DIV, axons had almost passed through the entire channel and entered into one of the three axonal compartments (Figure 8 F). Axons were either growing in direct paths or changing the growing direction in the crossing points (Figure 8 C and E). Regarding the whole length of the microchannel and counterpart reservoirs, axons could grow at least 3 mm in this device. The neuronal tissue mass inside the channels was increasing up to 27 DIV. Afterward, neural tissue was almost constant for one week (40 DIV) when axons inside the channels and the axonal compartments started to degenerate and thick axonal bundles appeared (Figure 12 A). In accordance to the morphology degeneration mainly started from the distal parts and then extended into the proximal sections. This was concomitant with activity drop especially in electrodes which were recording from more distal parts of the axons.

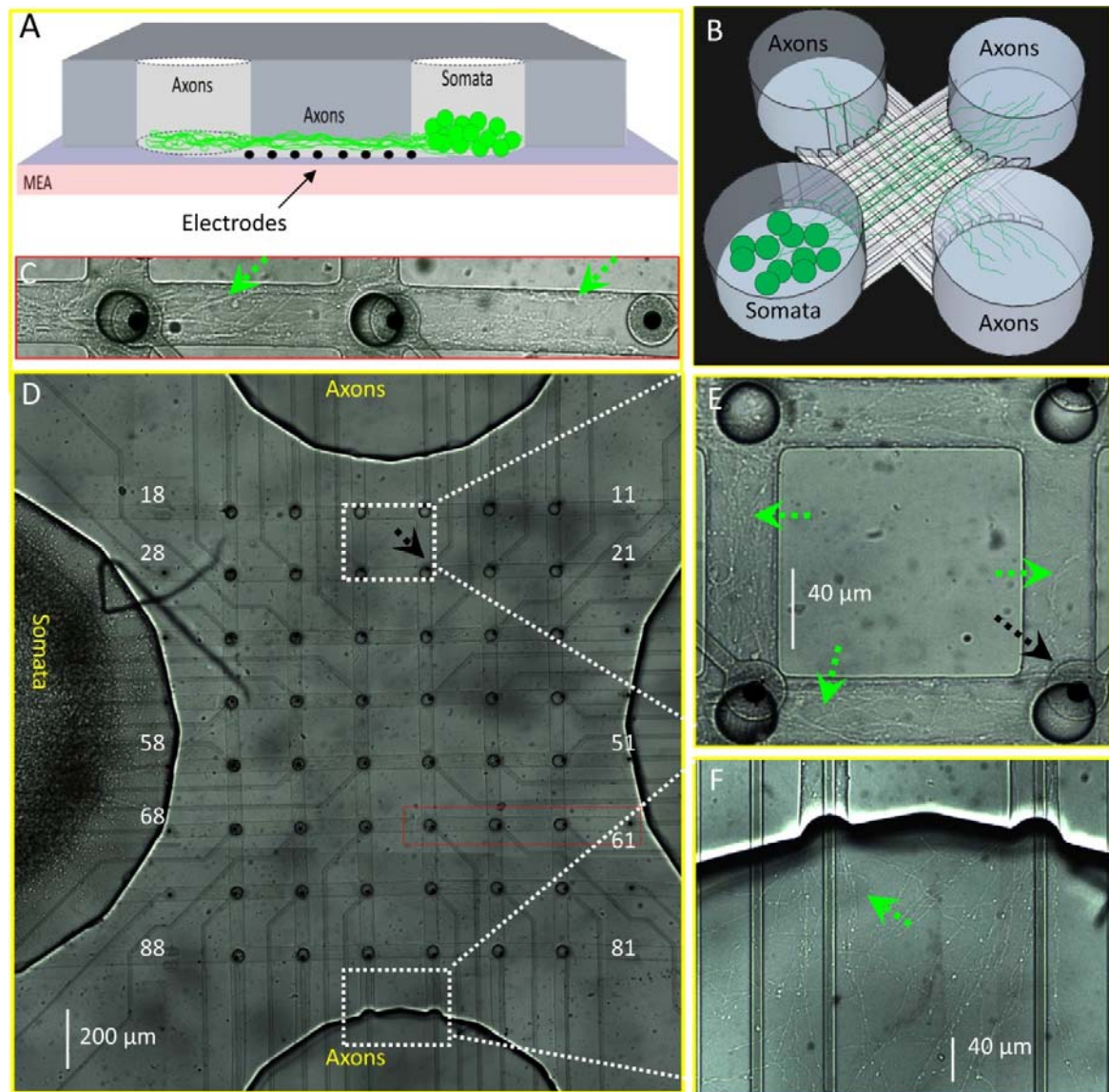


Figure 8 PDMS microchannel tiles on MEAs for neural network compartmentalization

A) A schematic cross-section of a microchannel and the reservoirs shows how microchannels selectively let axons grow on top of an electrode row while preventing cell bodies to enter. B) PDMS microstructure including four big reservoirs interconnected by an 8×8 matrix of channels. C) Growing axons inside a selected microchannel which is passing from 3 subsequent electrodes (marked by red frame in D). In the forehead there are few branches of the axons which will be filled completely by newly growing axons. D) Cells seeded in a somal compartment (left) had grown their axons after 9 DIV through the entire length of a microchannel into the empty axonal compartments. E) Magnified view of the axons inside the channels between electrodes 15-14 and 25-24. E) Magnified view of axons entering the axonal compartment. Black arrows indicate at an electrode and green arrows point at axons.

3.1.2 Recording activity from microchannel confined axons

Because the microchannels were aligned with the electrodes, axons were forced to grow over the electrodes. The small microchannel cross sections ($40\ \mu\text{m} \times 5\ \mu\text{m}$) increased the electrical resistance to ground, thereby amplifying the weak extracellular axonal signals. At 9 DIV, first signals could be recorded. They were similar in shape to random networks, but had higher amplitudes ($>100\ \mu\text{V}$; Fig.). The signal amplitudes increased up to $600\ \mu\text{V}$ after 20 DIV (Figure 10 B). The microchannels not only allowed to record from axons, but also forced the same axon to pass over or nearby all electrodes in one row of the electrode array (Figure 9; electrodes 28 to 21). This made it possible to record from the same axon at its different lengths. Therefore, the same signal appeared with short delay on subsequent electrodes as it propagated along the axon (Figure 9).

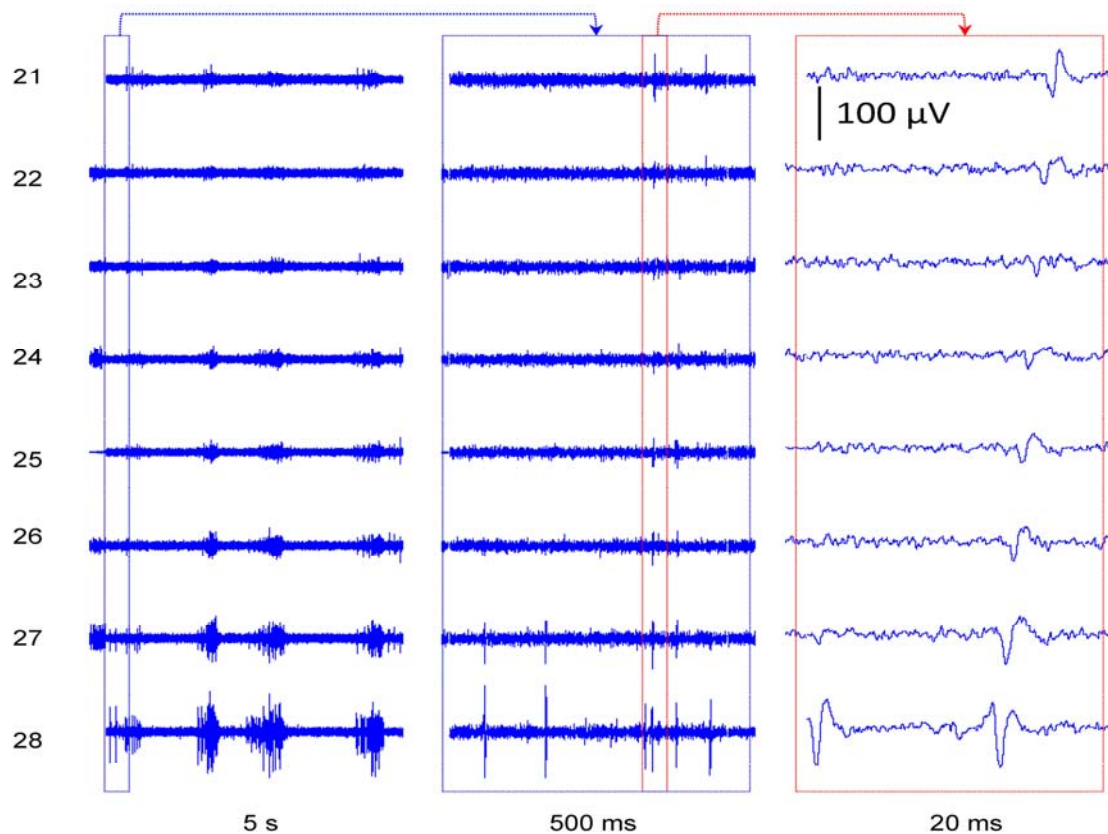


Figure 9 Sample recording and signal propagation in electrodes inside one microchannel

The right panel shows the magnified propagating signal along the full length of the channel from electrode 28 toward electrode 21 (see 8D).

Compared to the diameter of an axon ($\sim 1 \mu\text{m}$), the width of a microchannel was sufficiently large ($40 \mu\text{m}$) to let different axonal branches from the same network enter into it. Therefore, every electrode inside the microchannel could simultaneously record from different axons. Signals were sorted by shape to distinguish between the different axons (sources) (Figure 10 A). In general, two main signal categories were detected inside the microchannels; monophasic signals (mainly with negative wave) and biphasic signals (mainly with a negative followed by a positive wave). In contrast to quickly decaying biphasic signals, monophasic signals could propagate to distant electrodes inside a microchannel. This feature was amplitude-independent (Figure 10 B). Overlaying the signals recorded from subsequent electrodes inside the same channel showed the propagation delay and how the signal shape varied with location (Figure 10 D and C).

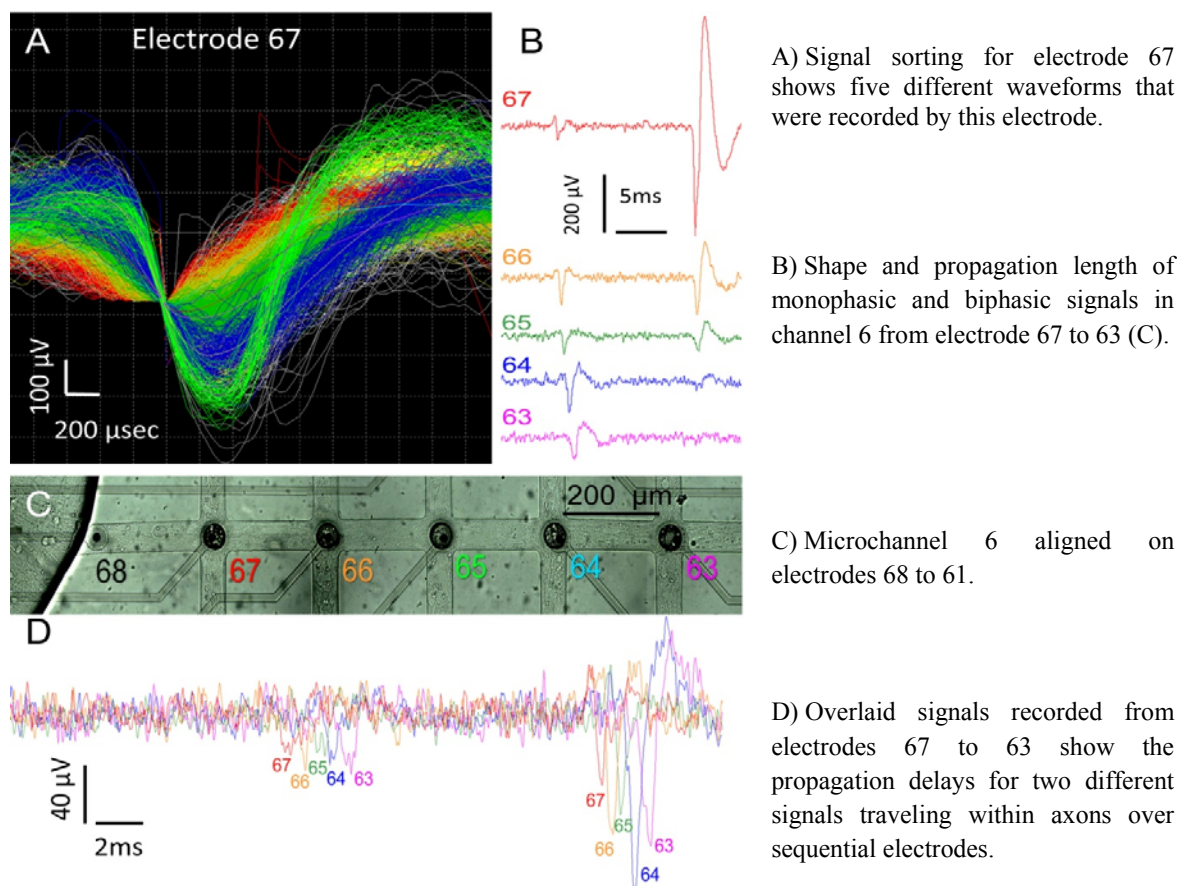


Figure 10 Signals with different amplitudes and shapes were propagating in channels.

3.1.3 Activity profile along the time in microchannel confined axons

To analyse the evolution of the axonal activity and the propagation velocity along the axons inside the microchannels over time, the electrical activity at 10, 20, 30 and 53 DIV was compared. To evaluate how activity levels change over time or along channels, two subsequent electrodes in a channel were considered as one segment, thereby dividing every channel into the following four segments: Seg 1 (0-250 μm), Seg 2 (250-650 μm), Seg 3 (650-1050 μm) and Seg 4 (1050-1300 μm) (Figure 12 A). A comparison of the overall number of spikes per minute in the proximal segments of all considered microchannels with that of their distal segments showed that the signal frequency decreases along the microchannel for all recording days ($P < 0.001$ at 10 and 30 DIV, $P < 0.01$ at 20 DIV; Figure 12 B). Monitoring the mean signal frequency in each segment over time (Figure 12 B) showed significant decrease in 53 DIV compared to 10 DIV in segments 1 and 2 and 3 ($p < 0.05$). Signal frequencies was also evaluated in detail for three selected microchannels, which was calculated by averaging all recorded signals from any of the electrodes inside a single microchannel. The mean signal frequency for each microchannel tended to decrease over time (Figure 12 C).

Propagation velocity was calculated by dividing the constant distance between a pair of electrodes (200 μm) by the temporal delay of the signal appearance on two subsequent electrodes. The mean propagation velocity for each microchannel was calculated by averaging the propagation velocities of all subsequent electrode pairs in that microchannel. For missing electrodes velocity was estimated by calculating the velocity between 2 nearby electrodes. The mean propagation velocity tended to increase with culture age, which was contrary to the observed decrease in the spike frequency (Figure 12 D). Propagation velocity increased with respect to DIV 10 in channel 2 ($p < 0.001$ vs. 20 DIV and $p < 0.01$ vs. 53 DIV; Figure 12 D), microchannel 5 ($p < 0.05$, $p < 0.001$ and $p < 0.001$ vs. 20, 30 and 53 DIV, respectively; Figure 12 D) and microchannel 6 ($p < 0.001$ vs. 20, 30 and 53 DIV; Figure 12 D). This increase was also significant when compared between 20 DIV and the subsequent recording days at 30 and 53 DIV in all microchannels ($p < 0.001$; Figure 12 D).

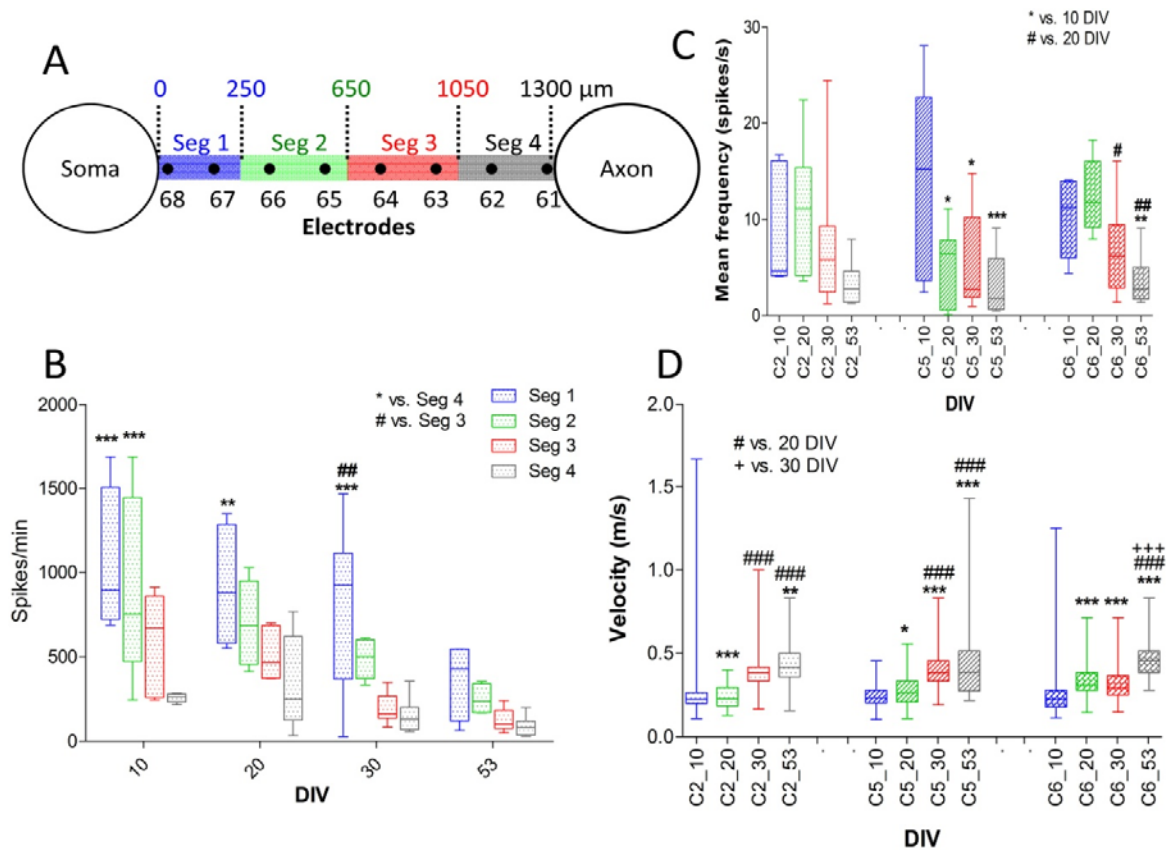


Figure 11 Changes in spike frequency and propagation velocity in axons growing inside crossing microchannels

A) To evaluate how activity levels change over time or along channels, two subsequent electrodes in a channel were considered as one segment, thereby dividing every channel into the following four segments: Seg 1 (0-250 μm), Seg 2 (250-650 μm), Seg 3 (650-1050 μm) and Seg 4 (1050-1300 μm). Each segment represents data that was collected from two adjacent electrodes. B) Spike frequency along the channel. Each bar represents the spike frequency range in one segment (color) on the mentioned day. The mean spike frequency was calculated by averaging the number of spikes per minute in a selected segment of channels 2, 5 and 6. A two-way ANOVA was applied for comparing the mean values between different segments on the mentioned day. * vs. Seg 4 and # vs. Seg 3 at the same DIV. C) Spike frequency evolution over time. Each line represents the changes in the mean spike frequency of the same segment (averaged over three microchannels) at different days. A one-way repeated measures ANOVA was applied for analyzing the mean frequency between different DIVs in each segment. * vs. DIV 30 and # vs. DIV 53 of the same segment. * or # $p < 0.05$, ** or ## $p < 0.01$ and *** or ### $p < 0.001$.) Each bar represents the range of spike frequencies in one channel on the mentioned day. X-axis denominators code for the channel number followed by the DIV on which the recording was performed. One-way repeated measures ANOVA applied for analyzing the mean frequency between different DIVs in each channel. * vs. DIV 10 and # vs. DIV 20 in same channel. B) Mean propagation speed in each channel for a given DIV. After calculating the velocity between each electrode pair in a channel, the mean propagation speed was determined by averaging the velocities of all pairs. Each bar represents the range of propagation speed in one channel at the mentioned day. One-way repeated measures ANOVA applied for analyzing the mean velocity between different DIVs in each channel. * vs. DIV 10, # vs. DIV 20 and + vs. DIV 30 in same channel. * or # $p < 0.05$, ** or ## $p < 0.01$ and ***, ### and +++ $p < 0.001$. Electrodes 27, 52 and 62 did not record any spikes at 10 and 20 DIV. Therefore, the velocity was estimated by dividing the time delay between two nearby electrodes by a distance of 400 μm .

Bursts propagation was analyzed for channels 2, 5 and 6 using the following criteria in NeuroExplorer: maximal interval to start burst = 0.02 s, maximal interval to end burst = 0.01 s, minimal interval between bursts = 0.01 s, minimal duration of burst = 0.02 s, minimal number of spikes in burst = 4, and bin size = 1 s). Figure 12 summarizes the mean burst rate in different segments of channels 2, 5 and 6. At 10 DIV, only a few bursts were detected (Figure 12 B). The burst frequency (bursts/min) increased over time and reached its maximum value after 30 DIV (Figure 12 C). A burst rate analysis for each segment of these three channels showed that bursts faded after 400-600 μm propagation length within a channel (Figure 12 C). The burst rate in segments 3 and 4 was significantly lower than in segment 1 ($p < 0.01$ and $p < 0.05$ at 20 DIV, $p < 0.001$ at 30 DIV, and $p < 0.001$ at 53 DIV).

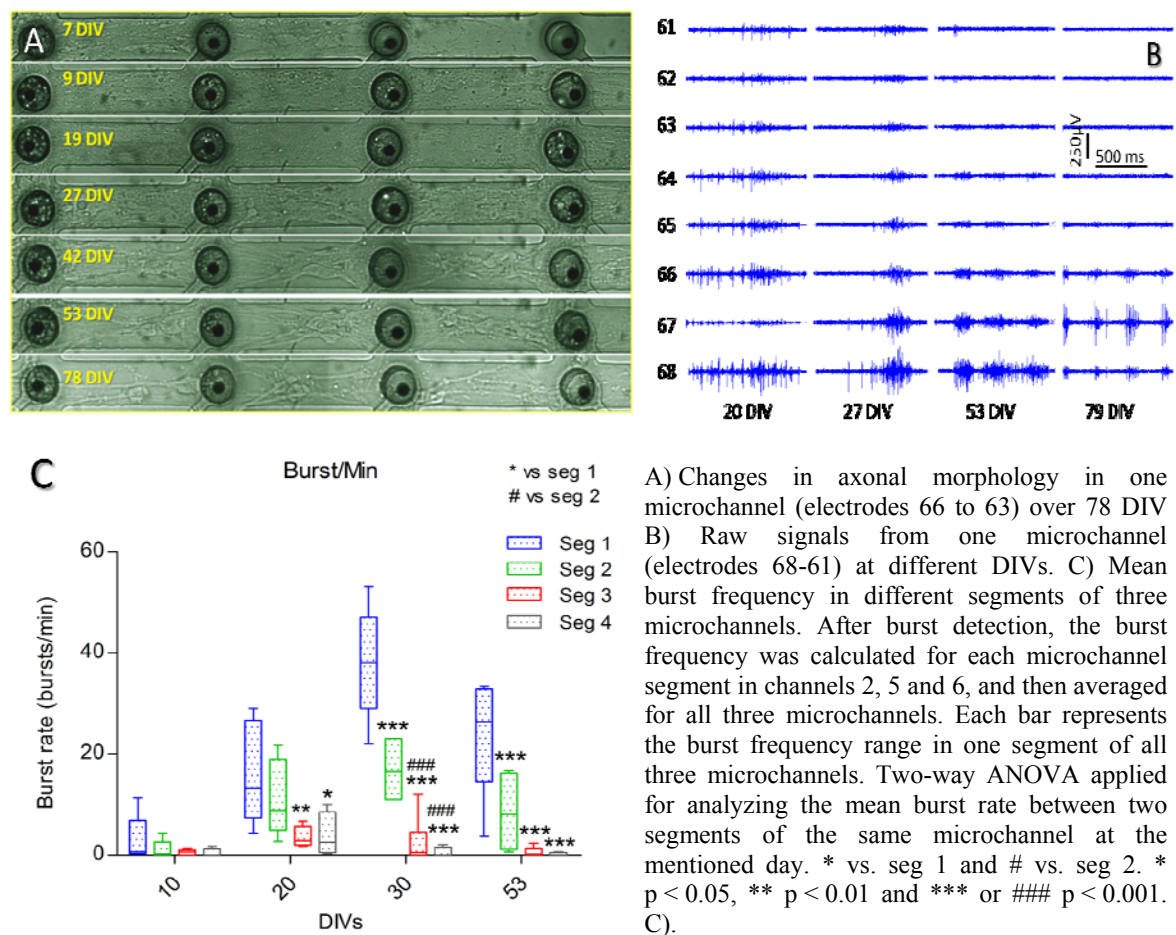


Figure 12 Burst propagation along channels and continuous monitoring of axonal morphology

3.1.4 Traverse action potential propagation in crossing microchannels

In the present device, microchannels were crossing each other which let axons to change their path and grow from one channel into another. Therefore, axons not only grew in direct path inside a single microchannel, but some of them also grew perpendicular to their main path (Figure 13). Either in the time stamp analysis or by overlaying the recorded signals from adjacent electrodes in nearby microchannels we found traverse propagation from one microchannel to another (Figure 13). This activity profile confirmed divergence from main path during axonal elongation inside the crossing microchannels.

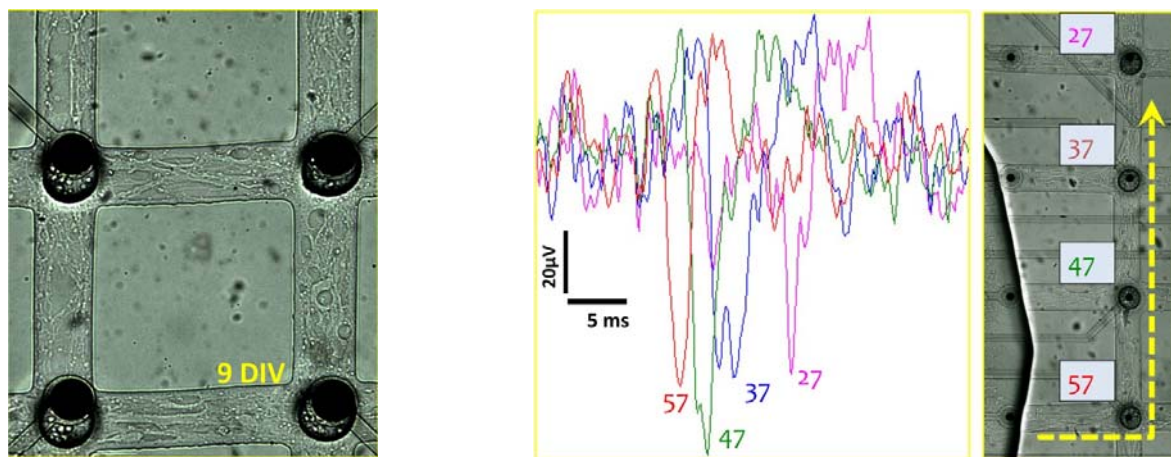


Figure 13 Traverse axonal growth and AP propagation in crossing microchannels.

The left picture shows the axons changing the path perpendicular to their main path (9 DIV). The right figures show the propagation of AP in traverse path from channel 57 to 27. Electrode pitch: 200 µm.

Regardless of the advantages of the crossing microchannel in providing useful framework for studying axonal electrophysiology in long-term and creating multiple pure axonal compartments from same cortical networks, it had few drawbacks. Because axons change their path inside the microchannel therefore the crossing points mix axons from different microchannels which make the analysis more difficult in every step toward the distal parts. Therefore we tried to decrease this complexity by fabricating direct microchannels with no crossing along their length. In addition, in the next generation of PDMS microdevices we decreased the microchannels length which left two electrode rows free, in both ends of the microchannels, for recording from reservoirs, soma.

3.2 Two compartment devices with open reservoirs

Fabrication protocol for the first generation of two-compartment devices was same as multicompartment devices and reservoirs, where the network supposed be formed, were perforated from top. The small reservoirs in these devices made it difficult to add cells into them and cells were spreading on top of the device as well as counterpart compartment, axonal compartment. Therefore we added few steps in cell seeding procedure. A PDMS mask with 1 mm hole was prepared and aligned on top of the device before cell seeding. This mask had only one through hole and aligned on top of the somal compartment. To prevent from detachment of mask from PDMS device a small droplet of silicon paste () applied as glue. Cells were added through the mask into the reservoir and after incubation PDMS mask has been gently removed from top of the PDMS device and cell culture medium added into the MEA ring (Figure 14). This procedure prevent from attachment of cells to PDMS device surface or their penetration into the counterpart reservoir.

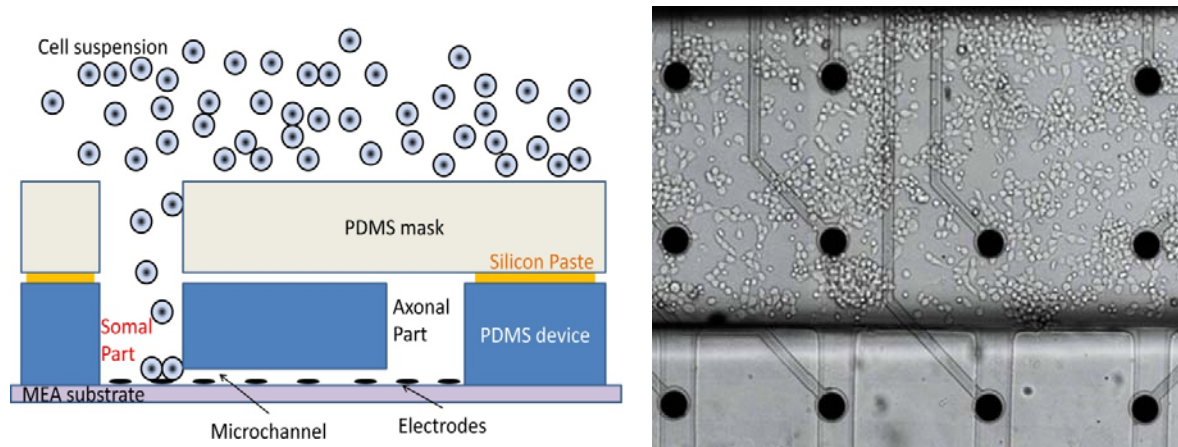


Figure 14 PDMS mask for cell seeding in the reservoirs of two-compartment PDMS device

The left cartoon shows PDMS mask ($\sim 200 \mu\text{m}$ thickness) attached by silicon paste on the backside of the PDMS device after alignment. PDMS mask with one perforated hole lets the cells to settle only in one reservoir. The right picture shows homogenously distributed cells ($< 2000 \text{ cell/ device}$) after seeding through a PDMS mask in the reservoir of two-compartment PDMS device and mask removal.

3.2.1 Recording issue from small networks in open reservoirs

Neurons in the open reservoirs and growing neurites inside the microchannels showed normal morphology same to random cultures on MEA surface or multicompartiment devices. Neurites grew into the microchannels after 3 DIV and reached counterpart reservoir in one week (because microchannels were shorter). First signals recorded after 7 DIV from growing axons inside the microchannels with no recordable activity in the reservoir section. This strange phenomenon in the reservoir section remained constant with very little changes even in older cultures more than 20 DIV (Figure 15).

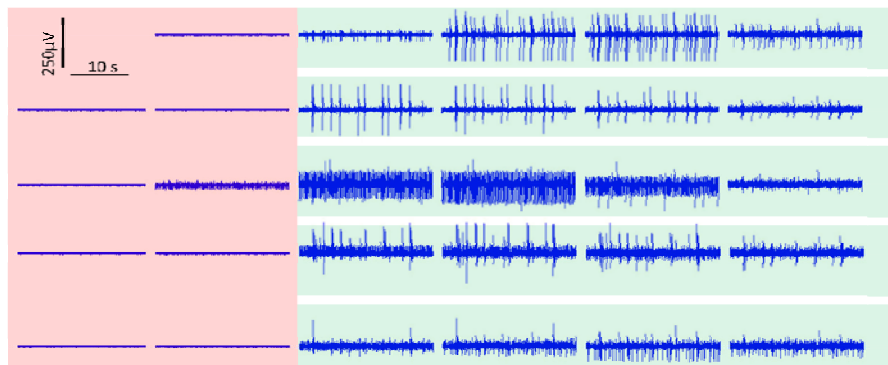


Figure 15 Very low or lack of recordable activity in the electrodes of open reservoirs.

Regardless of the activity in the electrodes inside the microchannels (green), almost no activity recorded by electrodes in the reservoir section (red).

The lack of the activity in the open reservoirs could have two possible reasons:

The small network size in the reservoir (< 2000 cell/ device) is not enough strong to provide detectable signals. In the very dense cultures in this device we could record from less than 3 out of 12 electrodes in the reservoir which shows that the density and number of the neurons are important factors. In addition device biophysical properties also could be another reason. The device was open in the place of the reservoirs. The bigger dimensions of the reservoir compared to microchannels and its opening from top could weaken the signal amplitude. To increase the signal amplitude in the reservoir section in two-compartment devices, with small changes in PDMS molding procedure we provided close chambers for cells in the next generation of two-compartment PDMS devices (Figure 2).

3.3 Two compartment devices with closed chambers

The main goal of designing the closed chambers instead of open reservoirs in the two-compartment devices was to increase the signal amplitude in the reservoir and facilitate the cell seeding procedure. In these devices after fabrication of the PDMS device with microchannels and closed chambers we punched two big openings ($r = 1\text{ mm}$) in two far edges of each closed chamber for adding the cells and connecting the closed chambers to outside environment (Figure 2 and Figure 3). Because the openings were big enough PDMS mask was not necessary to add cells into the reservoir, closed chambers. In addition, coating after device alignment and incubation of the device with cell culture medium for 12 to 24 hours before cell seeding increased device wettability, therefore adding the cells through one opening pool let the cells to settle homogenously inside the closed chamber and the rest of the cell suspension released into another pool in the same side (Figure 16).

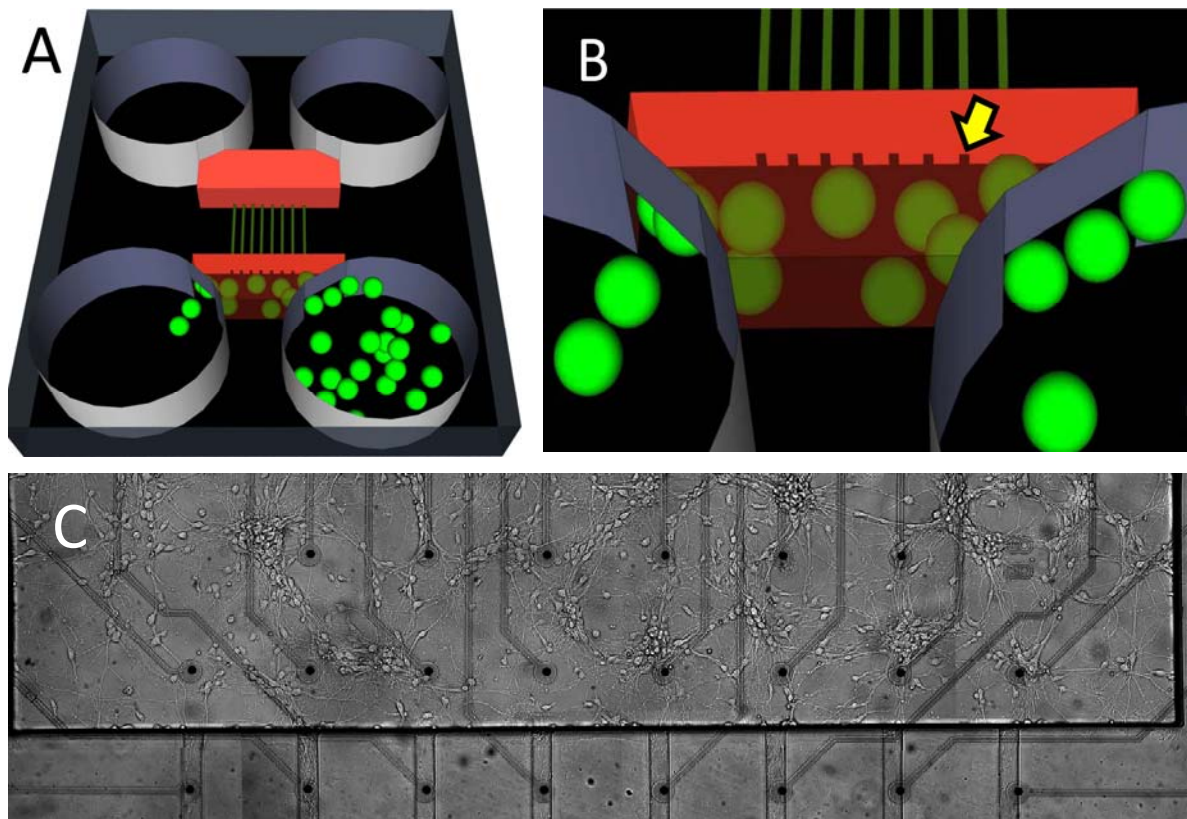


Figure 16 Cell seeding in two compartment device with closed chambers

A) Shows the cells seeding through one opening pool into the closed chamber. Because the device was already wet, cell suspension automatically found its way into the closed chamber and released into adjacent reservoir. Red: closed chamber, green: microchannels, gray opening pools. B) Magnified view of cells settled in the closed chamber in vicinity of the microchannels. Yellow arrow marks the microchannels openings into the closed chamber. C) Low density cortical neurons in DIV 6 after seeding inside closed chamber.

3.3.1 Improved recording in electrodes inside closed chamber

In the PDMS devices with closed chambers activity appeared around DIV 7 in microchannels. Activity in the reservoir appeared around DIV 10 and it improved days later when network morphology had been established completely (Figure 17). Regarding the network density in the closed chambers activity could be recorded from 4 to 10 out of 12 electrodes in that closed chamber which showed that sealing the reservoirs from top amplifies and improves signal to noise ratio (Figure 17). Comparing the signal amplitude recorded by electrodes in the reservoir section with electrodes inside the microchannels it was obvious that signal amplitude in the microchannels was at least 2 times more than the amplitude in the electrodes recording from reservoir (Figure 17). However, noise level has not been amplified significantly compared to the reservoir section. Biophysical properties of the microchannel improved signal to noise ratio and made it possible to record signals which had not been detected by electrodes in the reservoir section (Figure 17). Comparing the signal frequency between reservoir and microchannels confirmed higher activity recorded by electrodes inside the microchannels.

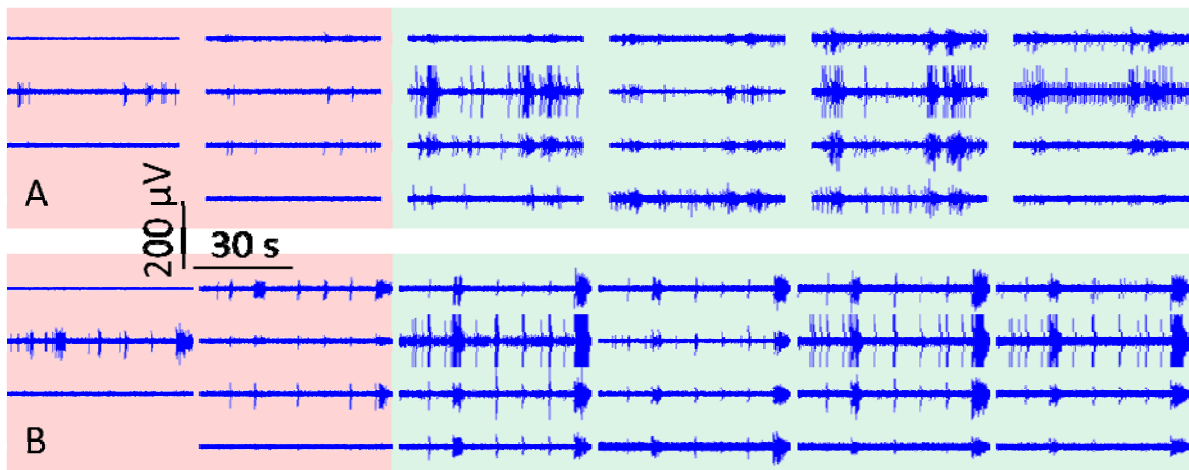


Figure 17 Recording the activity from network growing in the closed chambers

A) A sample activity profile recorded from cortical network inside the closed chamber (red area) and related axons inside the microchannels (green area) in DIV 10. B) Activity profile from the same network and axons in DIV 30. Each row in the green are represents 4 subsequent electrodes inside one microchannel.

3.3.2 Two layer cortical networks provided by sequential seeding

In the PDMS devices with direct microchannels we tried to culture two layer neuronal networks (Figure 2). The main idea was to see whether axons can grow into the already filled microchannels. First layer of cortical networks provided by seeding neurons in one side, one closed chamber, and wait for two weeks to let axons grow and release into the counterpart reservoir (Figure 19). After two weeks, all microchannels were filled with axonal bundles of the first population, which had exited into the counterpart reservoir and covered its surface by that time (Figure 19). To add new neurons into the counterpart reservoir, which already have been filled with axons from the first layer, the cell culture medium was drained up to the surface of the PDMS device and the solution inside the pools and closed chamber remained intact. Complete draining of the cell culture medium will kill cells and axons. Just before adding the cell suspension into the second compartment extra solution on device surface was removed and cells were seeded through one opening, same to the first compartment (Figure 2). New cortical neurons were added in DIV 13 on top of the axons (Figure 19). A younger network had formed within a few days and formed contact with axons from the first layer in other reservoir (Figure 19). Signals appeared earlier in the new networks (6 DIV after seeding).

Because the microchannels already had been filled with axons of the first compartment, it was almost impossible to distinguish newly growing axons from second compartment into the microchannels in the opposite direction. However, electrophysiological data recorded from electrodes inside the microchannels confirmed the axonal growth in the opposite direction (Figure 19). After about two weeks (DIV 30), in the first step and simply by overlaying the recorded signals in the subsequent electrodes we found that some signals first appeared in electrodes close to the second compartment (Figure 19), which suggested that this signal is originated from second layer. In addition cross-correlation showed how activity between two pairs of the electrodes inside the microchannel is correlated or not, and if there is a correlation whether it is synchronized or there is directionality between these two pairs. In all cases one electrode inside the microchannel is considered as reference electrode and the time stamp or appearance of the activity in other electrodes, target electrodes, is considered corresponding to this reference electrode (Figure 18).

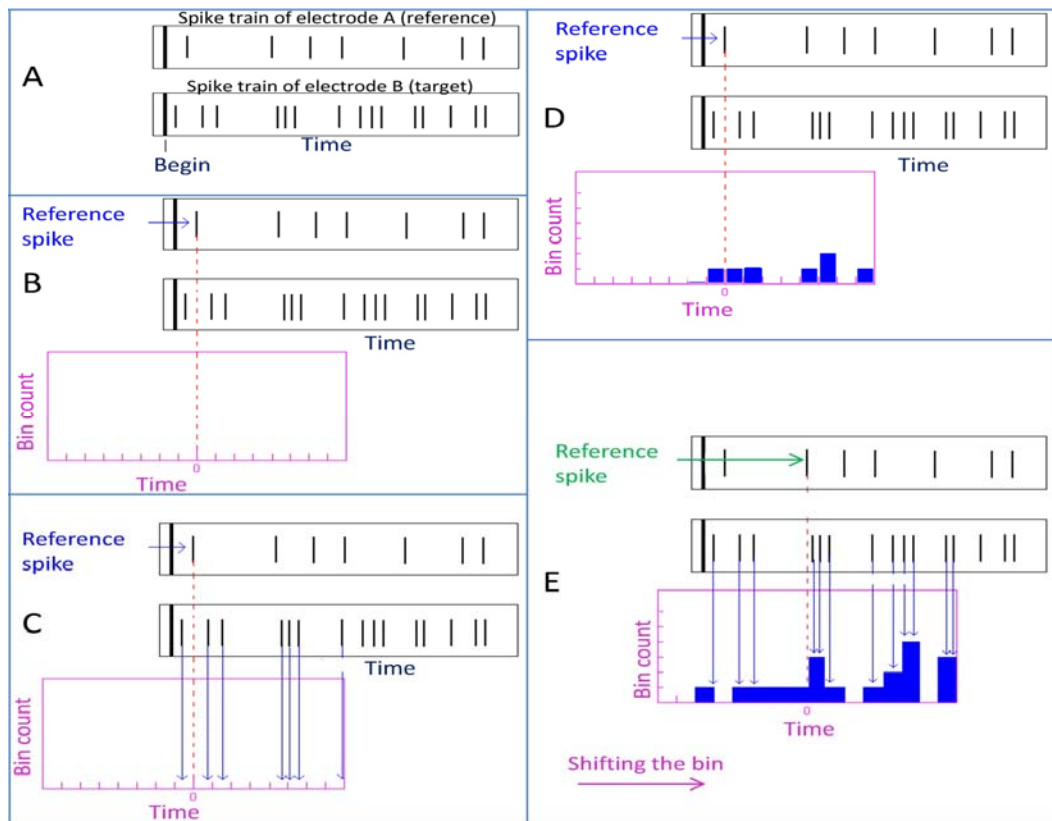


Figure 18 General concept of crosscorrelation between activity in different electrodes

A) Shows the spike trains recorded by two electrodes in the same time period. To find the correlation between two spike trains one electrode is considered as reference electrode and other as target. B) Depending on experiment a time bin is specified to monitor correlation between two spike trains in separated frames. To start, the zero point in the time bin is adjusted to the time stamp of reference spike. C) Time stamps of the target spikes is plotted corresponding to the reference spike, zero point. D) One spike adds one value to the total value in corresponding time stamp. E) After plotting the time stamps for all spikes present in specific bin, the bin window shifts along the time axis to fit its zero points with next reference spike, new reference spike. All values acquired from each reference spike are added to the previous values in crosscorrelogram. The procedure is repeated for all individual spikes inside the reference spike train for whole length of recording.

3.3.3 Bi-directional propagation in microchannels of two layer cortical cultures

Overlaying the signals in electrodes inside one microchannel and crosscorrelograms showed bi-directional action potential propagation in some microchannels 10 DIV after adding the new neurons into the second compartment. These findings proved the presence of axons from the second compartment growing in the opposite direction inside the microchannel (Figure 19 F, G and H). The delay between subsequent electrodes revealed that activity propagated at different velocities between the two compartments (Figure 19 F and H).

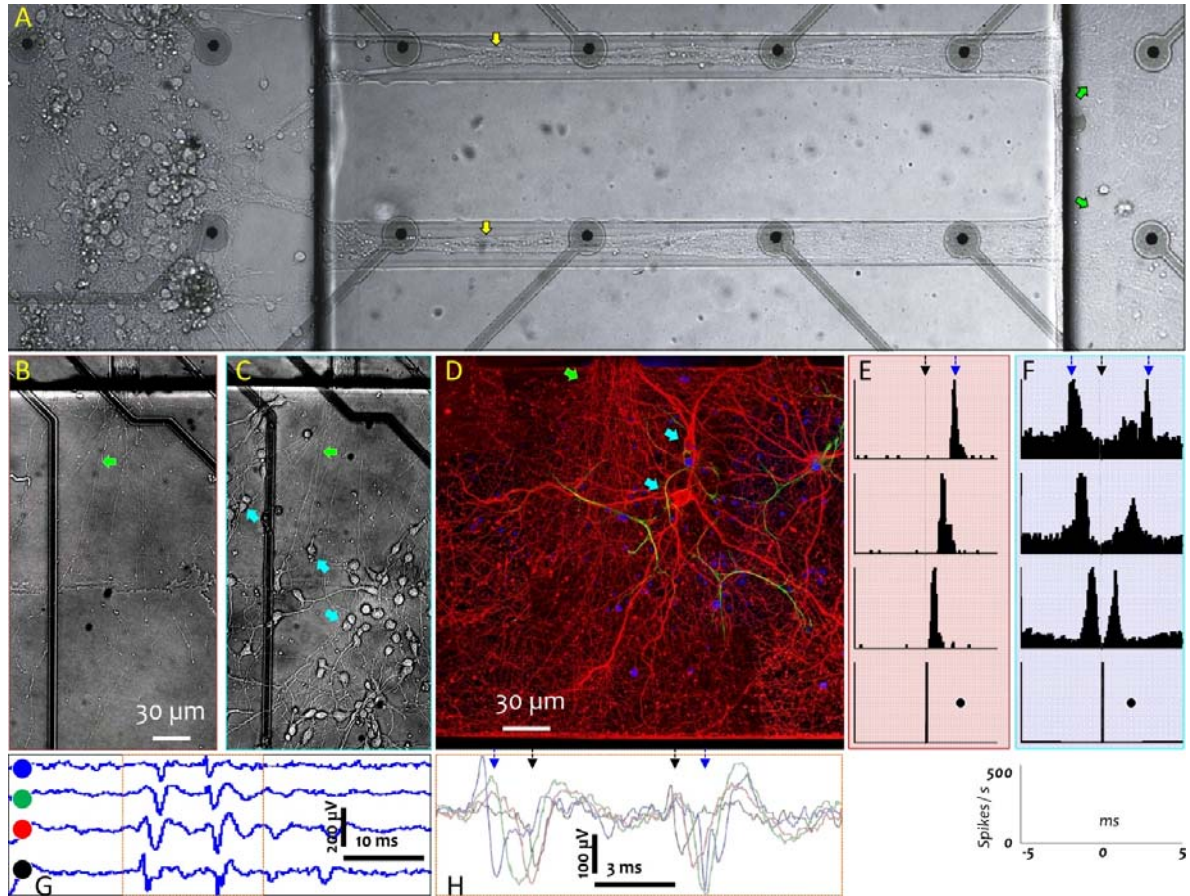


Figure 19 Two layer cortical networks and bi-directionally growing axons in microchannels

A) First layer cortical network in reservoir with growing axonal bundles into the direct microchannels (yellow arrows) and their release into the counterpart reservoir (green arrows). B) The counterpart reservoir before adding the fresh cortical neurons in DIV 13, and C) three DIVs after adding the cells on top of the axons from first layer (green arrows). Blue arrows show the new neurons which are in contact with axons from the first layer. D) Immunostaining the network in the second compartment showed interaction between axons from first layer and new neurons. Neurons were labeled by beta-Tubulin III (red), glial cells by anti-GFAP (green) and nuclei by DAPI (blue). E) Cross-correlogram of the activity in electrodes inside one microchannel which shows uni-directional propagation of the action potential in DIV 13. Delay in recording the same signal between first and last electrode inside the microchannel has been shown by black and blue arrows. F) Cross-correlogram from the same microchannel in DIV 30, in which neurons in the counterpart reservoir are already 16 DIV old and send their axons into the microchannels in reverse direction. Different directions of the propagation inside the microchannel has been confirmed by bifurcated histogram which shows almost half signals recorded by the first electrode inside the microchannel already has been recorded by the last electrode in the same microchannel. Bin size: 0.0001 sec, Xmin: -0.005s and Xmax: 0.005 s. Y-axis maximum in all graphs adjusted manually to 500 spikes which was the maximum number of correlation peak in all graphs. G) Sample recording window including two action potentials propagating in different directions with different velocities. H) Shows the orange border area in G which overlaid on each other to show the delays between electrodes and propagations in different directions. Each color representing the signal which has been marked by colored circle in G.

3.3.4 Laser microdissection of bi-directional and unidirectional axonal bundles

Physical confinements provided by device and its alignment on top of the electrodes made it possible to record from different compartments of the network including somata in the reservoir and axons inside the microchannel. In the same time compartmentalized axonal bundles were accessible for optical manipulation without affecting the other parts of the network. In further step, we tried to apply these devices for functional and morphological studies after selected axonal injury in specified locations inside the microchannels. Therefore, MEA and microfluidic device assembly was mounted on the microscopy stage equipped with laser microdissection (LMD) setup. Combining these technologies made it available to either provide local axonal damage or evaluate network functional response to this injury in different levels; soma, intact axons, dissected axons, proximal and distal parts of dissected axons.

In selected microchannels, axonal bundles were dissected 10 DIVs after seeding the second network and after confirming reverse axonal growth into the microchannels through uni- or bi-directional signal propagation (Figure 20). We dissected axonal bundles of both uni- and bi-directionally growing axons and compared the results (Figure 20 and Figure 22). Dissection was performed in a total of 19 microchannels in 11 cultures, 9 of which showed bi-directional propagation and 10 uni-directional activity as confirmed by cross-correlation analysis of baseline activity (DIV 25_1). Axons were dissected between two electrodes close to the older neuronal networks at 25 DIVs (Figure 20 and Figure 22). In all two-layer networks, the layer with higher baseline activity was considered¹ as the dominant reservoir and the first two electrodes inside each microchannel close to that network were considered the proximal electrodes. In all cultures with dominant activity in one reservoir, the propagation direction was mainly from that reservoir to the counterpart reservoir.

To see whether a dissection in the proximal or distal length of the axon can affect the activity over time, axons had been dissected on one end of a microchannel instead of the center (Figure 20 and Figure 21). In bi-directional axonal bundles, the dissections led to degeneration on both ends of the dissection point after 5 DIV. However, degeneration was more obvious on the side closer to one of the reservoirs (Figure 20 B and C). This was also

confirmed by analyzing the general activity level on electrodes at different distances from the dissection point (Fig. 13 D).

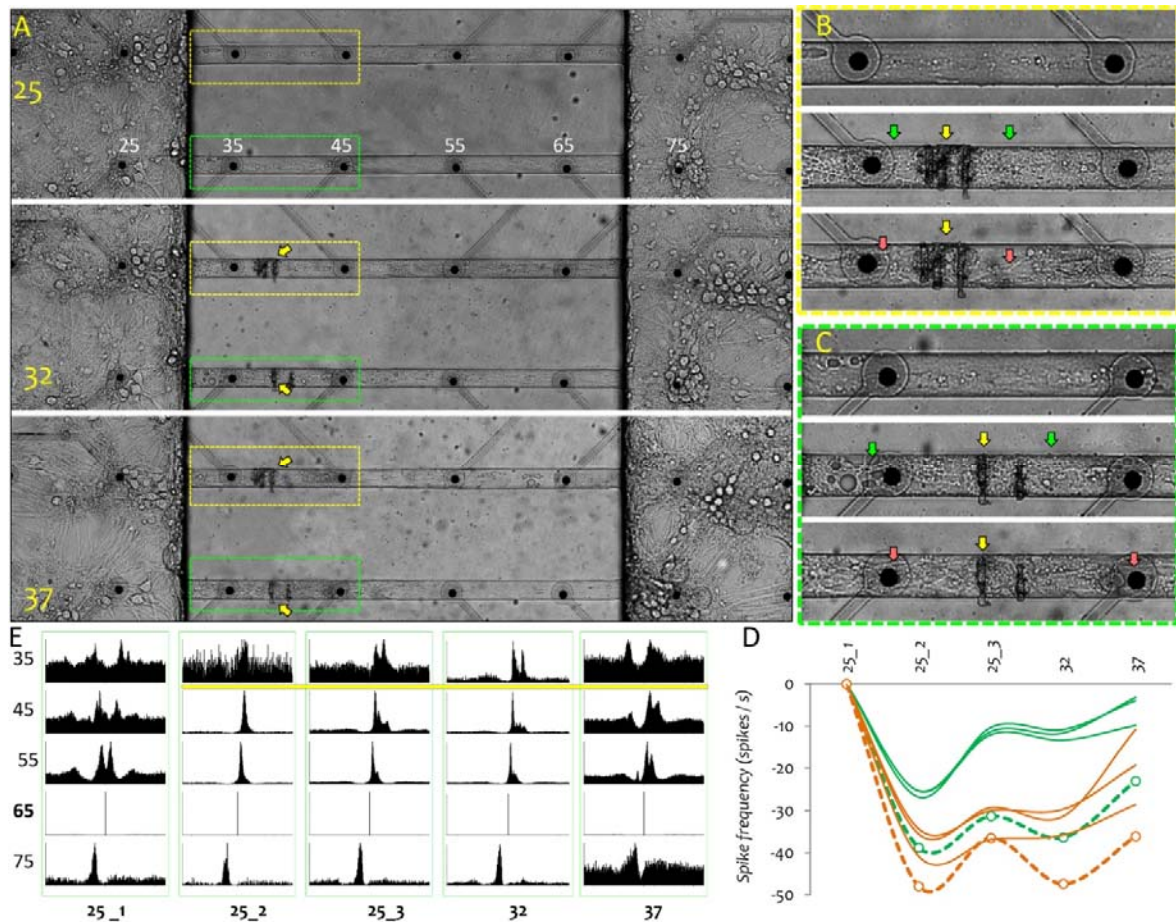


Figure 20 Morphology and activity after dissecting bi-directional axonal bundles connecting two layer cortical networks.

A) Sample picture of 2 Layer neuronal networks cultured in two reservoirs connected by 8 rows of direct microchannels. Second layer seeded 14 DIVs after first layer and the picture shows the image in DIV 11 of second layer (DIV 25 for first layer). Electrode 25 is recording from first layer and electrode 75 from second layer. Complete dissection was done in two microchannels between two proximal electrodes in DIV 25 in this culture. Second and third panels in “A” shows the morphology in DIVs 32 and 37, which was correspond to 7 DIVS and 12 DIVs after dissection. B and C) Magnified view of yellow and green marked areas in A, which shows two microchannels in baseline and 7 and 12 DIVs after axonal dissection. Yellow marks show the dissection loci, green arrows show the degenerating axons and red arrows representing the intact or regenerating axons. E) Cross-correlogram between the electrodes recording from highlighted electrodes in A. electrode 25 did not showed activity. Bin size: 0.0001 sec, Xmin: -0.005s and Xmax: 0.005 s. Y-axis maximum in all graphs adjusted manually to 500 spikes which was the maximum number of correlation peak in all graphs. Electrode 65 considered as reference electrode and the results showed bi-directional propagation in baseline (DIV 25_1). Yellow line shows the dissection location between electrodes. D) Spike frequency recorded by 8 electrodes from two dissected microchannels in A. Activity in baseline was subtracted from the activity in all DIVs for each individual electrode. Each color is representing the spikes recorded by electrodes inside one microchannel. The dashed lines show the most proximal electrode inside each microchannel, electrode 35

Because these microchannels encompassed axons originating from both reservoirs, cutting on one edge of the microchannel dissected some axons in their most proximal parts and others in their most distal parts. The dissection on one edge of the microchannel removed one arm of the bifurcated cross-correlogram and changed the propagation from being bi-directional at baseline to uni-directional within one week after the dissection (Figure 20 E). The unidirectional propagation and its latency with respect to the reference electrode showed that this propagation belonged to those axons which had been dissected in their most distal sections (Figure 20 E). In contrast, in axons which had been dissected in their most proximal parts propagation disappeared just after the dissection for two weeks (Figure 20 E). The difference in the propagation profile between these two groups of axons growing in the same microchannel was also confirmed by a sharp decrease in activity levels of axons which had been dissected in their proximal section compared to the axons dissected in the most distal parts (Figure 20 D and Figure 21). As shown in Fig 13 D, activity mainly lost in electrode 35 which is mainly recording from proximal part of axons dissected in their most proximal section (dashed lines), while in the rest of the electrodes which are recording mainly the activity from proximal parts of the axons dissected in their most distal sections activity decreased very slightly (continuous lines).

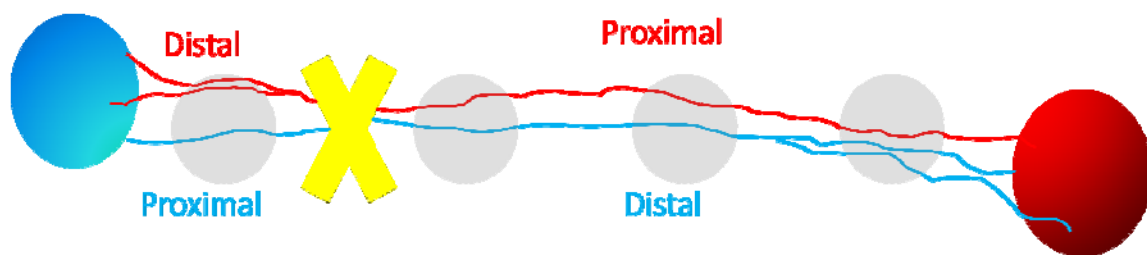


Figure 21 Schematic view of dissection in bi-directional growing axons

Dissection intentionally was performed in one edge of the microchannel to cut axons in one direction in their most proximal parts (blue axon), and cut the axons growing in the reverse direction in their most distal parts (red axons). yellow mark shows the dissection point. Gray circles representing four electrodes inside the microchannel recording from proximal or distal parts of axons.

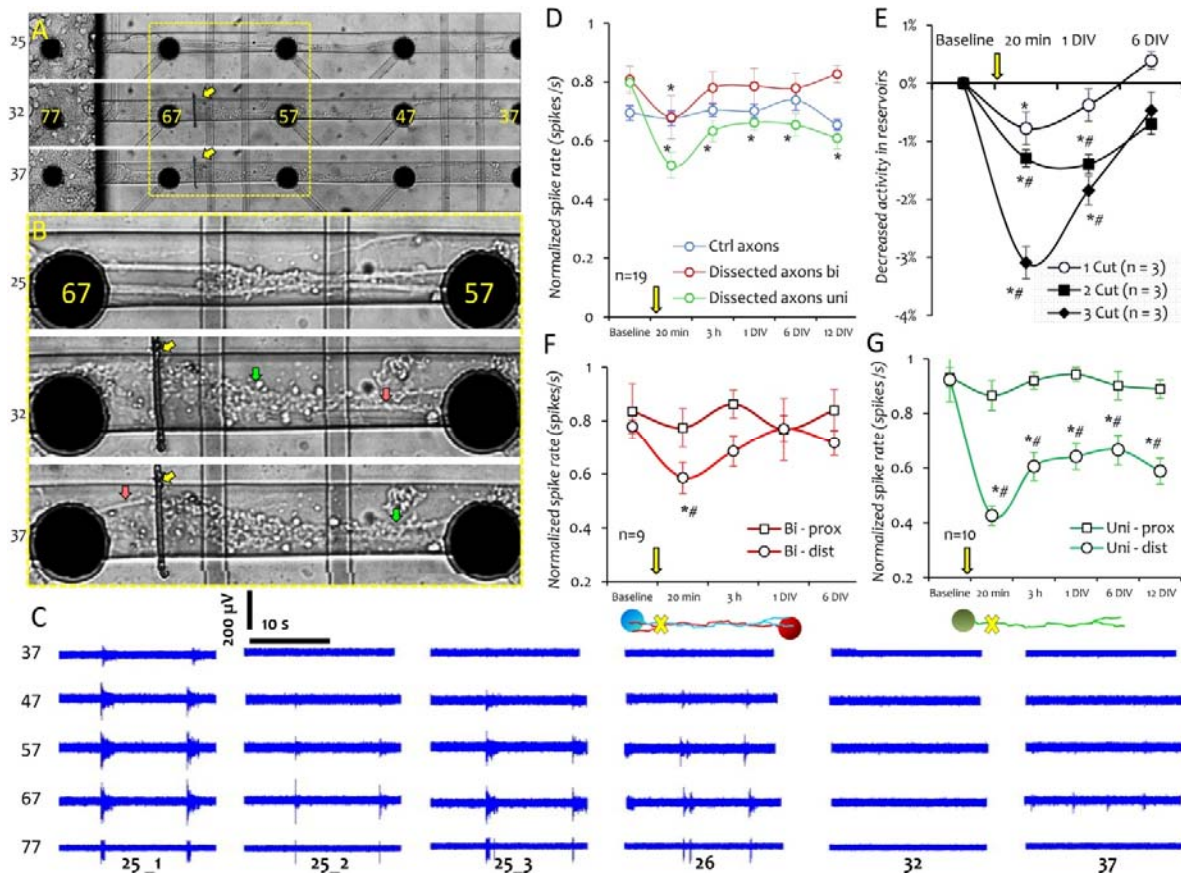


Figure 22 Morphology and activity after dissecting uni-directional axonal bundles connecting two layer cortical networks.

A) Dissection was done in DIV 25 and microscopy pictures prepared in baseline and one and seven DIVs after dissection. Yellow arrows show the dissection point. B) Yellow marked area in A, which shows the magnified view of the degeneration of the distal parts in 7 and 12 DIVs after dissection (green marks). Axons which have not been degenerated are pointed by red arrows. C) 20 seconds recording window from the electrode inside the reservoir (77), as well as proximal (67) and distal (57, 47, and 37) to the dissection point in baseline and different DIVs after dissection. Maximum signal amplitude is 200 μ V. D) Shows normalized spike frequency in control and dissected uni- and bi-directional axons. Each time point represents the mean \pm S.E.M in electrodes of same group across eleven cortical cultures. To normalize the activity in each channel type activity in each day divided by the maximum activity on that day in specific MEA, and the results were averaged over MEAs. E) Shows the percentage of activity decrease compared to the baseline in cultures which had endured different numbers of dissection; only in one microchannel, as well as two or three microchannels. Normalized activity in the baseline was subtracted from the activities in each DIV and the resulted value divided by the activity in baseline. F) Activity in the proximal vs. distal parts of bi-directional axonal bundles after dissection. Proximal and distal parts defined by position of the dissection regarding the dominant reservoir. G) Activity in the proximal vs. distal sections of un-directional. Repeated measure ANNOVA (* $p < 0.05$ vs. baseline) in all graphs. Two-way ANNOVA followed by post-hoc Tukey (# $p < 0.05$ vs. proximal section in F and G, and vs. culture with only one dissected microchannel in E).

In direct microchannels, a complete dissection of uni-directional axons in their proximal sections, between two first electrodes, led to a complete degeneration of the axonal bundles in distal sections after 7 to 12 DIV (Figure 22). In parallel, activity decreased to lower levels right after dissection and disappeared after 7 – 12 DIV (Figure 22 C).

Analysing the spike frequency recorded from control axons as well as proximal and distal parts of the dissected axons showed that at the same time, the activity of intact axons at different locations of dissected networks did not change significantly compared to baseline activity (Figure 22 D). However, in dissected bi-directional and uni-directional axons activity decreases just after dissection ($p < 0.05$). In dissected bi-directional axons activity returned to the baseline after three hours and remained constant over the next two weeks. However, in uni-directional axons activity remained at decreased levels for the rest of the experiment (Figure 22 D; $p < 0.05$ vs. baseline). In dissected bi-directional axons, activity in the distal section decreased for a few hours after dissection and returned to baseline levels on subsequent DIVs (Figure 22 F). In the uni-directional axons, dissection in the most proximal parts caused a sharp decrease in activity recorded from distal sections and remained at significantly lower levels compared to the proximal part (Figure 22 G; $p < 0.05$ vs. proximal part). Comparing the activity between cultures with different numbers of dissected axon bundles showed that increasing the number of dissections led to a severe and long-lasting decrease in network activity (Figure 22 E).

Even though this two compartment device with closed chamber and direct microchannels provide a useful framework for studying network response for selected axonal injury, it was difficult to provide partial damage to the axonal bundles inside the microchannels. In addition bi-directional growing axons increased the recorded signals complexity which made it difficult to extract a clear result from functional response of dissected axons to injury. In the next step we tried to fabricate microchannels with different features for separating axonal bundles and making them accessible for partial damage. In addition, we provided one layer and therefore uni-directional growing axons inside the microchannels to obtain more clear results.

3.4 Two compartment devices with working stations (MCh-ws device)

These devices included all properties of two-compartment devices with closed chambers plus 3 extended areas, working stations, along 3 out of 8 microchannels and a neurite filtering cavity in two ends of the microchannels.

To plate a sufficiently high density of cortical or hippocampal neurons into a cell culture chamber, we used cell suspensions with cell concentrations between 5000 to 12000 cell/ μl . Larger volumes caused the undesirable spreading of cells on top of the device or into the opposite compartment. The total volume of the closed chamber was 0.28 μl , which hosted a maximum number of 3360 neurons. In all cultures neurites started to grow homogeneously into the filtering area after 3 DIV and reached to the proximal electrodes at the microchannel entries (Figure 23 A). Within one week, axons had filled all microchannels and reached to the counterpart reservoir (Figure 23 B and C). Each microchannel guided axons over four subsequent electrodes. In all cases, axons tended to grow in axonal assemblies, which we named axonal bundles (Figure 23 C). Upon their entrance into the wider areas of the working stations or distal reservoir, these bundles branched out to distribute their individual axons over the entire width (Figure 23 C). In almost all networks, the first signals were recorded at 7 DIV from axons on electrodes inside the microchannels, but not from the electrodes in the somata reservoirs. Somal activity appeared at the earliest around 10 DIV. This phenomenon may be related to the larger dimensions of the reservoir, which decrease the extracellular resistivity and therefore the voltage amplitude according to Ohm's law.

Recording the signals from subsequent electrodes inside the microchannels confirmed the propagation of the activity including bursts and single spikes (Figure 23 D). Overlaying the recorded signals from the subsequent electrodes inside one microchannel allowed determine the latency of a signal travelling along the same axonal bundle (Figure 23 E). Time-stamp cross-correlograms, with the first electrode of a microchannel acting as the reference, had Gaussian distribution of increasing width along the microchannel, which suggests increasing variations in signal propagation latencies with distance (Figure 23 F and G). Most spikes had latencies ranging from 0.5 ms to 1 ms over an inter-electrode distance of 200 μm resulting in signal propagation speeds between 0.2 m/s and 0.4 m/s (Figure 23).

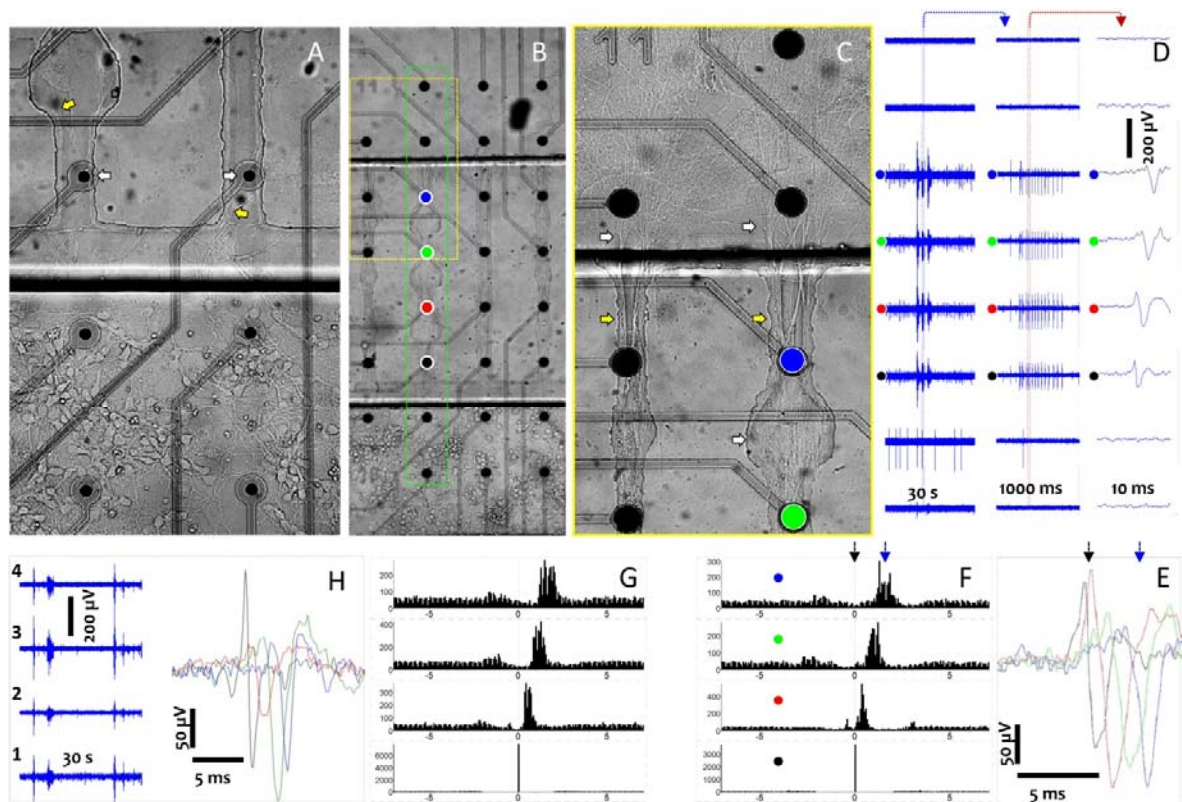


Figure 23 Sample morphology and recording from cultured neurons in MCh-ws device

A) Hippocampal culture in DIV 4 with homogeneously distributed neurons inside the closed chamber and growing neurites into the filtering area and proximal parts of the microchannels with straight geometry (MCh_direct) or with working stations (MCh_ws). Yellow arrows shows the individual axons which have found their way into the microchannel and white arrows show the axons passing from top of the electrodes (10 μm). B) Cortical culture in DIV 16, one day before first dissection. Four subsequent electrodes were recording from each microchannel or from same axons in different positions (marked by colored circles; black, red, green, blue). C) Magnified view of yellow marked part in B, which shows the axonal bundles in the narrow sections of the microchannel (yellow arrows) and branched axons in wider areas including working stations or releasing point into the counterpart reservoir (white arrows). D) Recording profile from the 8 electrodes inside the green frame in B, from which four are inside the microchannel and recording from same axonal bundles (colored circles in B, C and D). All three recording columns show the recording from same electrodes in the same time points with different magnification (window length; left: 30 s, middle: 1000 ms, and right: 10 ms). Left and longer window shows propagation of spike assemblies (burst activity), and the right column shows the propagation of single spikes from black marked electrode toward blue marked electrode. E) Right column in D after magnifying and overlaying the recordings from four electrodes inside the microchannel. Delay is shown by shift in the appearance of the same signal in subsequent electrode. F) Cross-correlogram of activity correlation between electrodes inside the microchannel regarding to reference electrode, the most proximal electrode inside the microchannel (black circle), Black and blue arrows show the delay between reference and most distal electrodes inside the microchannel. G) Histograms of activity correlation between electrodes inside the microchannel regarding to reference electrode, the most proximal electrode inside the microchannel (black circle). H) Shows a sample recording from four subsequent electrodes inside a direct microchannel (proximal to distal has been mentioned by numbers) with a sample single spike propagating over the same electrodes.

3.4.1 Laser microdissection in microchannels with working stations

In the device which had working stations in their microchannels we tried to provide one layer cortical and hippocampal cultures and dissect axonal bundles in the centre of the microchannel in middle of working stations. Dissection was performed only in the central working stations (ws) of microchannels which had working stations (MCh-ws) (Table 3 and Figure 6). Three different dissection levels in three different microchannels of each culture were applied at 17 DIV. In the first microchannel, all axons were completely dissected by passing twice across the working station (Table 4 and Figure 6 and Figure 31). In the second microchannel, only half of the axons were dissected by partially passing with the laser up to the center of the working station and leaving the rest of the axons intact (Table 4 and Figure 6). In the third microchannel, a very local point injury was induced in one corner of the working station (Table 4 and Fig. 6). One week later at 24 DIV, the dissection was completed for the previously partially dissected axons in the second microchannel by completely passing across the working station (Table 4). On the same day, a partial dissection was performed in the third working station with the local dissection (Table 4). Microchannels were selected randomly in each culture to provide complete, partial-partial or spot-partial dissections.

Table 4 Dissection protocol for each type of dissection

<i>Dissection type</i>	Baseline recording	First dissection	One week recovery	second dissection	3 weeks recovery
<i>Complete</i>	Yes	Complete	Yes	No	Yes
<i>Partial – partial</i>	Yes	Partial	Yes	Partial	Yes
<i>Local – partial</i>	Yes	Local	Yes	Partial	Yes

3.4.2 Morphology and activity in completely dissected axons

Imaging during and just after the dissection at 17 DIV showed a gap between the proximal and distal parts of axonal bundle (Figure 24 A and B). This gap later is gradually disappeared by reconnection of proximal and distal ends (Figure 24 B). One day after dissection, the degeneration signs were not yet obvious in the distal parts (Figure 24 A). However, within one week, most distal axonal bundles inside the microchannel experienced severe degeneration with only a few branches staying intact (Figure 24 C). Even though the

axonal mass decreased in the vicinity of the dissection point in the proximal part ($\pm 200 \mu\text{m}$), some dissociated branches reunited again and later filled almost all of the free distal areas (Figure 24 B).

In the present device degeneration of the control axons started after DIV 40, however cultures remained alive with recordable activity up to DIV 70. Recording and microscopy stopped in DIV 45.

Four electrodes were recording the activity from proximal or distal parts of dissected axonal bundles over time. It was therefore possible to monitor dissection-related activity variations to investigate how the activity is affected by morphological changes over time (Figure 24 D to F). We observed an overall activity decrease within the first few hours after dissection in cortical cultures (Figure 24 D and Figure 27). During the first days after dissection, the distal electrode in the vicinity of the dissection point showed a partial decrease in activity while activity had completely disappeared on the most distal electrode (Figure 24 D). Directly after dissection, activity in the proximal section had decreased and changed from bursting to single and separated spike activity (Figure 24 D). It returned to baseline after three hours and increased in the subsequent DIVs in parallel to the overall activity increase in the whole network. Dissecting the axons in the other microchannels at 24 DIV did not affect the activity in the already dissected axons, and at later DIVs activity returned to baseline levels even on the most distal electrode (Figure 24 D and Figure 31 a and Figure 32 a).

The cross-correlograms showed that activity on the first electrode inside the microchannel was preceded by activity on the closest electrode inside the reservoir (Figure 24 E). This suggests that axons inside the microchannel initiated from cell bodies closely located to the microchannel entrance. Dissecting axons in a microchannel abolished this correlation until the end of the study (Figure 24 E). The cross-correlograms for electrodes inside a microchannel showed decreased correlated activity between proximal and distal electrodes after dissection, which partially returned after three hours, but remained lost for the most distal electrode (Figure 24 E and F). This post-dissection correlation between distal and proximal activity reached its maximum at 45 DIV when activity reappeared on the most distal electrode (Figure 24 D and F and Figure 32 a).

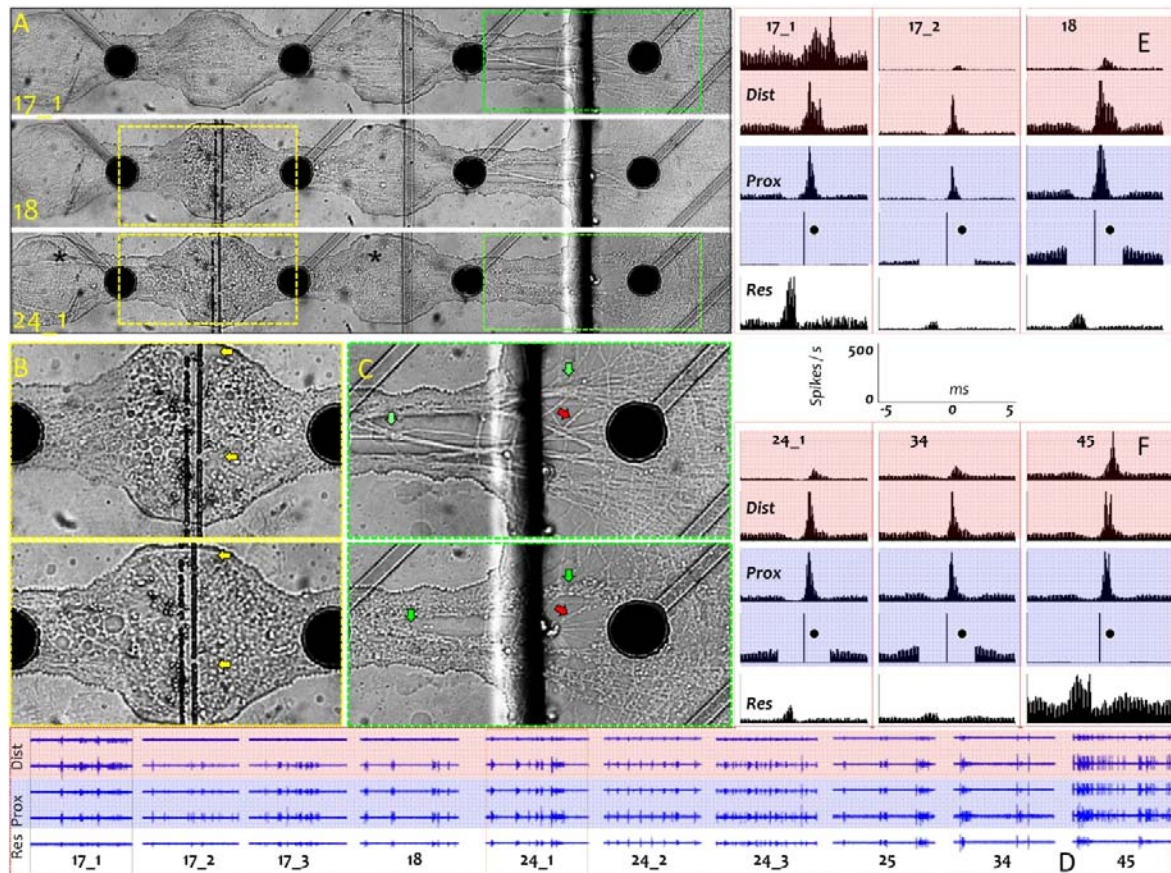


Figure 24 Axonal morphology and activity after complete dissection

Light microscopy pictures prepared before and every day after first dissection and before and every two days after second dissection for whole length of the experiment from all studied. Photos from different parts of the network were assembled and stitch together using Imagej or Photoshop software. A) Shows the baseline, one day and one week after complete dissection of all axonal bundles in a cortical culture (17_1 DIV, 18 DIV and 24 DIV, respectively). Laser line signature in the middle of the working station shows the dissection point (two parallel black lines). B) Magnified view of the yellow marked areas in A, with segregated proximal and distal parts of the axonal bundles in two sides of the dissection point in two different DIVs. Reunion of the proximal and distal parts between 18 DIV and 24 DIV has been marked by yellow. C) Magnified view of the green marked areas in A, which compares the more distal parts of the dissected axons in baseline and one week after dissection in DIV 24. Green arrows mark the degenerating axonal tissue and red arrows mark rare intact axons. D) Recording profile from electrodes recording from completely dissected axonal bundle. Each column shows 30 second recording window from two distal (red highlighted) and two proximal (blue highlighted) electrodes inside the microchannel and one most close electrode inside the reservoir in different DIVs. Maximum signal amplitude is 200 μ V. The column with black border shows the baseline and the column with red border shows the second dissection in the axons inside other microchannels. E and F) Show the cross-correlogram of the activity recorded from same electrodes in D in the selected DIVs. The first electrode inside the microchannel considered as reference electrode (black circle). Bin size: 0.0001 sec, Xmin: -0.005s and Xmax: 0.005 s. Each crosscorrelogram representing the correlation calculated from the spikes in 15 minutes of recording window. Y-axis maximum in all graphs adjusted manually to 500 spikes which was the maximum number of correlation peak in all graphs. This helps to better understand the variations which are happening over microchannel in the specific DIV or in same pairs of the electrodes in different DIVs. Correlation index between each electrode corresponding to the reference electrode is defined by the height of the correlation histogram

3.4.3 Morphology and activity in partial-partial dissected axons

A partial dissection at 17 DIV physically detached proximal and distal parts of an axon assembly while the rest of the axons in the non-dissected areas remained intact (Figure 25 A and B). Completing the axonal dissection at 24 DIV increased the gap between distal and proximal parts of the axonal bundle composed of both already degenerating and healthy axons (Figure 25 B). One week after the first dissection, degeneration was observed in distal parts including the axons entering into the opposite reservoir. However, some axons had stayed intact (Figure 25 C). Completing the dissection at 24 DIV induced the complete loss of axonal tissue in the distal section, which became particularly clear at the entry point of the opposite reservoir at later DIVs (Figure 25 C). A complete dissection in younger cultures (17 DIV) was found to be less detrimental compared to a complete dissection in older cultures (24 DIV) (Figure 24 and Figure 25).

After partial dissection, activity decreased on the distal electrodes by ...% within the first few days (Figure 25 D). In contrast, activity in the proximal section decreased for a few hours to then increase/recover again on subsequent DIVs before the second dissection was performed. The second dissection decreased the activity in the distal section, which had been regained during the week after the first dissection. Activity loss in the most distal section was permanent over the entire period (Figure 25 D). Besides changes in the overall activity level, the activity type had changed after a partial or complete dissection from burst to single spike activity or from longer to shorter burst durations (data are not shown).

Cross-correlograms showed that partial dissection decreased the activity correlation between the two sides adjacent to the dissection, which completely disappeared after the second dissection (Figure 25 E). The differences in morphology after a complete dissection at 17 and 24 DIV correlated with differences in the activity between the proximal and distal axonal regions (Figure 24 F and Figure 25 E). Furthermore, the activity in distal sections returned to baseline after four weeks after a complete dissection at 17 DIV which was not the case for axons that had been completely dissected at later DIVs (Figure 31 and Figure 32).

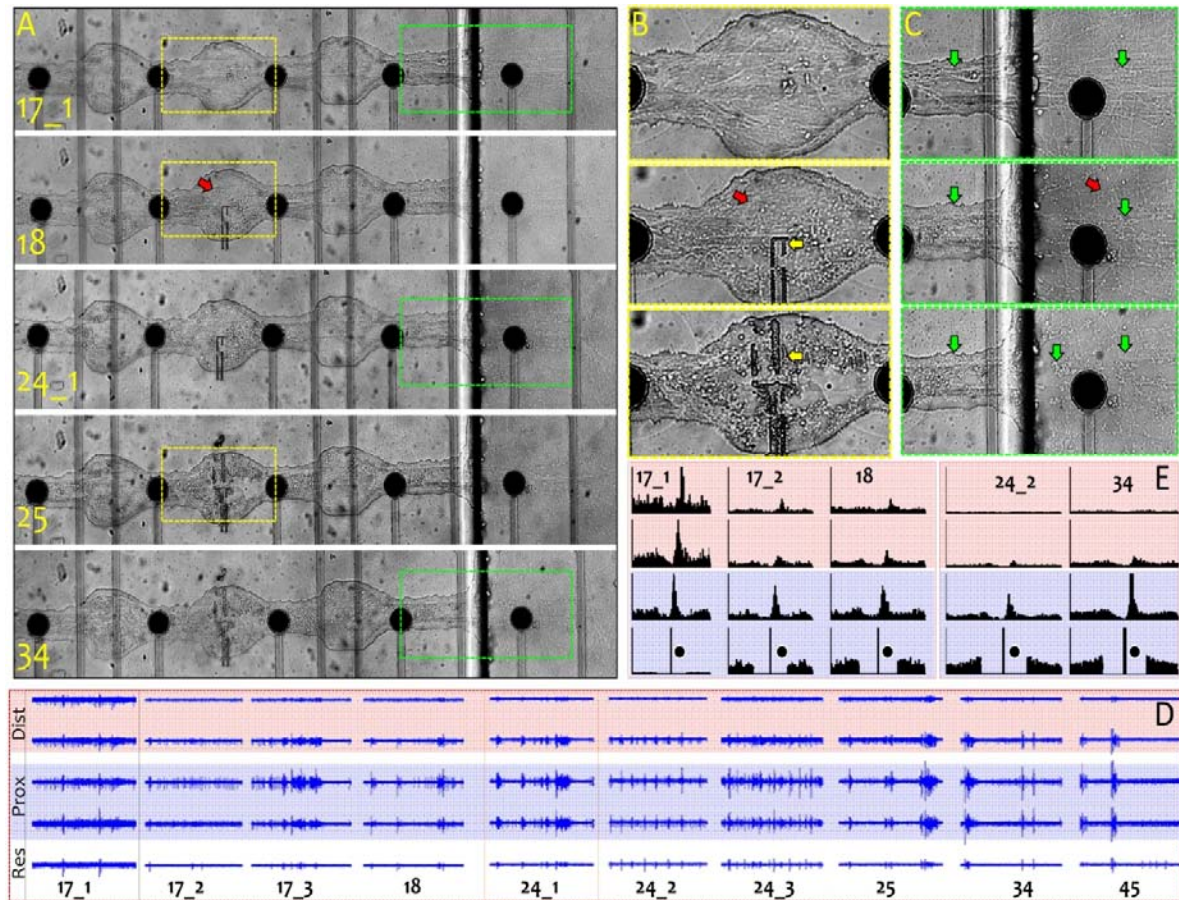


Figure 25 Axonal morphology and activity after first and second partial dissections

A) Shows the axonal morphology in baseline, one day and one week after first partial dissection, and one day and 10 days after second dissection in a cortical culture (17_1 DIV, 18 DIV, 24 DIV, 25 DIV and 34 DIV, respectively). Partial laser dissection was done in DIV 17 which is visible by laser mark on the substrate in DIV 18. Dissection was completed in DIV 24 by passing the whole wide of the working station, which is visible in the image prepared one day after in DIV 25. Pitches between each pair of the electrodes is 200 μm . B) Magnified view of yellow marked areas in A, with partial dissection of the axonal bundles in DIV 17 and completed dissection in DIV 24 (yellow arrows). The intact axons after first dissection in the non-dissected parts of the working station have been pointed by red arrows. C) Magnified view of the green marked areas in A, which compares the more distal parts of the dissected axons in baseline, one DIV after first dissection and 10 DIVs after second dissection. Green arrows mark the degenerating axonal tissue and red arrows mark the intact axons. D) Activity profile in electrodes which are recording from partially dissected axonal bundle of cortical culture. Each column shows 30 second recording window from two distal (red highlighted) and two proximal (blue highlighted) electrodes inside the microchannel and one most close electrode inside the reservoir in different DIVs. Maximum signal amplitude is 200 μV . The column with black border shows the baseline before first dissection and column with red border shows the recording at the baseline before second dissection in DIV 24. E) Cross-correlogram of the activity recorded from same electrodes in D in the selected DIVs. The first electrode inside the microchannel considered as reference electrode (black circle). Bin size: 0.0001 sec, Xmin: -0.005s and Xmax: 0.005 s. Each crosscorrelogram representing the correlation calculated from the spikes in 15 minutes of recording window. Y-axis maximum in all graphs adjusted manually to 500 spikes which was the maximum number of the correlation peak in all graphs.

3.4.4 Morphology and activity in local - partial dissected axons

For focal dissections the axonal morphology did not change notably neither at the dissection point in the working station (Figure 26 B) nor in the distal zones one week after dissection (Figure 26 C). Only very few axons at the reservoir exit showed degeneration signs one week after dissection while the majority of axons was intact (Figure 26 C). In a second dissection 7 DIV later, half of the axons of the already locally damaged axons were dissected by passing the laser twice from the edge to the center of the working station at different locations (Figure 26 A and Figure 26 B). This second dissection led to a larger segregation between the proximal and distal ends (Figure 26 B) with degeneration signs in most axons entering the opposite reservoir one week later (Figure 26 C). Comparing the effect of partial dissection in local–partial dissected axons in DIV 24 with partial dissection in partial – partial dissected axons in DIV 17 showed that partial dissection at 17 DIV was less deteriorating than at 24 DIV (Figure 25 and Figure 26).

Same to the complete or partially dissected axons in DIV 17, after very local dissection also activity decreased after dissection and returned to baseline after three hours (Figure 26 D). Activity decrease after dissection could be related to overall decrease in network activity related to complete and partial dissection in other microchannels. Even though, activity returned to normal levels one week after local dissection in the distal electrodes, second dissection decreased the activity in the distal section which had been regained during the week after first dissection. The loss of the activity in the most distal electrode last for longer time and improved in DIV 45 (Figure 26 D).

In accordance to crosscorrelograms prepared in different DIVs after first and second dissection, the connectivity between proximal and distal parts did not affect by local dissection in DIV 17, while after partial dissection in DIV 24 connectivity between two sides of the dissection point lost in subsequent weeks. This loss of connectivity was permanent in the most distal electrode inside the microchannel (Figure 26 E).

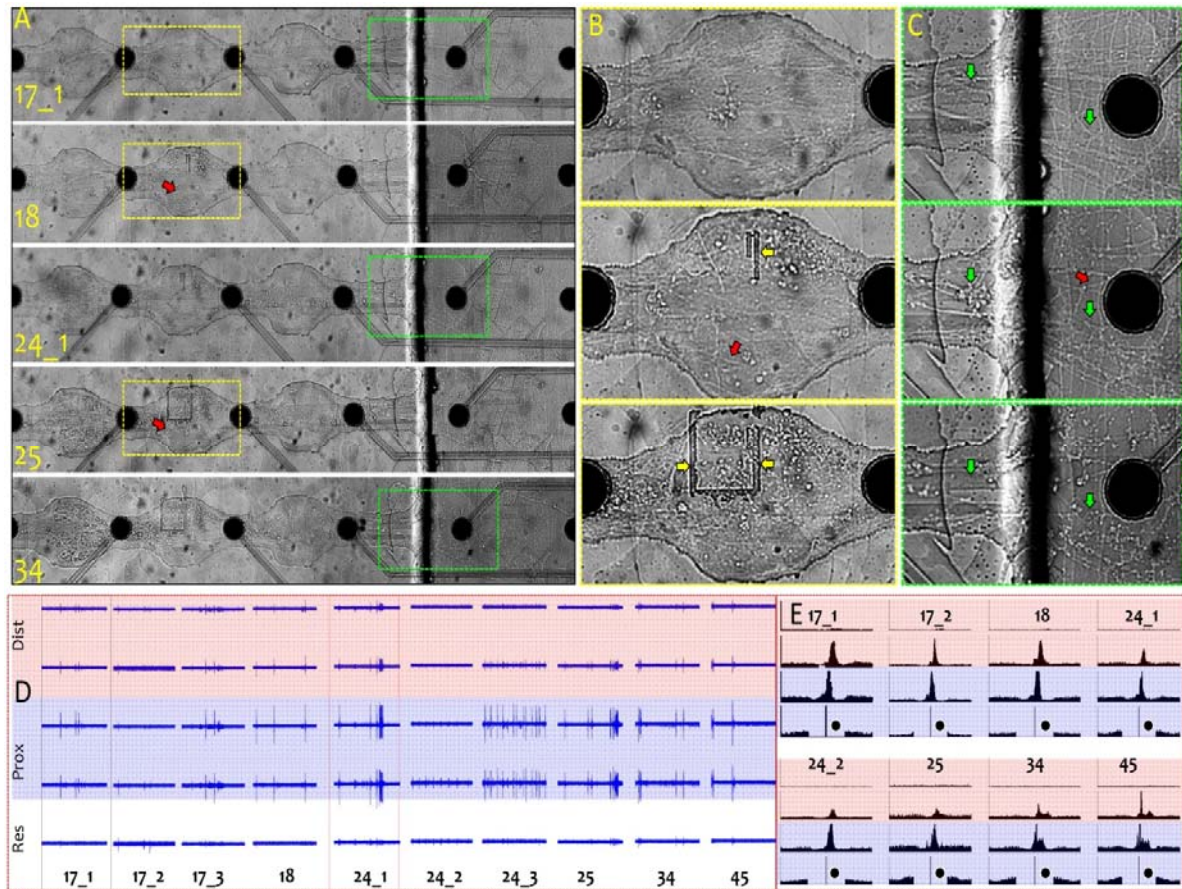


Figure 26 Axonal morphology and activity after first and second local – partial dissections

A) Shows the axonal morphology in baseline, one day and one week after local dissection, and one day and 10 days after partial dissection in a cortical culture (17_1 DIV, 18 DIV, 24 DIV, 25 DIV and 34 DIV, respectively). Very local laser dissection was done in DIV 17 which is visible by laser mark on the substrate in DIV 18. A partial dissection was done in the same side of the axonal bundles in DIV 24 by passing the half wide of the working station two times, which is visible in the image prepared one day after in DIV 25. Pitches between each pair of the electrodes is 200 μm . B) Magnified view of yellow marked areas in A, with Locally and partially dissected axonal bundles in DIV 17 and DIV 24 (yellow arrows). The intact axons after first and second dissections in the non-dissected parts of the working station have been pointed by red arrows. C) Magnified view of the green marked areas in A, which compares the more distal parts of the dissected axons in baseline, one DIV after first dissection and 10 DIVs after second dissection. Green arrows mark the degenerating axonal tissue and red arrows mark the intact axons. D) Activity profile in electrodes which are recording from locally-partially dissected axonal bundle in cortical culture. Each column shows 30 second recording window from two distal (red highlighted) and two proximal (blue highlighted) electrodes inside the microchannel and one most close electrode inside the reservoir in different DIVs. Maximum signal amplitude is 200 μV . The column with black border shows the baseline before first dissection and column with red border shows the recording at the baseline before second dissection in DIV 24. E) Cross-correlogram of the activity recorded from same electrodes in D in the selected DIVs. The first electrode inside the microchannel considered as reference electrode (black circle). Bin size: 0.0001 sec, Xmin: -0.005s and Xmax: 0.005 s. Each crosscorrelogram representing the correlation calculated from the spikes in 15 minutes of recording window. Y-axis maximum in all graphs adjusted manually to 500 spikes which was the maximum number of the correlation peak in all graphs.

3.4.5 Somata response to dissected cortical and hippocampal axons

Control cultures were treated in the same way and put in the microscopy stage for 10 min without dissection. Each cortical or hippocampal in dissected groups experienced three different types of dissection in DIV 17 and two partial dissections in DIV 24.

Activity, signal frequency, sharply increased during one week after the first dissection in cortical cultures ($p < 0.05$ vs. baseline). However, this change was not statistically significant when compared to control cultures (Figure 27 A). After the second dissection at 24 DIV, the mean firing rate was stable at ~ 5.5 spikes/s over the three subsequent weeks with no significant difference to the control group.

Both control and dissected hippocampal cultures showed a mild increase in the mean spikes frequency for the week between 17 and 24 DIVs ($p < 0.05$ vs. baseline). After second dissection activity level decreased in dissected cultures ($p < 0.05$ vs. baseline 24_1 DIV) and remained in lower levels for 10 DIVs (~ 2 spikes/s; Figure 27 B) compared to the activity in control group ($p < 0.05$), which was almost stable (~ 4 spikes/s).

To compare the activity changes over time in dissected cultures, the baseline values before the first and the second dissections (17_1 and 24_1, respectively) were subtracted from values after each dissection (17_2 to 24_1 and 24_2 to 45 DIV, respectively), and results have been summarized in Figure 27 C to F. After the first or second dissection almost all electrodes showed activity decrease which lasted for one day (Figure 27 C). This effect was more profound after the second dissection in cortical cultures (Figure 27 E). Activity returned to baseline one day after the first dissection and then increased over the subsequent week ($p < 0.001$ vs. baseline). However, after the second dissection activity did not change significantly with respect to the pre-dissection values at 24 DIV (24_1). In hippocampal cultures, activity increased mildly after the first dissection (Figure 27 D and Figure 27 F). However, activity dropped to lower levels after the second dissection and remained lower for 10 subsequent DIVs ($p < 0.001$ vs. baseline 24_1). Although most electrodes in both cultures showed slight activity changes over time, on some electrodes sharp changes in activity appeared just after dissection or at DIVs later (Figure 27 D). Excluding these electrodes from analysis showed that general network activity also changed after dissection (Figure 27 F)

which confirmed that not only in the affected neurons, but also in the whole network activity dynamics shifted after dissection.

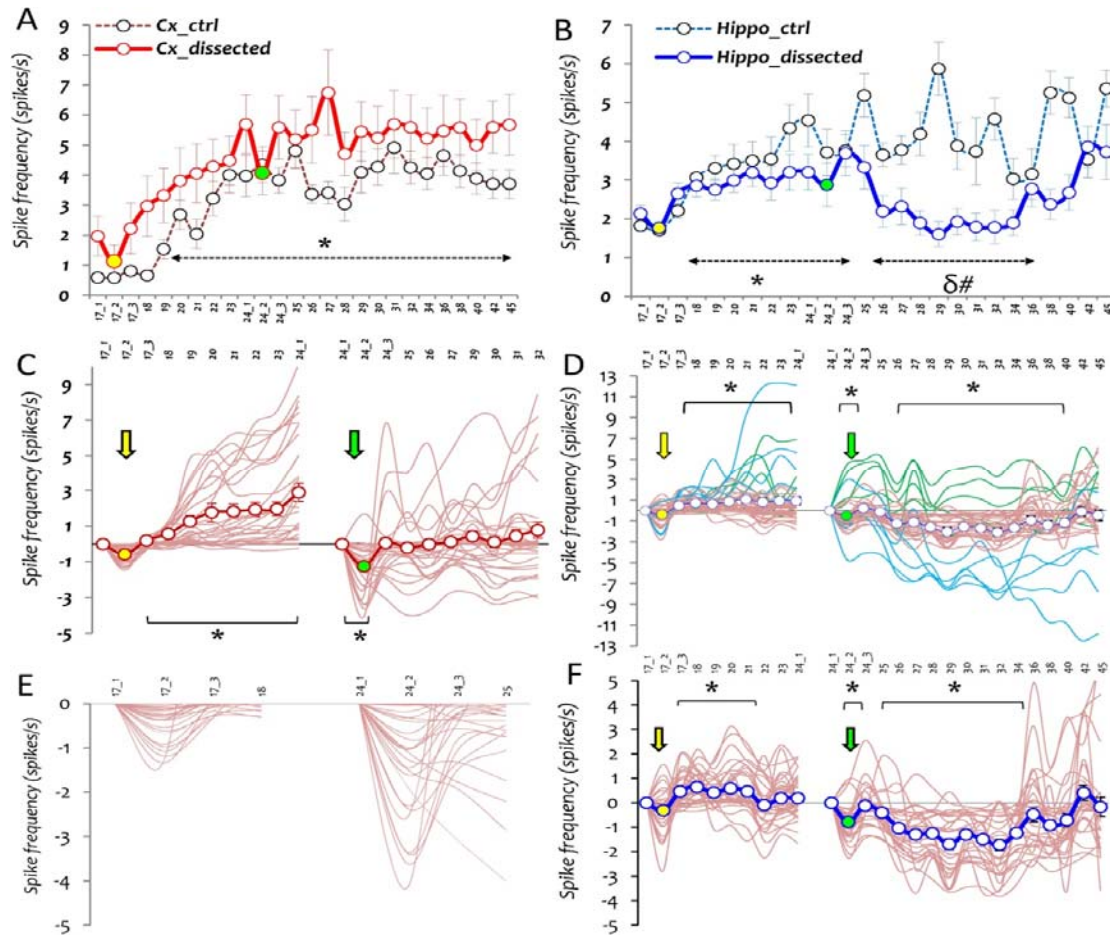


Figure 27 Somata response to axonal dissection in cortical and hippocampal cultures.

A) Shows the raw spike frequency (spikes / s) in electrodes recording from control (Cx_ctrl) and dissected (Cx_dissected) cortical cultures. B) Shows the raw spike frequency (spikes / s) in electrodes recording from control (Hippo_ctrl) and dissected (Hippo_dissected) hippocampal cultures. Data are represented as mean \pm S.E.M of spike frequency in all active electrodes of same group in each day. Mixed ANNOVA followed by post-hoc Tukey test was applied to compare dissected groups with ctrl groups in different time points. # $p < 0.05$ vs. ctrl group. Repeated measure ANNOVA based on estimated marginal means and multiple comparisons adjustment by Bonferroni used to compare vs. baseline in the same group. * $p < 0.05$ vs. 17_1 DIV, $\delta p < 0.05$ vs. 24_1 DIV. C) Shows the activity difference vs. baseline after first or second dissections in cortical cultures. Each thin red line represents activity in one electrode ($n = 36$) and the thick marked lines show the mean \pm S.E.M. yellow and green arrows representing the time of first and second dissections, respectively. E) Magnified view of decreased activity in most of the electrodes recording from cortical cultures for one day after first or second dissections. D) Activity difference vs. baseline in hippocampal cultures ($n = 44$). Each green and blue line represents an electrode which recorded sharp response to the dissection compared to other electrodes ($n = 9$). F) Individual and general activity in electrodes which showed mild response to the dissection ($n = 35$). The resulted data was compared to baseline values by repeated measure ANNOVA based on estimated marginal means and multiple comparisons adjustment by Bonferroni (* $p < 0.001$).

3.4.6 Activity recorded from axons in direct microchannels vs MCh_ws

To ensure that the changes in microchannel geometry had no significant effect on the biophysical properties of the recorded signals, we compared the spike rate in microchannels with working stations (MCh_ws) with control microchannels (MCh_direct) in control hippocampal culture. As shown in Fig. 8 A, there was no significant difference in the mean spike frequency on electrodes inside the MCh_direct and MCh_ws. Both cases showed the same fluctuations in somal network activity over time, as shown in Figure 28 A (Hippo_ctrl). To capture activity changes inside the microchannels beyond fluctuations in overall network activity, the spike rate in each microchannel type was normalized to the maximum activity recorded by one of the electrodes in that type of microchannel. Results are summarized in Figure 28 B. Regardless of the general decrease or increase in overall network activity, the mean activity remained stable in 50% to 80% of the cases (Figure 28 B). Because each microchannel contained a random number of axons, electrodes inside one microchannel could show different baseline activity compared to electrodes in other microchannels. Normalizing the data excluded the differences in baseline activity between different microchannels.

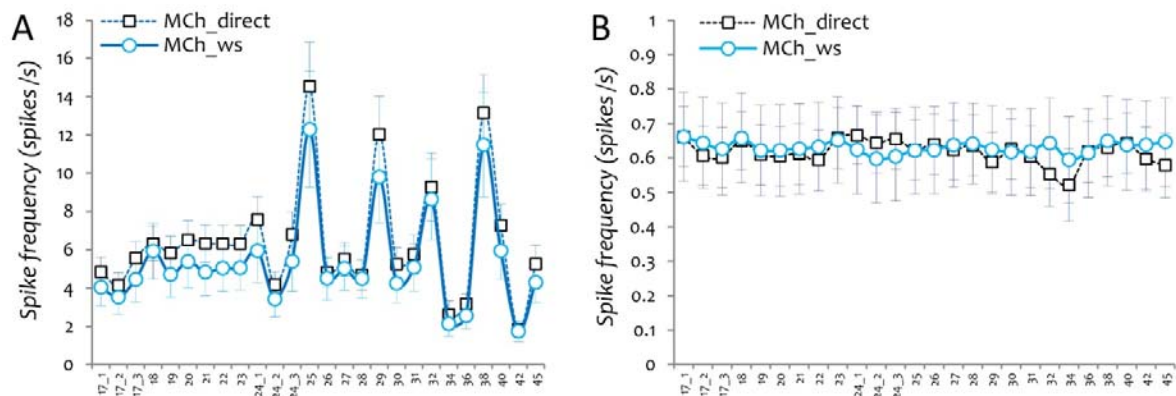


Figure 28 Activity recorded from MCh_ws vs MCh_direct

A) Raw and B) normalized spike frequency in direct microchannels (MCh_direct; black square) vs. microchannels with working stations (MCh_ws; blue circles) in control hippocampal cultures. Yellow and green arrows show the first and second dissection time points, respectively. Raw spike frequency is calculated by mean firing rate in all electrodes recording from each microchannel types in control hippocampal cultures ($n=19$ in MCh-direct and $n=12$ in MCh-ws). To normalize the activity in each channel type activity in each day divided by the maximum activity on that day in specific MEA, and the results were averaged over MEAs. Data were normalized to exclude normal fluctuation in activity of each culture over time, as well as the activity difference between cultures of same group in each recording DIV. Data are represented as mean \pm S.E.M.

3.4.7 Activity recorded from dissected axons vs. intact axons

To compare the activity between dissected and control axons of same cultures, all types of dissected axons including spot, half and completely dissected axons were considered as one group and the mean spike frequency in electrodes recording from these axons compared with control axons in each day. Figure 29 A and B summarized the effect of first and second dissections on general activity recorded from all electrodes inside the microchannels in *hippocampal cultures*. In spite of the similar baseline activity in dissected and control axons at DIV 17_1, a sharp and significant decrease of activity happens in dissected axons compared to control axons ($p < 0.01$). In one week after dissection activity increases both in control and dissected axons, however the mean spike frequency in dissected axons remained in significantly lower levels than the control axons ($p < 0.01$). In second dissection activity in control axons was not affected for three days, after which activity decreases over time up to DIV 45 (Figure 29 A). In contrast the decreasing trend of activity in dissected axons started just after second dissection and remained in significantly lower levels than the control axons up to DIV 45 ($p < 0.01$). The increase and decrease in control axons activity had the same profile as the activity recorded from somata in reservoirs (Figure 29 A and Figure 27 B) which suggested that such changes in axonal activity could be dictated from reservoir section. This hypothesis confirmed by running the same analysis for normalized data in control axons (Figure 29 B), which showed a stable activity in control axons for whole length of experiment. Interestingly, normalized data showed activity decrease in dissected axons after first dissection which was completely different from activity increase in accordance to raw data (Figure 29 A and B). These data clearly showed two different phases of activity drop in dissected axons after first and second dissections to 0.7 and 0.5 of maximum activity ($p < 0.05$ and $p < 0.01$ vs. ctrl axons, respectively).

In *cortical culture* similar results have been acquired in accordance to the raw and normalized data (Figure 29 C and D). After first and second dissections, activity in dissected axons dropped to lower levels, but it returned to basal level after three hours, increased significantly after one day ($p < 0.05$ vs. baseline 17_1), and remained in higher levels for subsequent week (Figure 29 C). In all time-points after first dissection activity in control cultures were significantly higher than dissected axons ($p < 0.01$). Same analysis on

normalized data showed a stable activity in control axons (Figure 29 D), but little drop in activity after first dissection and further changes after second dissection in the dissected axons (Figure 29 D; $p < 0.05$ vs. ctrl axons), even though these effect was not as strong as activity decrease in the dissected hippocampal axons. The difference responses in cortical and hippocampal axons to the same level of the injury will be clarified in next sections when we tried to compare the activity between proximal and distal parts of dissected axons.

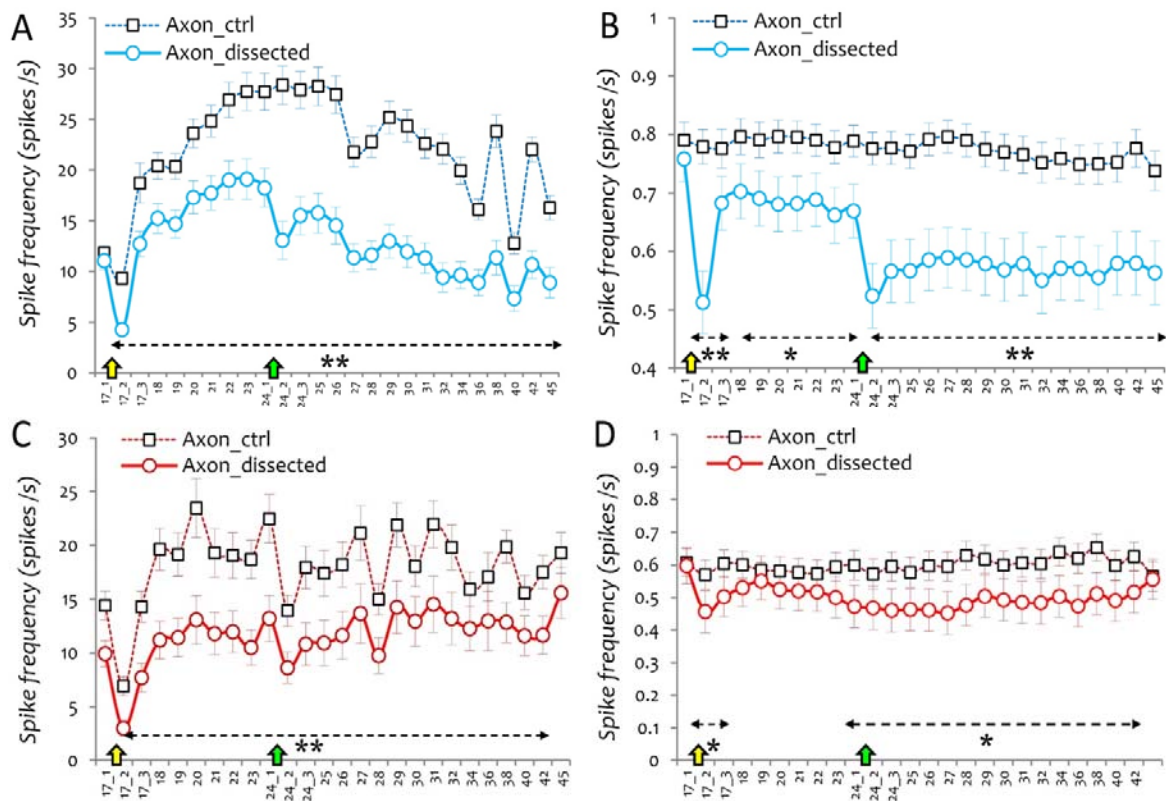


Figure 29 Activity recorded from dissected axons vs. intact axons

A) Raw and B) normalized spike frequency in electrodes recording from control axons (Axon_ctrl; black square), and dissected axons (Axon_dissected; blue circle), in hippocampal cultures which experienced dissection. The data for dissected axons has been averaged across axons inside all MCh-ws which experienced different types of dissection (spot, half, whole). In general 100 electrodes were recording from control axons in direct microchannels and 60 electrodes from different types of dissected axons in MCh-ws microchannels of hippocampal cultures. C) Raw and D) normalized spike frequency in electrodes recording from control axons (Axon_ctrl; black square), and dissected axons (Axon_dissected; red circle), in cortical cultures which experienced dissection. The data for dissected axons has been averaged across axons inside all MCh-ws which experienced different types of dissection (spot, half, whole). In general 80 electrodes were recording from control axons in direct microchannels and 44 electrodes from different types of dissected axons in MCh-ws microchannels of hippocampal cultures. Mixed ANNOVA followed by post-hoc Tukey test was applied to compare dissected Axons with control axons of same cultures in different time points. * $p < 0.05$ and ** $p < 0.01$ vs. control axons of same cultures in that specific time point (DIV).

3.4.8 Axonal response to different types of dissection

Axons of same culture in different microchannels experienced different level of injury by providing very local to complete dissection in axonal bundles. Before comparing the data between different types of dissection, baseline activity (DIV 17_1) has been subtracted from the activity in other DIVs in each individual electrode recording from specific part of axons in individual microchannel and then data averaged across electrodes belonging to the same group. This is done because axons in different dissection groups had different basal activity (Figure 30).

In *hippocampal cultures*, regardless of different levels of axonal damage (spot, half, complete dissection of axonal bundle), activity decreased just after dissection ($p < 0.05$ vs. baseline), returned to basal level after three hours and increased over the subsequent week (Figure 30 A; $p < 0.05$ vs. baseline). At 24 DIV, the dissected axonal bundles (half and spot) were subjected to a second dissection (extra half dissection in both of them), which sharply decreased activity in both cases ($p < 0.05$ vs. baseline 24_1) while it had no effect on completely dissected axons which left intact in DIV 24. During the subsequent weeks, activity gradually decreased in local and half dissected axons which had an extra dissection in DIV 24 ($p < 0.05$ vs. baseline 24_1). However, the activity remained stable in dissected axons which left intact in DIV 24 (Figure 30 A) and its level was significantly higher than the activity in axons which experienced an extra dissection in DIV 24 ($p < 0.05$). Completely dissected axons endure a sharper decrease in activity for the week after the first dissection compared to locally or half dissected axonal bundles (Fig. 9 B; $p < 0.05$). After the second dissection, the activity profile in three different types of dissected axons were almost the same, with a sharp activity decrease of axons which experienced an extra dissection and stable activity in axons which were left intact at 24 DIV (Figure 30 B).

In *cortical cultures*, the same decrease after the first dissection appeared which returned to baseline levels in three hours and remained at normal levels thereafter, except for the locally dissected axonal bundles which showed significant increase in activity after 18 DIV (Figure 30 C; $p < 0.05$ vs. baseline 17_1, $p < 0.05$ vs. completely dissected axons). The same activity profile appeared after the second dissection. Activity decreased after the first dissection and remained at the same levels thereafter (Figure 30 D).

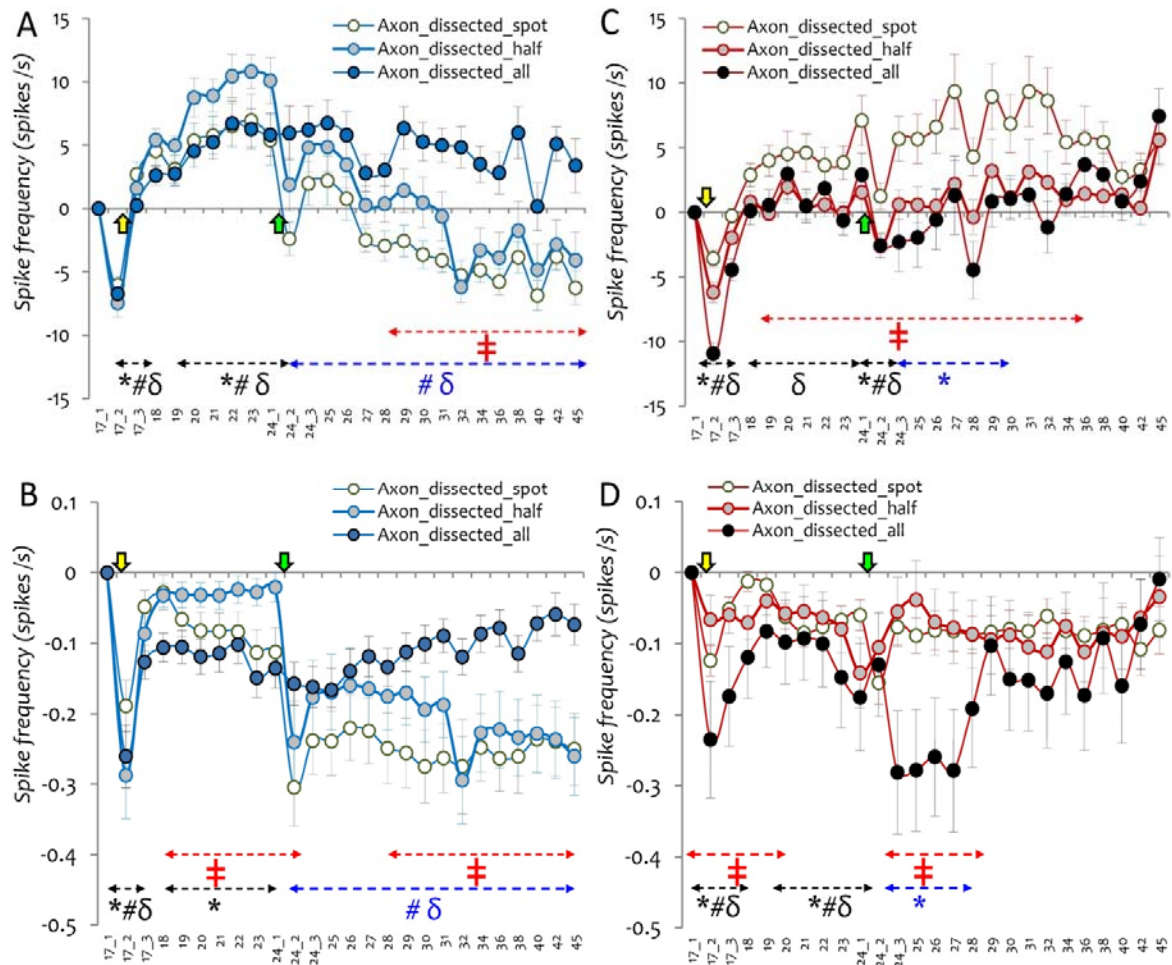


Figure 30 Axonal response to different types of dissection

A) Raw and B) normalized spike frequency in completely (all) vs. half vs. locally (spot) dissected axonal bundles in hippocampal culture. C) Raw and D) normalized spike frequency in completely (all) vs. half vs. locally (spot) dissected axonal bundles in cortical culture. Activity in completely dissected axons is shown by dark red circle, in half dissected axons by gray circle, and in local dissection is shown by free circles. Because axons in different dissection groups had different basal activity, in all cases basal activity (17_1) has been subtracted from the raw activity in each time point for each individual electrode recording from the dissected axons. Activity in completely dissected axons is shown by dark blue circle, in half dissected axons by gray circle, and in local dissection is shown by free circles. Each graph representing the data gathered from 20 electrodes recording activity from one type of dissected axons. To normalize the activity in each channel type activity in each day divided by the maximum activity on that day in specific MEA, and the results were averaged over MEAs. Data are represented as mean \pm S.E.M. The resulted data in each group of dissected axons was compared to baseline values by repeated measure ANNOVA based on estimated marginal means and multiple comparisons adjustment by Bonferroni. * $p < 0.05$, # $p < 0.05$ and $\delta p < 0.05$ vs. baseline (17_1) in completely dissected, half dissected and local dissected axons, respectively. # $p < 0.05$ and $\delta p < 0.05$ vs. baseline (24_1) in half dissected and local dissected axons, respectively. In addition mixed ANNOVA followed by post-hoc Tukey test was applied to compare the mean difference between groups in each time point. † $p < 0.05$ vs. completely dissected axons in the same DIV.

3.4.9 Activity in proximal vs. distal parts of dissected axons in *hippocampal cultures*

For all analysis comparing the activity between proximal and distal parts, two proximal electrodes were considered as one group as well as two distal electrodes (Figure 6). To normalize the data or subtract the baseline values, each electrode treated individually and resulted values were averaged across the same group.

As shown in Figure 31 B, the distal section of axons was affected profoundly by a complete dissection. Its spike frequency remained significantly lower compared to that in the proximal parts of same axonal bundles where the activity actually increased on later DIVs (Figure 31 A; $p < 0.05$). In partially and locally dissected axonal bundles, even though the activity in the distal section was lower than in the proximal section, the difference was not significant. However, after completing the dissection at 24 DIV for partially dissected axons and inflicting partial damage to locally dissected axons, activity in the distal sections of both types of dissected axonal bundles dropped significantly compared to their proximal sections (Figure 31 A; $p < 0.05$). Equally, the normalized data showed activity loss for the distal section of completely dissected axons and remained at significantly lower levels compared to both its previous baseline activity ($p < 0.05$ vs. DIV 17_1) and activity in the proximal section ($p < 0.01$).

After a second dissection in other axonal bundles, activity in the distal section of already completely dissected axons remained constant (vs. DIV 24_1) and gradually returned to baseline levels over the days (Figure 31 a). In contrast, half and locally dissected axons left a clear activity loss signature after their first (DIVs 17_1) and second (24_1) dissection (Figure 31 b and c). In both cases, the activity in the distal section decreased mildly after the first dissection ($p < 0.05$ vs. baseline 17_1), whereas completing the dissection in half-dissected axons and partially dissecting locally dissected axonal bundles at 24 DIV led to a very sharp and permanent activity decrease ($p < 0.01$ vs. baseline DIV 24_1). Activity in the distal section was significantly lower than in the proximal parts of the same axonal bundles in the week after the first ($p < 0.05$) and second dissections ($p < 0.01$) in half or locally dissected axons. In contrast, there were no significant activity changes in proximal axonal compartments when compared to the baseline either after the first or second dissection (Figure 31 b and c).

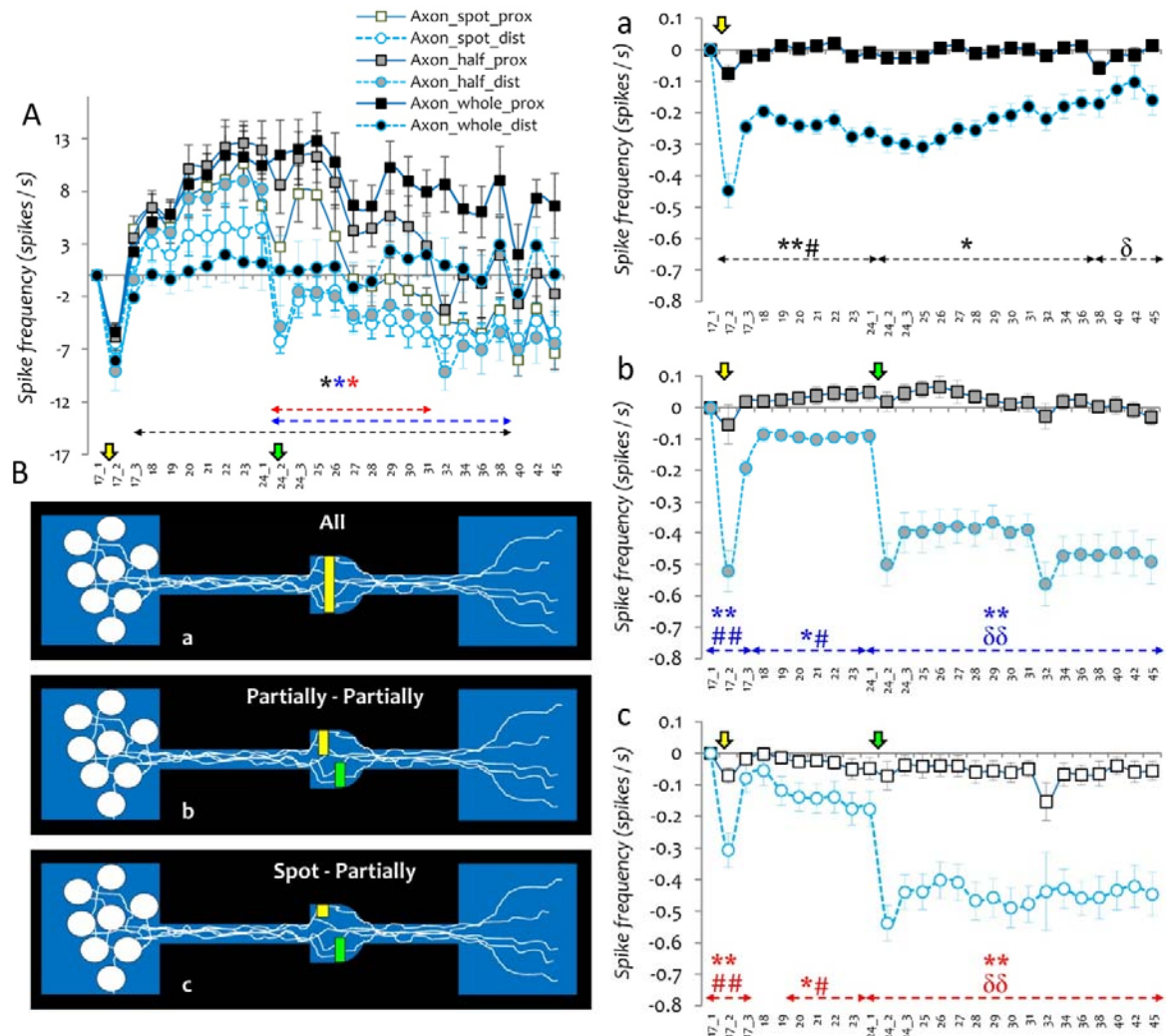


Figure 31 Activity in the proximal and distal parts of dissected hippocampal axons

In each microchannel two electrodes and in general 30 electrodes were recording the activity from proximal parts of dissected axons in hippocampal cultures and the other 30 electrodes were recording from distal parts of the same axons. A) After subtracting the basal activity from the mean activity in proximal or distal parts in different types of dissected axons in each DIV, results were compared between proximal and distal sections. Results are represented as mean \pm S.E.M. Mixed ANNOVA followed by post-hoc Tukey test was applied to compare the mean difference between activity in proximal and distal sections of each type of dissected axons in specific DIV. * $p < 0.05$, * $p < 0.05$ and * $p < 0.05$ vs. activity in proximal section of completely, half, and locally dissected axons, respectively. B) Shows the different types of dissection in axons including; a) complete dissection in DIV 17, b) partially dissection in DIV 17 and completing the dissection in DIV 24, c) locally dissecting few branches in DIV 17 and partially dissecting in DIV 24. Yellow marks representing the dissection in DIV 17 and green marks show the dissection in DIV 24. a, b, c) Are representing the results of normalized activity recorded from electrodes in proximal and distal parts of completely, partially and locally dissected axons to the maximum activity. In each type of dissected axon baseline value for distal or proximal sections were subtracted from the activity in other DIVs and results compared to baseline values by repeated measure ANNOVA. # $p < 0.05$, and ## $p < 0.01$ vs. baseline (DIV 17_1) and δ $p < 0.05$ and $\delta\delta$ $p < 0.01$ vs. baseline (DIV 24_1). Mixed ANNOVA followed by post-hoc Tukey test was applied to compare proximal and distal section. * $p < 0.05$, ** $p < 0.01$ vs. proximal section in the same DIV.

3.4.10 Activity in proximal vs. distal parts of dissected axons in cortical cultures

In accordance to the spike rate data collected from proximal and distal electrodes in dissected cortical cultures, activity was dramatically affected in the distal section of all types of dissected cortical axons (Figure 6). It remained significantly lower compared to the activity in the proximal parts of same axonal bundles, which actually showed an activity increase over the entire study (Figure 32 A; $p < 0.05$). As Figure 32 A suggests, activity was affected more in completely dissected axons.

The normalized activity (Figure 32 a) in the distal section of completely dissected axons revealed a loss in activity, which remained at significantly lower levels compared to both baseline activity ($p < 0.05$ vs. DIV 17_1) and that in the proximal section ($p < 0.01$). Proximal parts of these axonal bundles experience a non-significant increase of activity over whole length of the study (Figure 32 a). After second dissection in other axonal bundles, activity in the distal section of completely dissected axons which had been left intact during the second dissection, remained constant (vs. DIV 24_1) and in very later DIVs activity in the distal parts of the completely dissected axons increased to the higher levels (Figure 32 a). In the locally dissected axons first and second dissections provided clear signature on activity loss after DIVs 17_1 and 24_1 (Figure 32 b and c). In both cases activity in the distal section decreased mildly after first dissection ($p < 0.05$ vs. baseline 17_1 in half dissected axons), however completing the dissection in half dissected axons and providing partial dissection in locally dissected axonal bundles in DIV 24, produced further decrease in the activity in the distal sections ($p < 0.01$ vs. baseline DIV 24_1; locally dissected axons). Activity in the distal section was significantly lower than the proximal parts of same axonal bundles in the week after first dissection ($p < 0.05$) in half dissected axons, and second dissection ($p < 0.01$) in half or locally dissected axons. Proximal parts in all kind of dissections did not show significant changes in activity compared to the baseline either after first dissection or after second dissection (Figure 32 b and c).

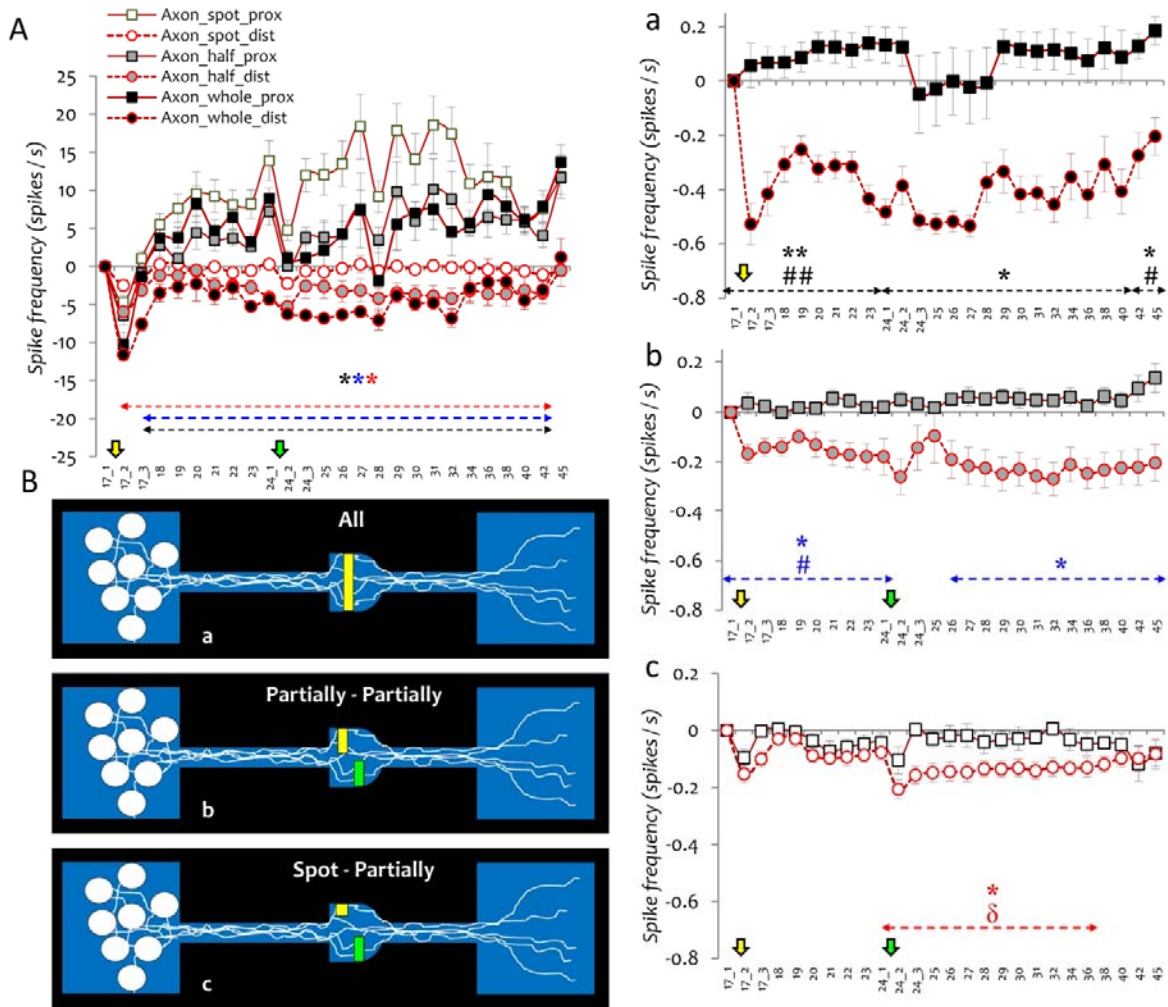


Figure 32 Activity in the proximal and distal parts of dissected cortical axons

A) After subtracting the basal activity from the mean activity in proximal or distal parts in different types of dissected axons in each DIV, results were compared between proximal and distal sections in different DIVs. Results are represented as mean \pm S.E.M. Mixed ANNOVA followed by post-hoc Tukey test was applied to compare activity in proximal and distal sections of each type of dissected axons in specific DIV. * $p < 0.05$, * $p < 0.05$ and * $p < 0.05$ vs. activity in proximal section of completely, half, and locally dissected axons, respectively. B) Shows the different types of dissection in axons including; a) complete dissection in DIV 17, b) partially dissecting axons in DIV 17 and completing the dissection in DIV 24, c) locally dissecting few branches in DIV 17 and partially dissecting in DIV 24 in the same microchannel. Yellow marks representing the dissection in DIV 17 and green marks show the dissection in DIV 24. a, b, c) Are representing the results of normalized activity recorded from electrodes in proximal and distal parts of completely, partially and locally dissected axons to the maximum activity. In each type of dissected axon baseline value for distal or proximal sections were subtracted from the activity in other DIVs and results compared to the baseline values by repeated measure ANNOVA based on estimated marginal means and multiple comparisons adjustment by Bonferroni. # $p < 0.05$, and ## $p < 0.01$ vs. baseline (DIV 17_1) and δ $p < 0.05$ vs. baseline (DIV 24_1). Mixed ANNOVA followed by post-hoc Tukey test was applied to compare the mean difference between proximal and distal section in each type of dissected axons. * $p < 0.05$, ** $p < 0.01$ vs. proximal section in the same DIV.

D

iscussion

Over different trials we tried to optimize the PDMS devices in a way which is more compatible with MEA electrophysiology and optical imaging or manipulations. The device thickness in all cases was less than 200 μm which increased its transparency to trace the neurite growth inside microchannel by bright-field or phase contrast up-right or inverted microscopy. In addition, to limit the network size for electrode-included areas in the MEA substrate and simplify it for studying we developed feasible and simple cell seeding method (Figure 16 and Figure 14).

The presented examples in the first step demonstrated combined replica-molding process for PDMS microchannel scaffolds and extracellular recording by MEAs as a tool for compartmentalizing the network functional modules, soma and axons, and studying activity dynamics in these two compartments separately. Because the device makes it possible for non-invasive extracellular recording of very weak activity from axons and soma, it is possible to trace the activity fluctuations for long-term experiments. Regardless of the small network sizes used in the present study we could keep cultures alive for more than 3 months in most cases. In addition the physical confinements provided by microchannels and reservoirs provide a constant microenvironment for axons and cell body and prevent from sharp fluctuations in cell culture environment due to temperature changes or adding the fresh medium which shifts the activity in whole network (). The similar devices already have been developed by Taylor et la., successfully separated the axons from cell body and have been applied in different approaches for understanding axonal biology without intervening effects of somata (). For instance the same device used for studying protein and gene expression in axons () or for axonal degeneration () as well as axon and glial cell interactions (). In the present study, we tried to combine PDMS provided physical confinements with

commercially available MEAs for exploiting their advantages in studying axonal electrophysiology.

After validating the first generation combined PDMS – MEA setup by providing axonal modules and recording separately from each module very local axonal injury provided inside the selected microchannels by laser microdissection (LMD), to see whether the subjected axon and intact axons respond to the local injury. In the same time it was possible to record network activity from which axons had been originated. Because the damage was done by laser light without affecting the cell culture environment or infecting the culture medium, it was possible to study the pure effect of the local damage on network dynamics in different levels (soma, intact axons, damaged axons, as well as proximal and distal parts of dissected axons) over weeks after dissection. Because regeneration is a time dependent procedure and occurs in log-term (), beside the structural changes happening during the regeneration, it would be great to understand the functionality of regenerating network, axons. Definitely, adding other approaches to the present combined setup will help to unravel complex questions either in normal developing networks or in degenerating and regenerating networks.

4.5 Multicompartment device for axon guidance and electrophysiology

We showed that axons can be easily guided in crossing microchannels that were aligned on top of the recording electrodes of a MEA. This allowed the detailed evaluation of axonal morphology, the different types of activity and their propagation velocity along channels over time. In the crossing microchannels we found that the signal frequency decreased between proximal and distal segments of a microchannel. This could have two reasons: axons may leave the straight path by changing their growth direction at the channel crossing points (Figure 13). Axonal bundles were getting diluted in subsequent crossing by diverting from main root and growing into other microchannels or releasing into the compartment in one side (Figure 8). Furthermore, the signal could be fading along the channel as it was evident in most cases (Figure 9 and Figure 10 and Figure 11).

The effect of microchannel geometry on signal quality has been evaluated by Wang et al. (Ling, 2011) They showed that in microchannels with lengths between 200 μm and 3000 μm the signal amplitude decreases along the channel length. Therefore, signals could become

too small to be detected by electrodes in distal sections. In accordance with Figure 9, large amplitude signals in proximal sections (electrode 68) decrease as they propagate within the channel. In accordance to Wang et al. (Ling et al., 2012), the high microchannel resistance combined with its stray capacitance act like a first-order low pass filter that attenuate high frequency signal amplitudes (i.e. the **negative peaks of an action potential**). Equally, the channel cross-section can affect signal properties (Ling, 2011). Although all microchannels had the same cross-section, the number of axons and the thickness of the axon bundles inside the microchannel varied with channel depth and over time, thereby changing the total cross-section of a microchannel at different channel locations. In 2009, Dworak and Wheeler showed that the growth of neurites inside the microchannels (750x10x3 μm) increased the resistivity from 75 $\Omega\text{ cm}$ of empty channels to 300 $\Omega\text{ cm}$ for microchannels filled with neural tissue) due to an effective decrease of the channel cross section (Dworak and Wheeler, 2009).

The increase of neural tissue mass inside the microchannels between 20 and 30 DIVs (Figure 12) could be correlated with an increased spike frequency for almost all channels and all channel segments (Figure 11). Equally, a decrease in neural tissue density after 53 DIV led to a decrease in the firing frequency in all channels (Figure 11). A significant decrease of the signal frequency after 53 DIV in all segments could be related to the axonal degeneration and the formation of axonal bundles (Figure 12).

Recording an action potential from subsequent electrodes along a microchannel enabled us to determine the propagation velocity and direction. The propagation velocities varied between 0.1 to 2.5 m/s, which is in same range as previously reported by Pan et al., (0.18 to 1.14 m s^{-1} in unmyelinated axons; (Pan et al., 2011)). In the presented study, we also evaluated changes in the propagation velocities in different segments of the same microchannel as well as in same segment of different microchannels over time. Changes in action potential velocity along the axon could be related to changes in thickness and curvatures along the axon. We also observed an increased propagation velocity in all channels between 30 and 53 DIV, which could possibly be related to increased axonal diameters or the fasciculation of axons. similar spatial and temporal changes in stimulus-driven action potential propagation velocity have recently been reported by Bakkum et al.,

(Bakkum et al., 2013a). In the present study, we evaluated the propagation velocity of signals derived from normal activity of network over time.

Bursts are spike flares within a short time window. Bursts are usually recorded simultaneously from different MEA electrodes, which shows that burst activity involves and propagates within large parts of the network (Maeda et al., 1995). We also evaluated how bursts propagate inside the crossing microchannels. While individual monophasic spikes are able to propagate over long distances within a channel, bursts failed in reaching the microchannel endings in most cases (Figure 12). A significant difference in burst frequency on electrodes in proximal and distal parts of the crossing microchannels confirmed the observed burst propagation fading along the crossing microchannel (Figure 12). Because bursts are composed of individual spikes with different shapes, each of them will have its specific half-life for traveling along the channel. Fading spikes inside a burst will cause the burst to disintegrate along the channel. In consequence, a spike sequence that was categorized as a burst at the proximal end of a channel may not be recognized as a burst anymore at the distal end of a channel. Another mechanism for burst fading could be based on a phase cancelling effect. Signals with different shapes and phases can cancel each other out while traveling along the channel (Ling et al., 2012).

4.1.1 Advantage and disadvantages of multicompartment device

The PDMS device with four compartments, one as somal compartment and three other as axonal compartments and crossing microchannels provided a feasible setup for studying axonal growth and guidance into the microchannels with the availability of recording from them in different positions. . Similar device has already been developed by Park et al., for in vitro CNS axon-glia interaction and axonal myelination research, capable of conducting up to six independent experiments in parallel for higher-throughput (Park et al., 2009a; Park et al., 2009b). In the same device it is possible to apply growth factors or degenerating agents through one compartment and run parallel experiments on the affect and no-affect axons from the same culture. Fluidic isolation between neuronal cell body and axonal compartments gives the opportunity to add desired cell type or agents into the axonal compartment and study axonal response without intervening effects of the cell body. In our device we designed the configuration compatible with commercial MEAs to give the

opportunity for studying the axonal electrophysiology and morphology inside the microchannels along other approaches.

Even though crossing microchannel configuration provide useful information about axonal electrophysiology, action potential propagation properties, as well as burst propagation up to 70 DIVs, it suffered from few drawbacks related to design, including:

- a) Long crossing microchannels (1400 μm – 2000 μm) covered all 8 electrodes in each row. However most signals were faded beyond 800 μm because of axonal divergence from main root and signal fading along the microchannel related to its biophysical properties (wide microchannels; 40 μm).
- b) The crossing points in microchannel structures mixed axons from different microchannels together which made it difficult to trace the specific axonal bundle inside the microchannel.
- c) Because of large microchannel area (> 1400 x 1400 μm), it was not possible to align also the reservoir section with part of the electrodes to obtain simultaneous recording from network inside the reservoir.

4.2 Two compartment devices with straight microchannels

4.2.1 Opening the reservoirs from top and recording issue

This device overcame most deficiencies in multicompartiment devices by including straight and shorter microchannels (800 μm) connecting two small reservoirs. Microchannels covered only 4 electrodes in each row and 2 electrodes in each side of the microchannel left for recording from the small area of the reservoirs. However, it was not possible to record from small network in the reservoirs which had openings from the top side (Section 3.2.1).

4.2.2 Closed chamber two-compartment device for optimal electrophysiology

Closing the reservoirs from top side by simple modifications in the PDMS molding procedure (Figure 2) improved the signal quality in the reservoir section (Section 3.3.1). In this device we kept small world networks (< 3000 neuron/device) alive with recordable activity for more than 3 months. In accordance to the previous studies it is difficult to keep low density networks alive for longer periods () and in most cases they do not give enough

activity to be used for analysis or interpreting the network functional properties (). The main intention in decreasing the network sized was to simplify its complexity. Therefore, providing small networks with rich activity for weeks and months could be exploited for different types of experiment in developing neurons *in vitro*.

In addition, closed chambers keeps the cell culture environment almost in stable conditions and prevents from rapid changes in pH, temperature and mechanical disturbance even during medium exchange. These closed chambers connected by tiny gates ($\sim 100 \mu\text{m} \times 200 \mu\text{m}$) into the opening pools (Figure 3 and Figure 16), which dampens the changes happening in the cell culture medium outside of the reservoirs. This could be a great advantage for devices with applications in electrophysiology, because network activity is prone to even slight fluctuations in culture environment which can affect the results of the experiment (). For instance, in any recording trial the whole MEA and device assembly had to be taken out of the incubator and carry to the recording stage, a procedure composed of mechanical and thermal changes affecting the activity profile.

4.2.2.1 Providing bi-directional axonal bundles in microchannels

Fabricating two big openings in two far edges of the microchannel and increasing the device wetability, by incubating it with cell culture medium overnight, facilitated cell seeding into the small area of the closed chambers ($0.4 \times 1.6 \text{ mm}$) without spreading the cells in the surface of the device or counterpart reservoir (Figure 16). It was also feasible to add new neurons into the counterpart reservoir without affecting the network in the first compartment (Figure 2 and Figure 19). This concept is used to provide two layer neuronal networks inside the PDMS device and let them connect together through bi-directionally growing axons inside the microchannels (Figure 19).

Two layer networks were provided for three major goals:

- a) Provide neuronal tracts, pathways, or nerves composed of axons originating from different modules and study their electrophysiology.
- b) Examine the device functionality in detecting bi-directional wiring inside the microchannels.

- c) To cut axons inside the same bundle in their different location compare their functional recovery.

Using different approaches to analysis the signals obtained from four subsequent electrodes inside the microchannels we confirmed that uni-directional propagation in one layer neuronal network gradually changed to bidirectional, started 10 DIV after seeding the next layer in the counterpart reservoir. This feature is confirmed by overlaying the raw signals recorded from four electrodes inside one microchannel, as well as crosscorrelogram of the activity between these electrodes. This kind of bidirectional tracts or pathways is common either in central nervous systems (CNS) or peripheral nervous system (PNS) (Neubauer et al., 2010; Schmahmann et al., 2007). Bidirectional connectivity could be provided between different types of the neurons in the two compartment microfluidic device (Kanagasabapathi et al., 2012) and be used as an in vitro model for studying electrophysiological properties of bidirectional tracts in CNS or mixed nerves in PNS.

In present work connecting microchannels between two network modules showed mixture of unidirectional and bidirectional propagation and we used this system for induction of axonal injury either in unidirectional or in bidirectional axonal tracts and studying network response to the localized injury in different compartments: somata, intact axons, dissected axons, as well as proximal and distal segments of the dissected axons (Figure 20 and Figure 21).

4.2.3 Controlled laser microdissection in specific unidirectional or bidirectional axonal tract

Besides providing pure axonal compartments with separate chemical and physical environment for axons, microchannels also isolating axonal bundles from each other which makes the device an interesting option for studying focal axonal damage in selected microchannel.

Recently, few studies have been conducted in similar microfluidic devices to understand axonal biology and pathology after dissection. In most cases, axonal injury produced by applying suction with fine tip glass pipettes to the entrance of the axonal channel, where axons releasing into the counterpart reservoir. This needs pipetting up all medium in the axonal compartment and then washing the compartment for several times to assure complete axonal dissection (Kim et al., 2012; Park et al., 2006; Taylor et al., 2005; Tsantoulas et al.,

2013). Regardless of its capability in providing pure axonal injury without affecting the cell body and studying the gene and protein expression in the injured axons, it was not possible to provide very local axonal injury without affecting other axons in adjacent microchannels or in the axonal compartment. In addition, almost in all cases these experiments were dealing with axonal biology and structural changes after dissection without evaluating the axonal electrophysiology or network functional response to the focal injury. In most cases, functional evaluations were restricted to calcium imaging or patch clamping the dissected neuron and studying its electrophysiology by providing artificial stimulus (Tsantoulas et al., 2013).

Laser light could be exploited for inducing very local dissection in the developing axons. For instance, pulsed laser microbeams have been applied for axonal microdissection in vivo in *C. elegans* and *Drosophila* (Bourgeois and Ben-Yakar, 2008; Yanik et al., 2004; Yanik et al., 2006). Femtosecond laser radiation (kHz or MHz) was the most common pulsed laser type used for axonal microdissection, because of its ability to produce extremely localized damage zones in single cells (Bourgeois and Ben-Yakar, 2008). However, this laser is high cost and the resulted setup is complex to work with. As an alternative it is possible to use picoseconds pulsed laser for axonal microdissection which is less expensive and does not provide reactive oxygen species (ROS) during the procedure, which are toxic for cell (Hellman et al., 2010).

To decrease the effect of the dissection in the local parts of an axon to other cellular compartments like cell body and dendrite, as well as other axons in the same culture dish, laser microdissection applied on the patterned cultures which had been provided by microfluidic system (Hellman et al., 2010; Kim et al., 2009). In 2009 Kim et al, Applied femtosecond laser to spatially isolate individual axons in microchannel for precise and reproducible axotomy on CNS and PNS axons and monitor the axonal regeneration after injury by mounting the culture into a mini-incubator (Kim et al., 2009). Hellman et al, in 2010 provided a combined micropatterned cell culture and picoseconds pulsed laser microbeam methods to study the initial dieback response and subsequent regrowth of CNS neurons in standard cell culture media (Hellman et al., 2010). Even though, both methods successfully applied much localized axonal injury and studied different aspects of axonal

degeneration and regrowth after injury, however it was not possible to record network electrophysiological response to the injury.

In a recent study by Tsantoulas et al, in 2013, they tried to analyse cellular activity in response to the axotomy by seeding the neurons in multicompartiment microfluidic device and recording the activity after axotomy using patch clamp recording from already stained cell bodies by DiO and calcium imaging from dissected axons. In this model dissection was provided by applying the suction into the axonal compartment and all axonal branches in that compartment were dissected. Combined Ca imaging and electrophysiology recording showed that axotomy in DRG or nociceptor neurons increases action potential (AP) amplitude and altered AP threshold in subpopulations of the regenerating axons. In addition they showed accumulation of Nav.18 channels in the regenerating axons (Tsantoulas et al., 2013). In this study the recordings from axon or cell body was performed after stimulation through an electrode inserted into the axonal compartment. In addition it was not possible to address the whole network response to the injury. In addition, the axonal injury, as well as recording, was not focalized to specific microchannel.

In our setup, we combined the laser microdissection with microfluidic culture method to provide focal axonal dissection. Combining the microfluidic cell culture setup with MEA technology on the other hand provide spatial access for locally recording from different compartments of the network as well as different sections of dissected axons. In general 12 electrodes were recording the activity from small-world network in the reservoir, two electrodes from proximal and 2 from distal parts of dissected axons, and four electrodes from intact axons in other microchannels. The increased signal amplitude recorded by non-invasive extracellular recording in combined microfluidic-MEA setup gave the opportunity to keep cultures alive after dissection for more than 6 weeks and monitor the activity dynamics in different parts of the network.

In spite of the miniaturized reservoir structures in our device, updated seeding protocol facilitated providing bidirectional axons inside the microchannels in two-layer networks. These axonal bundles resemble mixed nerves in the PNS or bi-directional tracts in the CNS (Neubauer et al., 2010; Schmahmann et al., 2007). Therefore we utilized the system for the first time to perform dissection on axonal bundles composed of bi-directionally growing

axons. In addition, dissecting these axons in one edge of the microchannels provided us the opportunity to cut some axons in most distal parts and the rest in their most proximal sections (Figure 21). It has already been shown that axonal dissection in the proximal and distal sections could provide different outcomes (Navarro et al., 2007; Ygge, 1989).

4.2.4 Bi-directional axons morphology and electrophysiology after focal microdissection

Even though mixed nerves in the PNS are mixture of sensory and motor neurons growing in different directions and the combined neuronal tracts in CNS might composed of axons from different types of neurons (Navarro et al., 2007; Schmahmann et al., 2007), here we cultured the same type of the neurons in two sides of the microchannels to provide bi-directional axons which had similar biophysical properties. Sequential seeding of neurons in two reservoirs and bi-directional growth of the axons was confirmed by crosscorrelograms obtained from electrophysiological data in microchannels (Figure 19). Dissection was performed after establishment of bi-directional propagation in few out of eight microchannels in each cortical culture.

The first morphological signs of degeneration in both sides of the dissected axonal bundles were appeared around 24 hours after dissection with segmented pieces of degenerating axons which progressed during the subsequent weeks (Figure 20). It has already been shown that in peripheral nerve injury the first signs are observed after one DIV with progression into proximal and distal sections in one to two weeks later (Guertin et al., 2005).

In accordance to the crosscorrelation analysis after dissection propagation disappeared in one direction (Figure 20). Considering the latencies between the recorded activities in subsequent electrodes recording from same axonal bundle, we realized that propagation is mainly lost in axons which had been cut in their most proximal parts (Figure 20 and Figure 21). In the rat model of sciatic nerve dissection it has been shown that dissection in the proximal sections is more deteriorative than the distal section which includes higher percentage of cell loss when dissection is performed in the proximal parts (Ygge, 1989). In the same cultures or other cultures dissection was done in microchannels encompassed uni-directionally growing axons and the results compared with bi-directional axonal bundles. In accordance to the morphology, uni-directional axons showed severe distal degeneration

compared to bi-directional axons (Figure 20 and Figure 22) which is also confirmed by recorded activity in distal electrodes (Figure 22 F and G).

In parallel we analysed the recordings from somal compartment and intact axons in other microchannels. In intact axons activity did not change for DIVs after dissection however in reservoir a sharp decrease and return to baseline in activity happened post-dissection (Figure 22 E).

4.2.5 Direct microchannels limitations in studying axonal morphology and electrophysiology

By further analysing the acquired data from microchannels, time stamps and cross correlations, it was possible to predict whether axonal bundle inside the microchannel is unidirectional or bi-directional. However, it was difficult to correspond clearly the obtained results from electrophysiology data to distinct axonal bundle. In the direct microchannels axons tended to form big bundles or fascicles in which morphological changes in separate branches was not accessible for evaluation, especially in the bi-directional bundles which had filled almost all microchannel width (Figure 20).

In the previous studies it has been shown that upon the releasing point into the counterpart reservoir the composing axonal branches separated from each other (Peyrin et al., 2011) (Figure 23). We applied the same concept in the next generation of the devices by adding extended areas, working stations, to the microchannels (Figure 3 and Figure 6). In the alignment procedure these wider areas left between electrode pairs to have access for dissection. Big axonal bundles branched in the working stations, in which morphology was simple to be monitored (Figure 23). In the next step, we simplified the network by seeding neurons in one reservoir and producing different levels of dissection for same axonal bundle for quantitative evaluation of the severity of the injury on axonal activity, as well as network dynamic.

4.3 Working stations in microchannels for step wise dissection

Branched axons in the working stations was accessible for dissecting few branches (local or spot dissection), half of the axonal bundle or complete axonal bundle. In addition we performed dissection before and after establishment of network morphology in DIVs 17

and 24, respectively (Table 4). In addition response to the dissection was compared between hippocampal and cortical cultures by following same procedure for both types of the neurons.

4.3.1 Axonal response to different levels of dissection

Different levels of dissection in the same culture provided different axonal activity and distal morphology depending upon the severity of the dissection. In complete dissection almost all distal section experienced progressive degeneration in two subsequent weeks with few branches repaired at later DIVs (Figure 24). Regardless of the significant activity decrease in distal section it has not been disappeared in the first distal electrode either in first hours after dissection or in later DIVs (Figure 24 and Figure 31 a and Figure 32 a). Crosscorrelation confirmed the presence of the propagation between two adjacent electrodes in two sides of the dissection point (Figure 24). This could be happened because of the small gap between distal and proximal sides. In the regenerating or repairing nerves axonal diameter and excitability as well as propagation speed remains lower than baseline and the amount of the regeneration is depends on the gap length between two sides (Cho, 2009; Navarro et al., 2007; Reyes et al., 2005). In our model the dissection gap was maximally 20 μm . It has been shown that nerves can reconnect for the dissection gaps less than 4 cm (Krarup et al., 2002). The presence of the activity in the first distal electrode could be related to the passive propagation along the degenerating axons in distal part. In the study by Kretschmer et al., they showed that axotomy leads to local accumulation of transported vesicles and insertion of the contained proteins including ion channels into the membrane which changes the membrane property and local hyper excitability (Kretschmer et al., 2002). In the axotomy of the hippocampal axons in microfluidic device, Tsantoulas et al., showed that after injury Nav1.8 channel accumulates in the regenerating axons and increases their excitability (Tsantoulas et al., 2013). Pictures prepared after one week of dissection showed signs of reorganization and bridges across the dissection point (Figure 24 B) which followed by slight increase in the activity after DIV 30 (Figure 31 a).

Slight or partial damage to the axonal bundles in DIV 17 caused a slight decrease of the activity in the recorded activity from whole hippocampal or cortical axonal bundles (Figure 31 b-c and Figure 32 b-c). However, partial dissection or completing the dissection in DIV 24 for axonal bundles which had already experienced local or partial dissections,

respectively, provided very sharp activity decrease in distal axons (Figure 31 b-c and Figure 32 b-c). This effect could be either related to the severity of the dissection or the age dependent consequence of the injury. Comparing the complete dissection in DIV 17 and DIV 24, we found that dissection in DIV 24 was more deteriorating than the dissection in DIV 17 (Figure 31 and Figure 32). Rapid axonal growth in the developing CNS neurons is an actin/myosin dependent mechanism which is facilitated by high cyclic AMP (cAMP) concentrations (Cai et al., 2001; Hellstrom and Harvey, 2014). In the younger neurons axotomy increases cAMP concentrations (Qiu et al., 2002), while in older neurons these types of growth promoting molecules are decreased both in basal condition and after axotomy (Cai et al., 2001; Selzer, 2003). Step wise activity decrease after first and local axonal dissections in cortical and hippocampal cultures proved the feasibility of the technique in providing desired axonal damage (Figure 31 and Figure 32).

In spite of the activity loss in distal axons activity increased in the proximal parts especially after first dissection in both types of the neurons (Figure 31 A and Figure 32 B). This increase in the activity could be related to accumulation of the ion channels in the proximal membrane which increases the membrane excitability (Kretschmer et al., 2002; Tsantoulas et al., 2013). This increased activity remained stable in the completely dissected axons which left intact in DIV 24, while it dropped down in local or partial dissected hippocampal axons which experienced an extra dissection in DIV 24. These data suggested that compared to the cortical axons, hippocampal axons are more susceptible to dissection induced activity loss (Figure 30). Difference response to the dissection could be related to the different activity levels in corresponding cortical vs. hippocampal network (Figure 27 A and B).

4.3.2 Network response to the dissection

In the PNS nerve injury increases the activity in the related CNS centers by sensitizing neuronal structures, long term potentiation as well as expansion of the CNS neurons receptive field (McMahon and Koltzenburg, 2006; Melzack et al., 2001; Navarro et al., 2007). Such increase in the activity was also confirmed after axotomy in cultured hippocampal neurons in younger DIVs (Tsantoulas et al., 2013). In our study, cortical and hippocampal network activity increased in response to the dissection in DIV 17 and remained

higher for subsequent week (Figure 27). This activity had been obtained from mixture of axotomized and non-axotomized neurons in the reservoir. However, after second dissection in DIV 24 cortical and hippocampal neurons showed different activity profiles (Figure 27). Cortical networks activity remained stable while in hippocampal culture activity decreased and remained in lower levels for 10 subsequent DIVs (Figure 27). This could be related to the electrophysiological properties of two neuron types. For instance oxygen and glucose deprivation in hippocampal neurons increased the AMPA receptor (AMPA) subunit GluA2 endocytosis which is absent in cortical neurons (Blanco-Suarez and Hanley, 2014).

It has been suggested that neuronal hyperactivity after axotomy could either prevent from cell death or promote axogenesis in hypothalamic magnocellular neurons (Shahar et al., 2004). Neuronal activity and depolarization increases the survival in different types of CNS neurons including hippocampal (Ma et al., 2009) (Cortes et al., 2007) and cortical neurons (Morimoto, 2012; Wagner-Golbs and Luhmann, 2012). In addition to the increased cell survival, higher electrical activity beside neurotrophic factors could improve neurogenesis and axogenesis (Corredor and Goldberg, 2009). In our study the loss of the activity in the hippocampal cultures were concomitant with severe activity loss in the dissected axons in DIV 24 (Figure 31 and Figure 27). This could be related to the intrinsic properties of the hippocampal neurons which are more susceptible to stress compared to the cortical neurons which consequently affects the neurogenesis after dissection.

4.4 Conclusion

In present study three technologies combined together to: 1) provide localized axonal dissection in the context of a rich and active network and 2) study network electrophysiology in different levels in response to the dissection. Combining the MEA and microfluidic cell culture chambers provide useful template for recording weak signals from axons, record propagation direction and velocity and amplify activity in the small and simplified cortical or hippocampal networks. In addition physical confinements provided by microchannels gave the opportunity to manipulate axons in specific parts of the network and leave the other axons or cell body intact. Because of the PDMS device fabrication flexibility it was possible to improve and optimize the device in each generation for specified task. For instance to provide different levels of axonal injury in different microchannels we simply added wider areas into the microchannels which axons to branch and separate from each other and made it possible to dissect few branches in some microchannels. Laser microdissection on the other hand provided a sterile and precise tool for providing axonal injury in reproducible format. The major aspect of the present study was to functionalize these three combined technologies for studying axonal injury and regeneration. Combined with other approaches like molecular biology and chemical manipulations it is either possible to trace the involved mechanisms in degeneration or look after regenerating mechanisms and in a more practical way test the effect of different compounds on increasing the axiogenesis after injury.

4.5 Limitations

- A) In the culture neurons in the planar electrodes recordable activity always starts from DIV 7 to 10 in few electrodes and reaches to optimal levels after 2 weeks. Therefore, and in accordance to the capabilities of the combined setup we preferred to perform the dissection in DIV 17 when cultures show rich electrophysiological activity. In accordance to the previous studies on laser microdissection and axonal regeneration, in younger ages starting from DIV 3 axons can regenerate with higher speed and more obvious way. However, in all these cases the experiments are limited in time because for recording the activity in very low density and young networks it is necessary to apply calcium imaging or patch clamp recording which are invasive (Difato et al., 2010; Difato et al., 2011; Tsantoulas et al., 2013). In addition these young neurons are different from adult neurons in response to injury.
- B) Even though the PDMS device is quite transparent, regarding the higher number of growing axons inside the microchannels it was not possible to trace individual axonal branches after dissection. This was mandatory to keep the number of the neurons in the reservoir in optimal amounts; otherwise it was not possible to obtain enough extracellular activity from very low density and small network. Increasing the number of the neurons in the reservoir increases the number of the growing axons inside the microchannels.
- C) Tiny microchannel environment prevents from penetration of the immunostaining dyes and therefore it's difficult to visualize the axons inside the microchannels by fluorescent dyes. In addition retrograde labeling in the present device was not feasible because the device was very thin and to provide enough nutrients for cells we had to merge both compartments in cell culture medium. Even adding very carefully DiI into the counterpart reservoir lead to labeling of the neurons in both compartments.

4.6 Future works

- A. MEA technology also gives the opportunity to stimulate the cultured neurons from multiple sites and for long term. In present study we didn't tried to define separate groups for electrical stimulation or even chemical stimulation by glutamate receptor agonists or GABA receptor antagonists. In addition it is possible to add new compartments or modify the design in an optimized way to understand the effect of dissection in one side of the complex network on the network dynamics in other parts.

- B. Axonal transport is an important factor either in axonal function and regeneration. Diluting the number of the axons inside the microchannels we can concomitantly study axonal electrophysiology and transport either in normal conditions or after injury.

R

ferences

- Alle, H., Geiger, J.R., 2006. Combined analog and action potential coding in hippocampal mossy fibers. *Science*. 311, 1290-3.
- Andersson, H., van den Berg, A., 2004. Microfabrication and microfluidics for tissue engineering: state of the art and future opportunities. *Lab Chip*. 4, 98-103.
- Bakkum, D.J., Chao, Z.C., Potter, S.M., 2008. Long-term activity-dependent plasticity of action potential propagation delay and amplitude in cortical networks. *PLoS One*. 3, e2088.
- Bakkum, D.J., Frey, U., Radivojevic, M., Russell, T.L., Muller, J., Fiscella, M., Takahashi, H., Hierlemann, A., 2013a. Tracking axonal action potential propagation on a high-density microelectrode array across hundreds of sites. *Nat Commun*. 4, 2181.
- Bakkum, D.J., Radivojevic, M., Frey, U., Franke, F., Hierlemann, A., Takahashi, H., 2013b. Parameters for burst detection. *Front Comput Neurosci*. 7, 193.
- Baruchi, I., Volman, V., Raichman, N., Shein, M., Ben-Jacob, E., 2008. The emergence and properties of mutual synchronization in in vitro coupled cortical networks. *Eur J Neurosci*. 28, 1825-35.
- Belanger, M.C., Marois, Y., 2001. Hemocompatibility, biocompatibility, inflammatory and in vivo studies of primary reference materials low-density polyethylene and polydimethylsiloxane: a review. *J Biomed Mater Res*. 58, 467-77.
- Berdichevsky, Y., Sabolek, H., Levine, J.B., Staley, K.J., Yarmush, M.L., 2009. Microfluidics and multielectrode array-compatible organotypic slice culture method. *J Neurosci Methods*. 178, 59-64.
- Berdichevsky, Y., Staley, K.J., Yarmush, M.L., 2010. Building and manipulating neural pathways with microfluidics. *Lab Chip*. 10, 999-1004.
- Blanco-Suarez, E., Hanley, J.G., 2014. Distinct subunit-specific alpha-amino-3-hydroxy-5-methyl-4-isoxazolepropionic acid (AMPA) receptor trafficking mechanisms in cultured cortical and hippocampal neurons in response to oxygen and glucose deprivation. *J Biol Chem*. 289, 4644-51.
- Blau, A., Neumann, T., Ziegler, C., Benfenati, F., 2009. Replica-moulded polydimethylsiloxane culture vessel lids attenuate osmotic drift in long-term cell cultures. *J Biosci*. 34, 59-69.
- Blau, A., Murr, A., Wolff, S., Sernagor, E., Medini, P., Iurilli, G., Ziegler, C., Benfenati, F., 2011. Flexible, all-polymer microelectrode arrays for the capture of cardiac and neuronal signals. *Biomaterials*. 32, 1778-86.
- Blau, A., 2013. Cell adhesion promotion strategies for signal transduction enhancement in microelectrode array in vitro electrophysiology: An introductory overview and critical discussion. *Current Opinion in Colloid & Interface Science*. 18, 481-492.
- Bourgeois, F., Ben-Yakar, A., 2008. Femtosecond laser nanoaxotomy properties and their effect on axonal recovery in *C. elegans* (vol 15, pg 8521, 2007). *Optics Express*. 16, 5963-5963.

- Buitenweg, J.R., Rutten, W.L., Marani, E., 2002a. Modeled channel distributions explain extracellular recordings from cultured neurons sealed to microelectrodes. *IEEE Trans Biomed Eng.* 49, 1580-90.
- Buitenweg, J.R., Rutten, W.L., Marani, E., Polman, S.K., Ursum, J., 2002b. Extracellular detection of active membrane currents in the neuron-electrode interface. *J Neurosci Methods.* 115, 211-21.
- Cai, D., Qiu, J., Cao, Z., McAtee, M., Bregman, B.S., Filbin, M.T., 2001. Neuronal cyclic AMP controls the developmental loss in ability of axons to regenerate. *J Neurosci.* 21, 4731-9.
- Campenot, R.B., 1977. Local-Control of Neurite Sprouting in Cultured Sympathetic Neurons by Nerve Growth-Factor. *Developmental Brain Research.* 37, 293-301.
- Chakraborty, S.K.M.a.S.C.S.M.a.S.K., 2011. Chapter 8. SU-8 Photolithography and Its Impact on Microfluidics. In *Microfluidics and Nanofluidics Handbook*. Vol. 2, ed.^eds. CRC Press, pp. 231-268.
- Chiappalone, M., Bove, M., Vato, A., Tedesco, M., Martinoia, S., 2006. Dissociated cortical networks show spontaneously correlated activity patterns during in vitro development. *Brain Res.* 1093, 41-53.
- Cho, M., 2009. Reconnecting injured nerves. *Nature Neuroscience.* 12, 1085-1085.
- Claverol-Tinture, E., Ghirardi, M., Fiumara, F., Rosell, X., Cabestany, J., 2005. Multielectrode arrays with elastomeric microstructured overlays for extracellular recordings from patterned neurons. *J Neural Eng.* 2, L1-7.
- Claverol-Tinture, E., Cabestany, J., Rosell, X., 2007. Multisite recording of extracellular potentials produced by microchannel-confined neurons in-vitro. *IEEE Trans Biomed Eng.* 54, 331-5.
- Corredor, R.G., Goldberg, J.L., 2009. Electrical activity enhances neuronal survival and regeneration. *Journal of Neural Engineering.* 6.
- Cortes, R.Y., Arevalo, J.C., Magby, J.P., Chao, M.V., Plummer, M.R., 2007. Developmental and activity-dependent regulation of ARMS/Kidins220 in cultured rat hippocampal neurons. *Dev Neurobiol.* 67, 1687-98.
- Cullen, D.K., Vukasinovic, J., Glezer, A., Laplaca, M.C., 2007. Microfluidic engineered high cell density three-dimensional neural cultures. *J Neural Eng.* 4, 159-72.
- Debanne, D., 2004. Information processing in the axon. *Nat Rev Neurosci.* 5, 304-16.
- Demerens, C., Stankoff, B., Logak, M., Anglade, P., Allinquant, B., Couraud, F., Zalc, B., Lubetzki, C., 1996. Induction of myelination in the central nervous system by electrical activity. *Proc Natl Acad Sci U S A.* 93, 9887-92.
- Dertinger, S.K.W., Jiang, X.Y., Li, Z.Y., Murthy, V.N., Whitesides, G.M., 2002. Gradients of substrate-bound laminin orient axonal specification of neurons. *Proceedings of the National Academy of Sciences of the United States of America.* 99, 12542-12547.
- Difato, F., Marconi, E., Maccione, A., Berdondini, L., Chierigatti, E., Ronzitti, G., Benfenati, F., Blau, A., 2010. Combining Optical Tweezers, Laser Microdissectors and Multichannel Electrophysiology for the Non-Invasive Tracing and Manipulation of Neural Activity on Single Cell and Network Level. *Biophysical Journal.* 98, 138a-138a.
- Difato, F., Dal Maschio, M., Marconi, E., Ronzitti, G., Maccione, A., Fellin, T., Berdondini, L., Chierigatti, E., Benfenati, F., Blau, A., 2011. Combined optical tweezers and laser dissector for controlled ablation of functional connections in neural networks. *Journal of Biomedical Optics.* 16.

- Dworak, B.J., Wheeler, B.C., 2009. Novel MEA platform with PDMS microtunnels enables the detection of action potential propagation from isolated axons in culture. *Lab on a Chip*. 9, 404-410.
- Fayaz, I., Tator, C.H., 2000. Modeling axonal injury in vitro: injury and regeneration following acute neuritic trauma. *J Neurosci Methods*. 102, 69-79.
- Feinerman, O., Segal, M., Moses, E., 2007. Identification and dynamics of spontaneous burst initiation zones in unidimensional neuronal cultures. *J Neurophysiol*. 97, 2937-48.
- Feinerman, O., Rotem, A., Moses, E., 2008. Reliable neuronal logic devices from patterned hippocampal cultures. *Nature Physics*. 4, 967-973.
- Fields, R.D., 2005. Myelination: an overlooked mechanism of synaptic plasticity? *Neuroscientist*. 11, 528-31.
- Filbin, M.T., 2003. Myelin-associated inhibitors of axonal regeneration in the adult mammalian CNS. *Nat Rev Neurosci*. 4, 703-13.
- Francisco, H., Yellen, B.B., Halverson, D.S., Friedman, G., Gallo, G., 2007. Regulation of axon guidance and extension by three-dimensional constraints. *Biomaterials*. 28, 3398-407.
- Frey, U., Egert, U., Heer, F., Hafizovic, S., Hierlemann, A., 2009. Microelectronic system for high-resolution mapping of extracellular electric fields applied to brain slices. *Biosens Bioelectron*. 24, 2191-8.
- Greenbaum, A., Anava, S., Ayali, A., Shein, M., David-Pur, M., Ben-Jacob, E., Hanein, Y., 2009. One-to-one neuron-electrode interfacing. *J Neurosci Methods*. 182, 219-24.
- Gross, G.W., 1979. Simultaneous single unit recording in vitro with a photoetched laser deinsulated gold multimicroelectrode surface. *IEEE Trans Biomed Eng*. 26, 273-9.
- Guertin, A.D., Zhang, D.P., Mak, K.S., Alberta, J.A., Kim, H.A., 2005. Microanatomy of axon/glia signaling during Wallerian degeneration. *J Neurosci*. 25, 3478-87.
- Hellman, A.N., Vahidi, B., Kim, H.J., Mismar, W., Steward, O., Jeon, N.L., Venugopalan, V., 2010. Examination of axonal injury and regeneration in micropatterned neuronal culture using pulsed laser microbeam dissection. *Lab Chip*. 10, 2083-92.
- Hellstrom, M., Harvey, A.R., 2014. Cyclic AMP and the regeneration of retinal ganglion cell axons. *International Journal of Biochemistry & Cell Biology*. 56, 66-73.
- Illes, S., Theiss, S., Hartung, H.P., Siebler, M., Dihne, M., 2009. Niche-dependent development of functional neuronal networks from embryonic stem cell-derived neural populations. *BMC Neurosci*. 10, 93.
- Jun, S.B., Hynd, M.R., Dowell-Mesfin, N., Smith, K.L., Turner, J.N., Shain, W., Kim, S.J., 2007. Low-density neuronal networks cultured using patterned poly-L-lysine on microelectrode arrays. *J Neurosci Methods*. 160, 317-26.
- Kanagasabapathi, T.T., Massobrio, P., Barone, R.A., Tedesco, M., Martinoia, S., Wadman, W.J., Decre, M.M., 2012. Functional connectivity and dynamics of cortical-thalamic networks co-cultured in a dual compartment device. *J Neural Eng*. 9, 036010.
- Kim, H.J., Park, J.W., Park, J.W., Byun, J.H., Vahidi, B., Rhee, S.W., Jeon, N.L., 2012. Integrated Microfluidics Platforms for Investigating Injury and Regeneration of CNS Axons. *Ann Biomed Eng*.
- Kim, Y.T., Karthikeyan, K., Chirvi, S., Dave, D.P., 2009. Neuro-optical microfluidic platform to study injury and regeneration of single axons. *Lab Chip*. 9, 2576-81.
- Kondo, M., Iwase, S., Mano, T., Kuzuhara, S., 2004. Direct measurement of human sympathetic nerve conduction velocity. *Muscle Nerve*. 29, 128-33.

- Krarup, C., Archibald, S.J., Madison, R.D., 2002. Factors that influence peripheral nerve regeneration: An electrophysiological study of the monkey median nerve. *Annals of Neurology*. 51, 69-81.
- Kretschmer, T., Happel, L.T., England, J.D., Nguyen, D.H., Tiel, R.L., Beuerman, R.W., Kine, D.G., 2002. Accumulation of PN1 and PN3 sodium channels in painful human neuroma-evidence from immunocytochemistry. *Acta Neurochirurgica*. 144, 803-810.
- Leclerc, E., Sakai, Y., Fujii, T., 2003. Cell culture in 3-dimensional microfluidic structure of PDMS (polydimethylsiloxane). *Biomedical Microdevices*. 5, 109-114.
- Li, N., Folch, A., 2005. Integration of topographical and biochemical cues by axons during growth on microfabricated 3-D substrates. *Exp Cell Res*. 311, 307-16.
- Ling, W., 2011. Microchannel enhanced neuron-computer interface: design, fabrication, biophysics of signal generation, signal strength optimization, and its applications to ion-channel screening and basic neuroscience research. In PhD Thesis. Vol. PhD, ed. ^eds. The Institute for Bioengineering of Catalonia, pp. 160.
- Ling, W., Michael, R., Jennifer Olmos, B., Enric, C.-T., 2012. Biophysics of microchannel-enabled neuron-electrode interfaces. *J Neural Eng*. 9, 026010.
- Luo, C., Li, H., Xiong, C., Peng, X., Kou, Q., Chen, Y., Ji, H., Ouyang, Q., 2007. The combination of optical tweezers and microwell array for cells physical manipulation and localization in microfluidic device. *Biomed Microdevices*. 9, 573-8.
- Ma, D.K., Kim, W.R., Ming, G.L., Song, H., 2009. Activity-dependent extrinsic regulation of adult olfactory bulb and hippocampal neurogenesis. *Ann N Y Acad Sci*. 1170, 664-73.
- Madhavan, R., Chao, Z.C., Wagenaar, D.A., Bakkum, D.J., Potter, S.M., 2006. Multi-site Stimulation Quiets Network-wide Spontaneous Bursts and Enhances Functional Plasticity in Cultured Cortical Networks. In *Engineering in Medicine and Biology Society, 2006. EMBS '06. 28th Annual International Conference of the IEEE*. Vol., ed. ^eds., pp. 1593-1596.
- Maeda, E., Robinson, H.P., Kawana, A., 1995. The mechanisms of generation and propagation of synchronized bursting in developing networks of cortical neurons. *J Neurosci*. 15, 6834-45.
- Maher, M.P., Dvorak-Carbone, H., Pine, J., Wright, J.A., Tai, Y.C., 1999. Microstructures for studies of cultured neural networks. *Med Biol Eng Comput*. 37, 110-8.
- Mandolesi, G., Madeddu, F., Bozzi, Y., Maffei, L., Ratto, G.M., 2004. Acute physiological response of mammalian central neurons to axotomy: ionic regulation and electrical activity. *FASEB J*. 18, 1934-6.
- Mata, A., Fleischman, A.J., Roy, S., 2005. Characterization of polydimethylsiloxane (PDMS) properties for biomedical micro/nanosystems. *Biomed Microdevices*. 7, 281-93.
- McDonald, J.C., Whitesides, G.M., 2002. Poly(dimethylsiloxane) as a material for fabricating microfluidic devices. *Accounts of Chemical Research*. 35, 491-499.
- McMahon, S.B., Koltzenburg, M., 2006. *Textbook of Pain- Wall, Pd, Melzack, R.* 91-105.
- Meeks, J.P., Mennerick, S., 2007. Action potential initiation and propagation in CA3 pyramidal axons. *J Neurophysiol*. 97, 3460-72.
- Mehling, M., Tay, S., 2014. Microfluidic cell culture. *Curr Opin Biotechnol*. 25, 95-102.
- Mehta, G., Mehta, K., Sud, D., Song, J.W., Bersano-Begey, T., Futai, N., Heo, Y.S., Mycek, M.A., Linderman, J.J., Takayama, S., 2007. Quantitative measurement and control of oxygen levels in microfluidic poly(dimethylsiloxane) bioreactors during cell culture. *Biomed Microdevices*. 9, 123-34.
- Melzack, R., Coderre, T.J., Katz, J., Vaccarino, A.L., 2001. Central neuroplasticity and pathological pain. *Ann N Y Acad Sci*. 933, 157-74.

- Millet, L.J., Stewart, M.E., Sweedler, J.V., Nuzzo, R.G., Gillette, M.U., 2007. Microfluidic devices for culturing primary mammalian neurons at low densities. *Lab Chip*. 7, 987-94.
- Millet, L.J., Stewart, M.E., Nuzzo, R.G., Gillette, M.U., 2010. Guiding neuron development with planar surface gradients of substrate cues deposited using microfluidic devices. *Lab Chip*. 10, 1525-35.
- Moriguchi, H., Wakamoto, Y., Sugio, Y., Takahashi, K., Inoue, I., Yasuda, K., 2002. An agar-microchamber cell-cultivation system: flexible change of microchamber shapes during cultivation by photo-thermal etching. *Lab on a Chip*. 2, 125-130.
- Morimoto, T., 2012. Role of electrical activity of neurons for neuroprotection. *Int Rev Neurobiol*. 105, 19-38.
- Morin, F., Nishimura, N., Griscorn, L., LePioufle, B., Fujita, H., Takamura, Y., Tamiya, E., 2006a. Constraining the connectivity of neuronal networks cultured on microelectrode arrays with microfluidic techniques: A step towards neuron-based functional chips. *Biosensors and Bioelectronics*. 21, 1093-1100.
- Morin, F., Nishimura, N., Griscorn, L., Lepioufle, B., Fujita, H., Takamura, Y., Tamiya, E., 2006b. Constraining the connectivity of neuronal networks cultured on microelectrode arrays with microfluidic techniques: a step towards neuron-based functional chips. *Biosens Bioelectron*. 21, 1093-100.
- Nam, Y., Chang, J., Khatami, D., Brewer, G.J., Wheeler, B.C., 2004. Patterning to enhance activity of cultured neuronal networks. *IEE Proc Nanobiotechnol*. 151, 109-15.
- Nam, Y., Wheeler, B.C., 2011. In vitro microelectrode array technology and neural recordings. *Crit Rev Biomed Eng*. 39, 45-61.
- Navarro, X., Vivo, M., Valero-Cabre, A., 2007. Neural plasticity after peripheral nerve injury and regeneration. *Prog Neurobiol*. 82, 163-201.
- Neubauer, D., Graham, J.B., Muir, D., 2010. Nerve grafts with various sensory and motor fiber compositions are equally effective for the repair of a mixed nerve defect. *Experimental Neurology*. 223, 203-206.
- Obien, M.E., Deligkaris, K., Bullmann, T., Bakkum, D.J., Frey, U., 2014. Revealing neuronal function through microelectrode array recordings. *Front Neurosci*. 8, 423.
- Pan, L.B., Song, X.D., Xiang, G.X., Wong, A., Xing, W.L., Cheng, J., 2009. First-Spike Rank Order as a Reliable Indicator of Burst Initiation and Its Relation With Early-to-Fire Neurons. *Ieee Transactions on Biomedical Engineering*. 56, 1673-1682.
- Pan, L.B., Alagapan, S., Franca, E., Brewer, G.J., Wheeler, B.C., 2011. Propagation of action potential activity in a predefined microtunnel neural network. *Journal of Neural Engineering*. 8.
- Park, J., Koito, H., Li, J., Han, A., 2009a. A multi-compartment CNS neuron-glia Co-culture microfluidic platform. *J Vis Exp*.
- Park, J., Koito, H., Li, J., Han, A., 2009b. Microfluidic compartmentalized co-culture platform for CNS axon myelination research. *Biomed Microdevices*. 11, 1145-53.
- Park, J.W., Vahidi, B., Taylor, A.M., Rhee, S.W., Jeon, N.L., 2006. Microfluidic culture platform for neuroscience research. *Nat Protoc*. 1, 2128-36.
- Park, J.W., Kim, H.J., Kang, M.W., Jeon, N.L., 2013. Advances in microfluidics-based experimental methods for neuroscience research. *Lab Chip*. 13, 509-21.
- Peyrin, J.M., Deleglise, B., Saias, L., Vignes, M., Gougis, P., Magnifico, S., Betuing, S., Pietri, M., Caboche, J., Vanhoutte, P., Viovy, J.L., Brugg, B., 2011. Axon diodes for the reconstruction of oriented neuronal networks in microfluidic chambers. *Lab Chip*. 11, 3663-73.

- Pine, J., 1980. Recording action potentials from cultured neurons with extracellular microcircuit electrodes. *J Neurosci Methods*. 2, 19-31.
- Pirlo, R., Peng, X., Yuan, X., Gao, B., 2008. Microfabrication, surface modification, and laser guidance techniques to create a neuron biochip. *Optoelectronics Letters*. 4, 387-390.
- Pirlo, R.K., 2009. Creation of defined single cell resolution neuronal circuits on microelectrode arrays. In Department of Bioengineering. Vol. PhD, ed. ^eds. Clemson University, pp. 189.
- Piruska, A., Nikcevic, I., Lee, S.H., Ahn, C., Heineman, W.R., Limbach, P.A., Seliskar, C.J., 2005. The autofluorescence of plastic materials and chips measured under laser irradiation. *Lab Chip*. 5, 1348-54.
- Qiu, J., Cai, C.M., Dai, H.N., McAtee, M., Hoffman, P.N., Bregman, B.S., Filbin, M.T., 2002. Spinal axon regeneration induced by elevation of cyclic AMP. *Neuron*. 34, 895-903.
- Quilty, M.C., Gai, W.P., Pountney, D.L., West, A.K., Vickers, J.C., 2003. Localization of alpha-, beta-, and gamma-synuclein during neuronal development and alterations associated with the neuronal response to axonal trauma. *Exp Neurol*. 182, 195-207.
- Ravula, S.K., McClain, M.A., Wang, M.S., Glass, J.D., Frazier, A.B., 2006. A multielectrode microcompartment culture platform for studying signal transduction in the nervous system. *Lab Chip*. 6, 1530-6.
- Ravula, S.K., Wang, M.S., McClain, M.A., Asress, S.A., Frazier, B., Glass, J.D., 2007. Spatiotemporal localization of injury potentials in DRG neurons during vincristine-induced axonal degeneration. *Neurosci Lett*. 415, 34-9.
- Recknor, J.B., Recknor, J.C., Sakaguchi, D.S., Mallapragada, S.K., 2004. Oriented astroglial cell growth on micropatterned polystyrene substrates. *Biomaterials*. 25, 2753-67.
- Reyes, O., Sosa, I., Kuffler, D.P., 2005. Promoting neurological recovery following a traumatic peripheral nerve injury. *P R Health Sci J*. 24, 215-23.
- Sasaki, T., Matsuki, N., Ikegaya, Y., 2011. Action-potential modulation during axonal conduction. *Science*. 331, 599-601.
- Schmahmann, J.D., Pandya, D.N., Wang, R., Dai, G., D'Arceuil, H.E., de Crespigny, A.J., Wedeen, V.J., 2007. Association fibre pathways of the brain: parallel observations from diffusion spectrum imaging and autoradiography. *Brain*. 130, 630-53.
- Selzer, M.E., 2003. Promotion of axonal regeneration in the injured CNS. *Lancet Neurology*. 2, 157-166.
- Shahar, T., House, S.B., Gainer, H., 2004. Neural activity protects hypothalamic magnocellular neurons against axotomy-induced programmed cell death. *J Neurosci*. 24, 6553-62.
- Shi, P., Nedelec, S., Wichterle, H., Kam, L.C., 2010. Combined microfluidics/protein patterning platform for pharmacological interrogation of axon pathfinding. *Lab Chip*. 10, 1005-10.
- Sia, S.K., Whitesides, G.M., 2003. Microfluidic devices fabricated in poly(dimethylsiloxane) for biological studies. *Electrophoresis*. 24, 3563-76.
- Siddique, R., Thakor, N., 2014. Investigation of nerve injury through microfluidic devices. *Journal of the Royal Society Interface*. 11.
- Taylor, A.M., Rhee, S.W., Tu, C.H., Cribbs, D.H., Cotman, C.W., Jeon, N.L., 2003. Microfluidic multicompartiment device for neuroscience research. *Langmuir*. 19, 1551-1556.
- Taylor, A.M., Blurton-Jones, M., Rhee, S.W., Cribbs, D.H., Cotman, C.W., Jeon, N.L., 2005. A microfluidic culture platform for CNS axonal injury, regeneration and transport. *Nat Methods*. 2, 599-605.
- Taylor, A.M., Jeon, N.L., 2010. Micro-scale and microfluidic devices for neurobiology. *Curr Opin Neurobiol*. 20, 640-7.

- Tooker, A., Meng, E., Erickson, J., Tai, Y.C., Pine, J., 2005. Biocompatible parylene neurocages. Developing a robust method for live neural network studies. *IEEE Eng Med Biol Mag.* 24, 30-3.
- Tsantoulas, C., Farmer, C., Machado, P., Baba, K., McMahon, S.B., Raouf, R., 2013. Probing Functional Properties of Nociceptive Axons Using a Microfluidic Culture System. *Plos One.* 8.
- van Pelt, J., Wolters, P.S., Corner, M.A., Rutten, W.L., Ramakers, G.J., 2004. Long-term characterization of firing dynamics of spontaneous bursts in cultured neural networks. *IEEE Trans Biomed Eng.* 51, 2051-62.
- Wagenaar, D.A., Pine, J., Potter, S.M., 2004. Effective parameters for stimulation of dissociated cultures using multi-electrode arrays. *J Neurosci Methods.* 138, 27-37.
- Wagenaar, D.A., Madhavan, R., Pine, J., Potter, S.M., 2005. Controlling bursting in cortical cultures with closed-loop multi-electrode stimulation. *J Neurosci.* 25, 680-8.
- Wagner-Golbs, A., Luhmann, H.J., 2012. Activity-dependent survival of developing neocortical neurons depends on PI3K signalling. *J Neurochem.* 120, 495-501.
- Wang, J., Ren, L., Li, L., Liu, W., Zhou, J., Yu, W., Tong, D., Chen, S., 2009. Microfluidics: a new cosset for neurobiology. *Lab Chip.* 9, 644-52.
- Wheeler, B.C., Brewer, G.J., 2010. Designing Neural Networks in Culture: Experiments are described for controlled growth, of nerve cells taken from rats, in predesigned geometrical patterns on laboratory culture dishes. *Proc IEEE Inst Electr Electron Eng.* 98, 398-406.
- Wheeler, B.C., Nam, Y., 2011. In Vitro Microelectrode Array Technology and Neural Recordings. *Critical Reviews in Biomedical Engineering.* 39, 45-61.
- Whitesides, G.M., Ostuni, E., Takayama, S., Jiang, X.Y., Ingber, D.E., 2001. Soft lithography in biology and biochemistry. *Annual Review of Biomedical Engineering.* 3, 335-373.
- Wu, M.-H., Huang, S.-B., Lee, G.-B., 2010. Microfluidic cell culture systems for drug research. *Lab on a Chip.* 10, 939-956.
- Yanik, M.F., Cinar, H., Cinar, H.N., Chisholm, A.D., Jin, Y.S., Ben-Yakar, A., 2004. Neurosurgery - Functional regeneration after laser axotomy. *Nature.* 432, 822-822.
- Yanik, M.F., Cinar, H., Cinar, H.N., Gibby, A., Chisholm, A.D., Jin, Y.S., Ben-Yakar, A., 2006. Nerve regeneration in *Caenorhabditis elegans* after femtosecond laser axotomy. *Ieee Journal of Selected Topics in Quantum Electronics.* 12, 1283-1291.
- Ygge, J., 1989. Neuronal Loss in Lumbar Dorsal-Root Ganglia after Proximal Compared to Distal Sciatic-Nerve Resection - a Quantitative Study in the Rat. *Brain Research.* 478, 193-195.